Preliminary Design and CFD Analysis of a Free-piston Engine with Uniflow Scavenging

Politecnico di Torino

Tomas Jano Rodriguez Lopez

Msc Mechanical Engineering

Academic Supervisors: Mirko Baratta & Daniela Misul
Company Supervisors: Carlo Beatrice & Dario Di Maio

2023

Contents

List of Figures

List of Tables

1 Abstract

Following the actual tendencies towards a reduction of greenhouse gases emissions and engines' downsizing, throughout this writing it is developed, in collaboration with CNR-STEMS, the geometrical modelling and CFD simulation of the gas filling in a heavy duty opposed-pistons two-stroke engine, which has a free piston layout and uniflow scavenging. The geometrical design is based on dimensions imposed by CNR-STEMS, recommendations found in literature and simplifications for the future mathematical complexity that the solver will need to face. After this is done, the geometry is inserted in the CFD software where the different boundary and initial conditions are set, based on a GT-Power model previously developed by CNR-STEMS. After establishing the previous parameters three verifications are done: first, a grid verification to properly set the fixed embeddings; second, a sealing verification to adapt the base grid size and triangulation; third, a temporal verification to properly configure the Adaptive Mesh Refinement settings, the duration of the whole simulation and its overall precision. Due to the satisfactory results that all the verfications showed, it is possible to perform the thermodynamic study which had positive and negative results. On the one hand, the model is able to properly represent the evolution of the relevant fields inside the engine, mainly the velocity, the air mass and fresh charge concentration; and reasonable values for an uniflow engine are obtained for different functionality parameters. On the other hand, a backflow problem is encountered due to an imprecise design decision for the ports' location and this situation should be fixed in future model upgrades before adding the combustion because it affects the reliability of the scavenging results: cylinder pressure profile and filling, among others.

2 Introduction

Considering the actual tendency towards a transition from conventional energy sources to renewable energy sources, an extended variety of engines have appeared with the objective of reducing greenhouse gases emissions in order to improve the air quality and counteract on global warming. A promising solution which is showing to have satisfactory results are engines which use **natural gas** as fuel because it is proven to: guarantee lower greenhouse gases emissions than typical diesel engines thanks to its higher hydrogen-to-carbon ratio; reduce the contribution for smog generation; and have the property of being carbon negative (capturing more carbon than the emitting).[1, 2]

Furthermore, it should also be remarked that natural gas engines present advantages in terms of noise generation, due to the lower sound pressure level; and odor emissions, due to the proper chemical composition of the fuel. Apart from these environmental benefits, the fuel, mainly constituted by methane, has demonstrated to be more cost-efficient than diesel and gasoline and to have higher performance: higher octane number, obtaining better compression and combustion efficiency due to an increased knock resistance; and cleaner combustion, resulting in a longer engine life, in comparison with conventional gasoline vehicles. [1]

Regardless the fuel type, one relevant aspect that should always be considered as one of the initial steps in the design process is the engine size, which is mainly dependent on the application in which it will be used. Light-duty engines are those used in passenger cars or trucks, whereas **heavy-duty** engines are placed in large and heavier vehicles like trucks, buses and ships, among others. Typically, heavy duty engines are designed for specific fields such as construction, mining and agriculture; and are characterized by their elevated torque and power output values. As a last point, it should also be mentioned the fact that heavy duty engines are able to resist heavy loads and extreme temperatures. [3, 4]

Similarly to the transition to renewable energy sources, another trend that is occurring nowadays is the downsizing of the engines to reduce costs and overall mass while increasing the specific power output. While in a conventional four-stroke engine a downsizing of more than 50% can generate negative consequences in terms of knocking combustion, maximum boost capability and peak cylinder pressure, among others; the **two-stroke engine** option occurs to be an effective alternative, because, as it has twice the firing frequency (one cycle every 360 crank angle degrees, instead of each 720), for the same output torque, the highest peak pressure can be almost halved, reducing the tendency for knocking and NOx production. Therefore, the two-stroke engine option is widely selected because it can guarantee an adequate downsizing without affecting the original boost. Additionally, by properly designing the scavenging in 2-stroke engines, it is possible to minimize the pumping power lost during intake, the thermal losses and the frictional losses during the cycle; increasing, as a consequence, the total efficiency. [5, 6]

One of the main aspects regarding two-stroke engines is the scavenging process, that is to say, the period in which the combustion exhaust products exit the cylinder and the new fresh charge enters, generating the gas exchange. The importance of this process is such that different engine configurations are adopted to guarantee certain type of scavenging. Throughout this project, the engine that will be considered works with **uniflow scavenging**, which consists in having evenly spaced inlet ports, so as to generate a swirling motion in

the charge flow that allows the cylinder filling with fresh charge at one end and the exhaust gases removal at the other, while reducing the possible short-circuiting (fresh charge exiting directly at the exhaust). As a matter of fact, this configuration tends to be particularly adequate for long stroke engines and provides the best scavenging efficiencies at any given scavenge ratio value. As a last remark, due to the fact that the gas flows towards the exhaust ducts after combustion, no backflow is possible when the exhaust opens. [7, 8]

As an example of uniflow scavenging two-stroke engines, the **opposed-pistons layout** is one of the most promising options. The previously mentioned layout consists of a pair of pistons inside their respective cylinders which are joined together with the absence of a cylinder head, that is to say, the clearance volume is delimited by each piston top when they both reach the top dead centre. This configuration eliminates the need for poppet valves because the same pistons are the ones which open and close the ports by blocking them or not while moving inside the cylinder. Moreover, the absence of the cylinder head significantly reduces the surface area of the combustion chamber enhancing further processes thanks to the additional heat available at the exhaust. It should also be mentioned the fact that, by properly designing the pistons' offset, this type of engine permits stronger turbulence to be generated inside the cylinder and so, improving the combustion process and increasing the thermal efficiency. In particular, the opposed-pistons layout has a **free piston** type in which both of the pistons move inside the cylinder without any mechanical join, diminishing the frictional losses in the engine and increasing the mechanical efficiency. [9, 10]

Having established all the previous information, throughout this project it is studied the design and CFD simulation of a heavy duty two-stroke engine with an opposed-piston layout, having the particularity of being a free piston type of engine. The objective is to generate and verify a predictive and robust 3D model able to adequately simulate the gas filling inside the engine, so that, in a future, it will be possible to upgrade the study by adding the combustion with natural gas.

3 Methodology

3.1 Engine Geometry Design

To begin with, in order to be able to develop a proper CFD model, it is needed to define the **control volume** inside the engine, that is to say, the complete volume that will be filled with air and fuel and where scavenging, combustion, expansion and exhaust will take place. For simplicity, this initial geometry will not be designed with the same CFD software (in this case, CONVERGE), but it will be developed a CAD file using SOLIDWORKS that, afterwards, will be converted to the appropriate format for the CFD analysis.

As a first step, it should be established which geometrical parameters must have a specific value due to requirements imposed by CNR STEMS. All this information is collected in Table 1:

Unitary stroke [mm]	144
Bore [mm]	120
Scavenging Type	Uniflow
Unitary stroke [mm]	144
Clearance volume [mm^3]	125277.04
Compression ratio	14

Table 1: Engine geometrical information provided by CNR STEMS

Having established all of the previous information, the cylinder occurs to be fully defined, but a new issue arises: the scavenging and exhaust ports' position, dimension, geometry and quantity are still undefined. This situation triggered an extensive research in order to find the best values for the previously mentioned parameters and the reasons for choosing them.

In first place, the ports' location is directly imposed by CNR-STEMS by establishing that the **position of the edge that will firstly open when scavenging begins** is **104,80 mm** away from the top dead centre and **96 mm** for the exhaust. It must be mentioned that these values were obtained from a preliminary research in which scavenging began at 131 crank angle degrees after the top dead centre and the exhaust at 120 crank angle degrees, but, as this kind of engine is of the free piston type, it does not seem reasonable to speak about "crank angle degrees", so a **linear relation** using the stroke (see Table 1) was applied in order to obtain analogous values in millimeters, considering that, in the conventional engines' theory, the top dead centre is placed at 180 crank angle degrees. As a last remark, it is necessary to highlight that each of the ports' positions are expressed as a distance with respect to the top dead centre and, as the opposed-piston engine presents two pistons ("intake and exhaust pistons" in Figure 8), each set of ports has a piston associated, so, for example, the scavenging ports location is expressed as a distance from the position where the intake piston is when it reaches the top dead centre (and in an analogous for the exhaust ports and piston).

In what respects to the dimensioning, for both types of ports it is selected a **rectangular shape with rounded corners** because it permits a sufficiently precise timing control together with an optimal use of the cylinder wall area [8]. Furthermore, an adequate starting point for the number of ports is **12** for the scavenging ones in order to guarantee an appropriate cylinder filling; and **8** for the exhaust ports to permit the proper exit of the combustion gases [11].

With the cross-section shape defined, it is now necessary to determine the dimensions for this cross-sectional area. In regards to the exhaust ports, the ports' width is decided as **75% of the bore dimension** to enable efficient gas outflow from the cylinder following the recommendation from Blair [7]. Similarly, the ports' height is chosen having as reference the work done by Mattarelli, Rinaldini, Savioli and Cantore [11] and adapting the values from that engine with the stroke shown in Table 1.

On the other hand, the dimensioning of the scavenging ports is more complex because more parameters should be defined, as it can be seen in Figure 1.

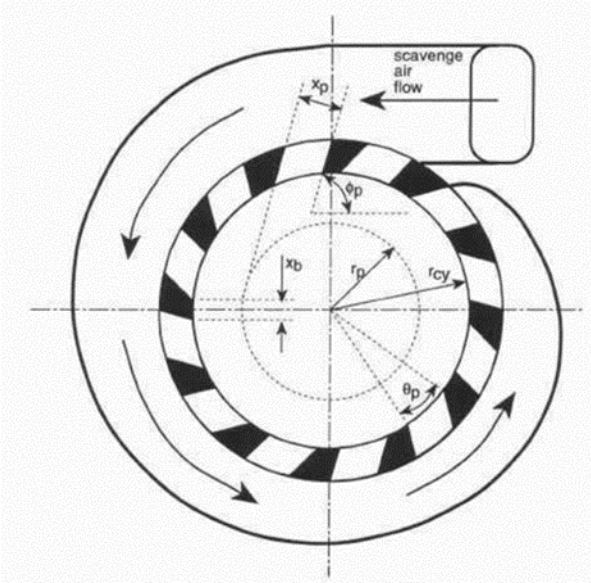

Figure 1: Generic layout for the scavenging ports of a uniflow scavenging engine (image taken from [7]).

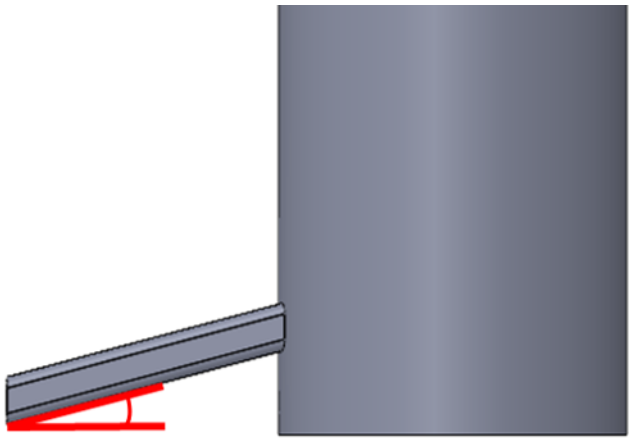

Figure 2: Tilt angle representation.

The swirl angle, Φ_P in Figure 1, and the tilt angle, shown in figure in Figure 2 are chosen as **15°** because they provide the best compromise between the swirl ratio, the delivery ratio and the charging efficiency; this means that they cause adequate swirling motion (for scavenging), filling and exhaust in the cylinder.[11]. In a similar way, the angle between ports, θ_P, is also **15°**, but in this case, the reason for this is to avoid piston ring pegging in the ports as the piston moves inside the cylinder[7]. With the previous angles already set and with the cylinder radius ("r_{cy}") known, it is possible to determine the scavenging ports width, "X_P", using the following formula [7] :

$$X_p = 2 \cdot r_{cy} \cdot \sin\left(\frac{\theta_P}{2}\right) \cdot \cos\left(\Phi_P\right) \tag{1}$$

As a last point, it must be mentioned that the ports' height is selected using the same criterion explained in the previous paragraph for the the exhaust ports.

In order to conclude the ports' design, it is required to talk about the corner radii. For both, the scavenging and the exhaust ports, the **top corner radii will be equal to the bottom corner radii**, taking [8] as a reference and, after analysing different examples of engines with uniflow scavenging, it is decided that the radii should have a value equal to the **25% of minimum cross-sectional dimension**, namely, the smallest between the height and the width. As a last remark, as, in a future, it will be necessary to study the inflow and outflow to and from the cylinder, the ports should be extended out of the cylinder, generating the "scavenging and exhaust ducts" which, in both cases, have a **length of 100 mm**, value arbitrarily defined in order to assure adequate correspondence between model and reality in what respects to flow analysis.

To sum up, below this paragraph it is placed Table 2 which shows all the results of the geometrical parameters previously discussed; and an image that clearly illustrates the actual geometry design:

Parameter	**Scavenging ducts**	**Exhaust ducts**
Shape	Rectangular with rounded corners	
Quantity	12	8
Width [mm]	15,13	11,25
Height [mm]	16,37	31,77
Swirl angle [°]	15	0
Tilt angle [°]	15	0
Angle between ports [°]	15	-
Corner radii [mm]	3,8	2,8
Length [mm]	100	

Table 2: Scavenging and exhaust ducts' dimensions. For the exhaust ducts, it is not necessary to impose the angle between ports; its value arises from setting the other dimensions.

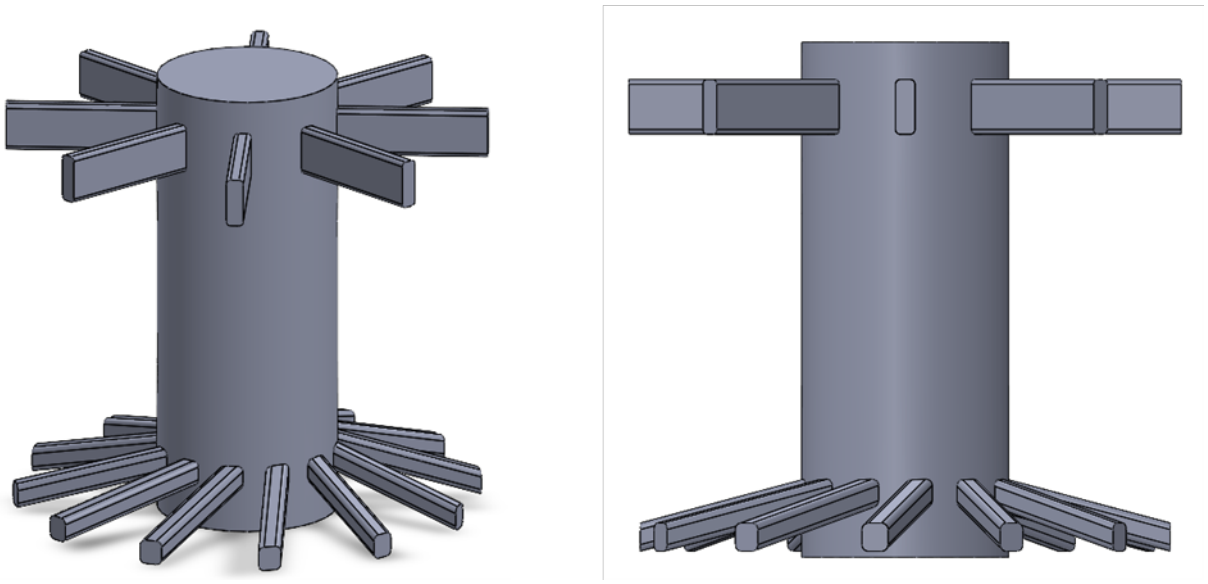

Figure 3: Isometric (left) and front (right) views of the engine control volume: at the bottom, the scavenging ducts; and at the top, the exhaust ducts.

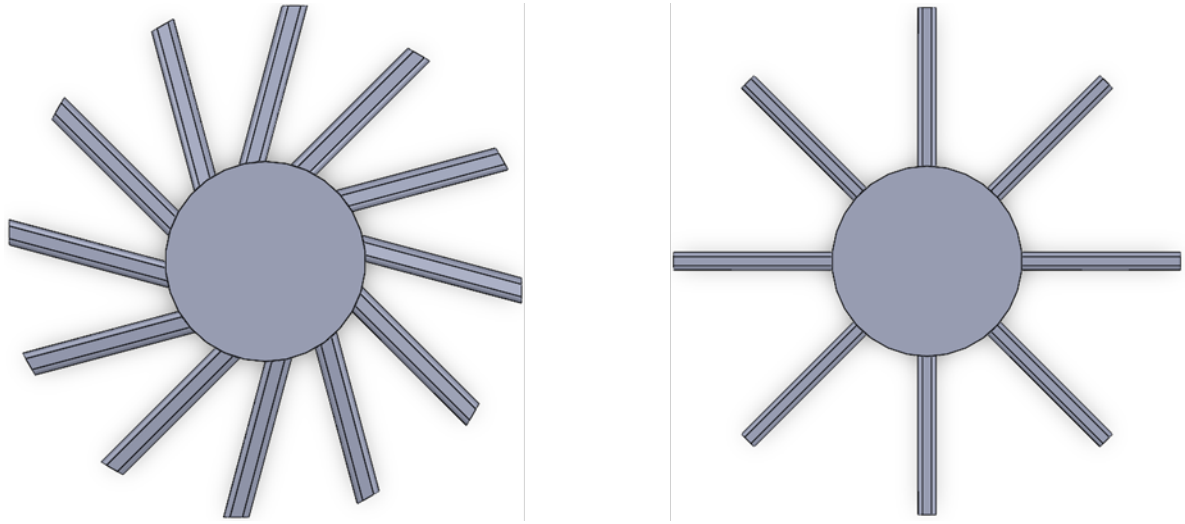

Figure 4: Top view of the scavenging ducts (left) and exhaust ducts (right).

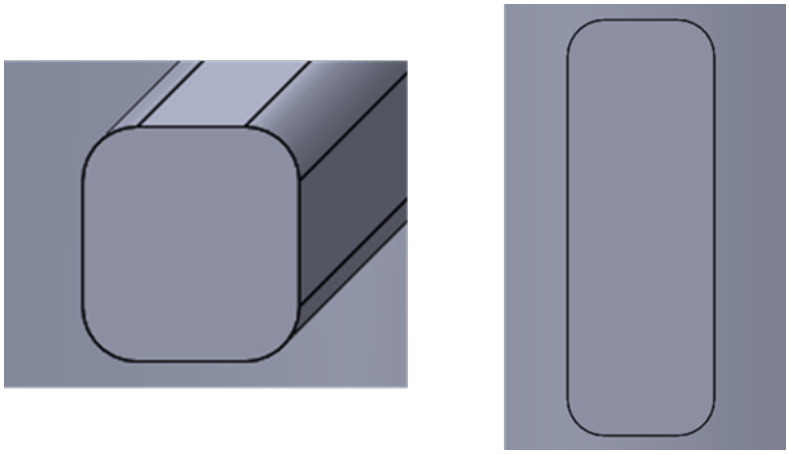

Figure 5: Front view of the scavenging ducts (left) and exhaust ducts (right).

From a physical point of view, the engine design is complete, but, actually, there are some modifications that should be done to simplify the future calculations and improve the quality of the future grid of the CFD model. In first place, the fact of imposing the boundary conditions at each of the 20 ports previously shown not only means a less realistic situation, but also implies an increased mathematical complexity for the solver. Therefore, to solve this, a collector that joins each set of ducts is added at the top and at the bottom, together with a pipe attached where the boundary conditions will be set. In this way, certain conditions are guaranteed:

- As the boundary conditions are imposed only in one port, the solver will be able to solve the corresponding equations faster.
- As the flow moves along the collectors before entering the scavenging ducts and after leaving the exhaust ducts, the fluid flow represented resembles more to the real one.
- As the circular shape of the collectors reaches all of the ducts, the fluid flow will still distribute itself between ducts in a relatively uniform way.

The dimensional information about each of the sets collector-duct is presented below:

Parameter	**Scavenging collector**	**Exhaust collector**
Height [mm]	36,37	51,77
Thickness [mm]	40	
Corner radii [mm]	2,5	
Duct's height [mm]	21,37	36,77
Duct's width [mm]	75	105
Duct's length [mm]	100	100

Table 3: Scavenging and exhaust collectors' dimensions.

Furthermore, as these collectors are just included for mathematical purposes, their impact on the physical results should be diminished as much as possible in order to maintain the correspondence between the model and the real engine, hence roundings are added at

any edge surrounding the collectors to generate a smoother flow by reducing the impact of sudden flow area changes. The rounding between each collector and its respective duct is chosen to be **5 mm** and the ones between each collector and each set of ducts **2,5 mm**.

After all this analysis, **the final control volume that will then define the CFD grid is finished** and it can be seen in Figure 6:

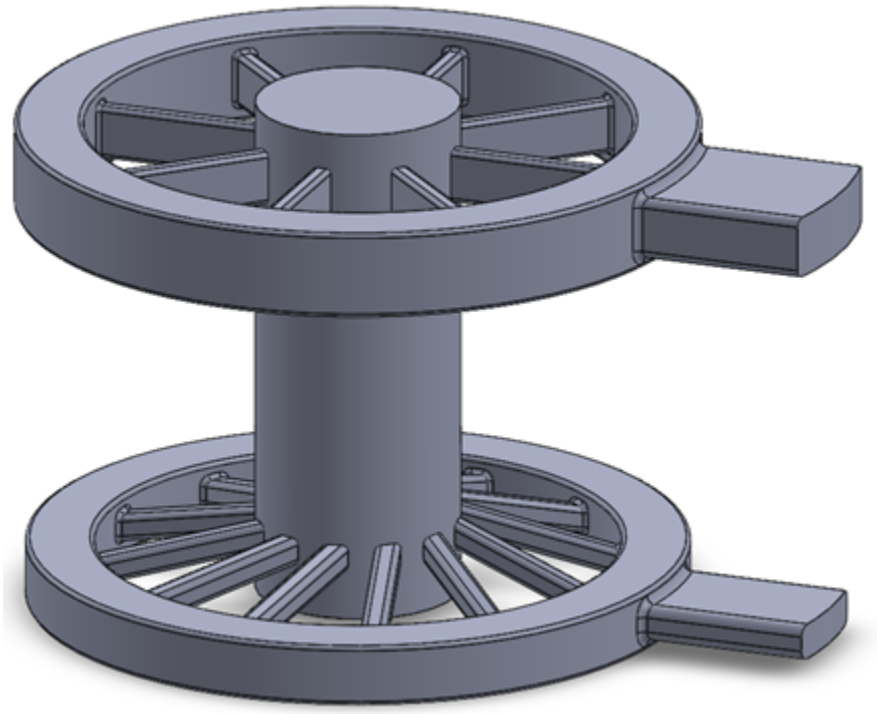

Figure 6: Isometric view of the control volume for the CFD model.

3.2 CFD Model Setup

With the CAD already defined, now it is possible to import the geometry in the CFD software pre-processing application: CONVERGE Studio. In CONVERGE Studio, the initial CAD is used as a starting point for defining the computational grid that will be used for the CFD analysis inside the domain. In addition, the application also enables the definition of the different physical parameters necessary for properly solving the mathematical equations that reign this case of study.[1]

3.2.1 Grid and Pistons

Once the CAD geometry is already imported in CONVERGE Studio, an automatically generated computational grid (with a grid size that will be modified afterwards) is produced in order to represent the corresponding engine control volume.

[1] Any physical or mathematical parameter that is not specifically mentioned in the following paragraphs is considered not fundamental for the analysis and the default values from CONVERGE Studio are maintained.

As a following step, it is needed to define the boundaries and the fences, that is to say, respectively, the different zones inside the engine (which have a difference in terms of functionality and/or boundary conditions) and the limits between them. After properly analyzing the whole system, it is determined that the best choice for the boundary definition is the following:

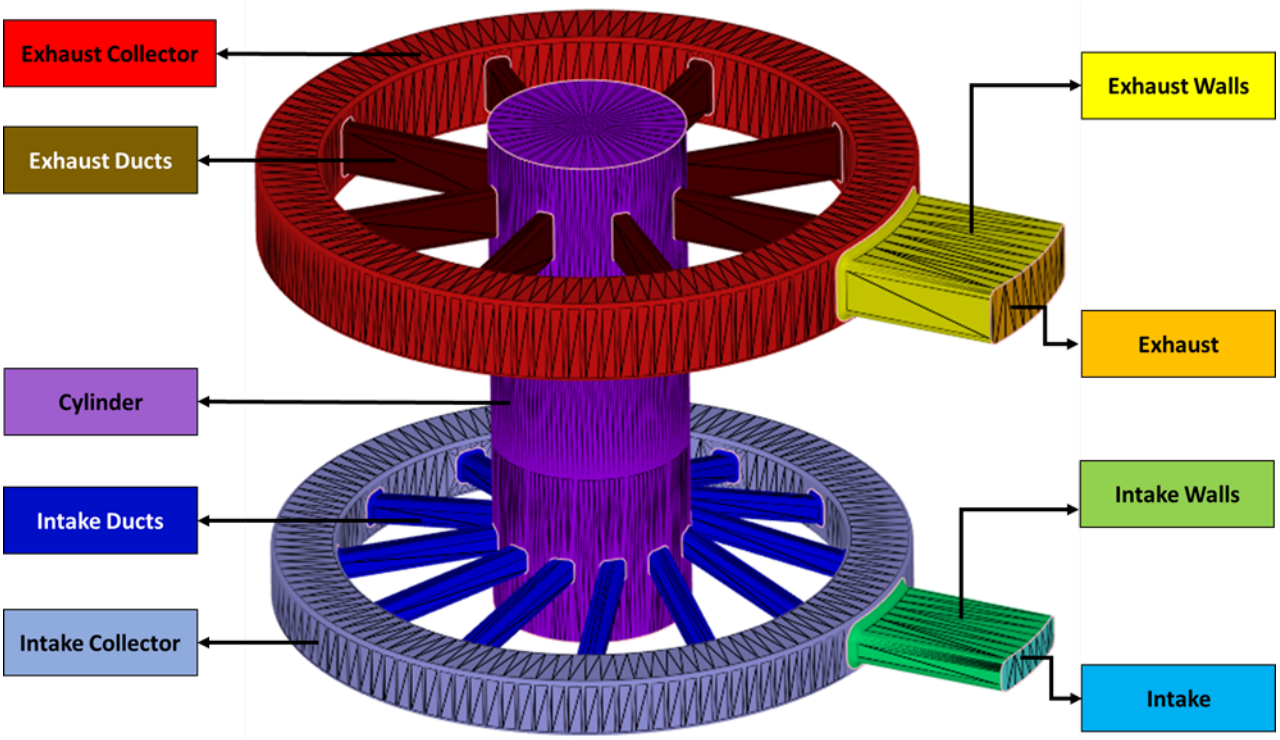

Figure 7: Isometric view of the computational mesh that will be used for the CFD analysis and each of its boundaries.

However, the grid is not completely defined because there are still two elements that are missing: the lower and the upper pistons. As the model shown should represent the bottom dead centre position, both of the pistons are located at each end of the boundary defined as "Cylinder" in Figure 7 and, initially, they have a diameter equal to the bore and a length equal to the unitary stroke (see Table 1).

Nevertheless, although this seems to be the reasonable layout for the system from a physical point of view, there are some mathematical issues that require some modifications in the actual layout. Taking as an example the intake piston that should be placed at the bottom of Figure 7 (the same analysis is valid and analogous for the exhaust piston at the top), when it is at the bottom dead centre, its top part is in the same position as the cylinder's bottom end and, in consequence, if the simulation was launched under this conditions, the solver would not know which values to consider in that location for the boundary conditions. In order to provide a solution to this problem, it is simply extended the length of the cylinder by 10 mm at both sides; in this way, it is guaranteed that, when the pistons are at the bottom dead centre, their ends, not the cylinder's, are the ones that act as a wall for the fluid inside the engine.

Nonetheless, now a new irregularity should be solved: with the actual layout including the last modification, when the pistons are at the top dead centre, two new "empty" volumes

appear between the cylinder ends and each of the pistons' ends and, due to the way in which the software works, the program will understand it as if it was full of fluid and will try to solve the problem in these enclosed volumes too. To fix this situation, the pistons' length is extended until their ends exceed the cylinder ends (in this case 30 mm); this condition prevents the formation of the previously mentioned enclosed volumes and do not affect the overall study because, in practical terms, the function of the pistons of being walls that avoid fluid flow in certain direction is still guaranteed.

Finally, it is also necessary to progressively increase the pistons' diameter until it reaches a value slightly higher than the cylinder's because, in this way, it will be possible to guarantee an adequate boundary sealing (elimination of gaps between boundaries) when it corresponds. This property will be useful mainly to block scavenging and exhaust ports with the pistons at certain instants of time, avoiding fluid from entering and exiting the cylinder volume.

After establishing all the previously mentioned information, the boundaries for each piston and the final mesh for the CFD analysis result in:

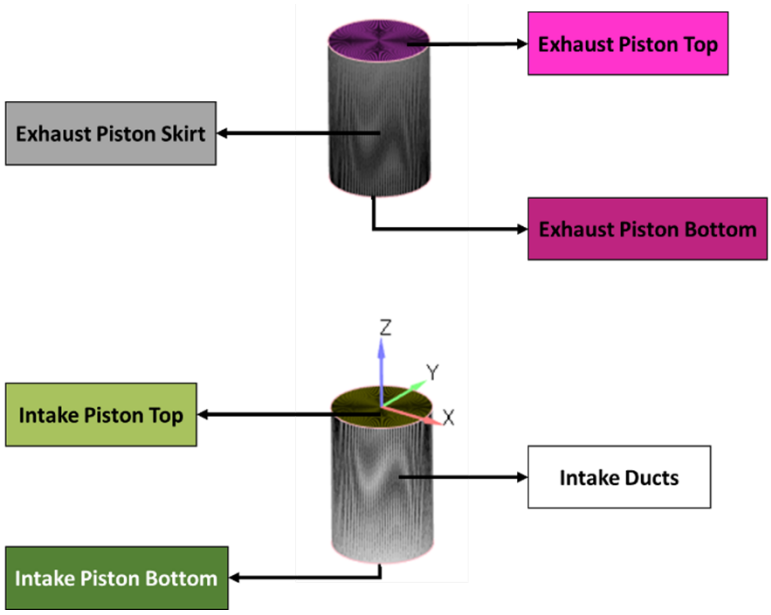

Figure 8: Isometric view of the boundaries present in the intake (bottom) and exhaust (top) pistons.

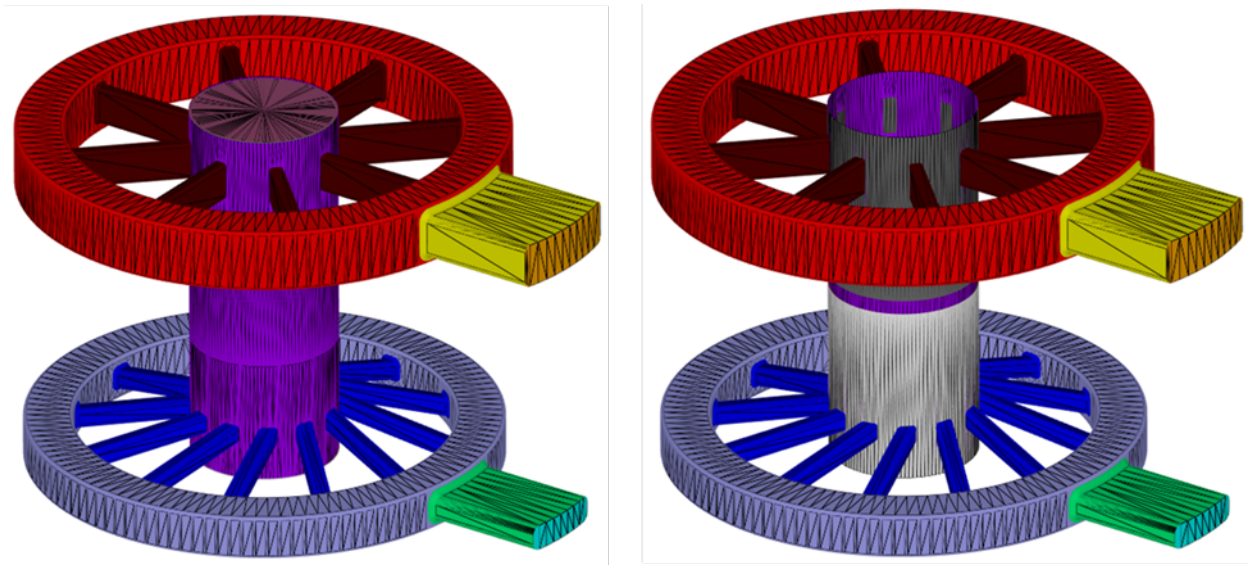

Figure 9: Isometric view of the computational mesh including the pistons at the bottom dead centre (left) and top dead centre (right).

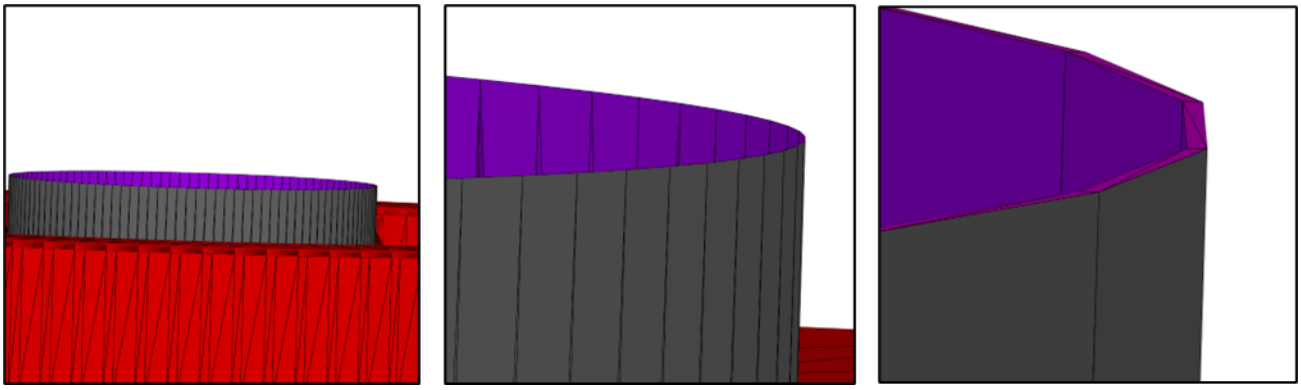

Figure 10: Zoom in to the upper end of the cylinder at the top dead centre to evidence that the cylinder is closed by the exhaust piston top. See Section 3.2.2 for the explanation.

3.2.2 Boundaries

Based on Figure 9, the boundaries in the system are already clearly separated one from each other, so the following step is to properly assign their corresponding **boundary conditions** which are unavoidably necessary to solve the reigning equations. The values of the different boundary conditions that will be shown are obtained based on a GT-Power model developed by CNR-STEMS which appeared to be a useful starting point for the current study. Throughout this section, the boundaries will be named following the denomination established in Figures 7 and 8.

To begin with, it should be mentioned that, in the whole domain, there is just **one INFLOW and one OUTFLOW** boundary types which are, respectively, **Intake and Exhaust** and, in both cases, **Dirichlet Boundary Conditions** are used based on, once again respectively, the scavenging and the exhaust results obtained by the GT-Power model; except for the **velocity** where **Neumann Boundary Conditions** are applied using the **Zero**

normal gradient approach that defines the velocity based on the pressure and the supersonic conditions. The values imposed to the formerly mentioned boundaries are evidenced in Table 4:

Parameter	**Intake**	**Exhaust**
Boundary Type	INFLOW	OUTFLOW
Pressure [bar]	2,53	1,92
Temperature [K]	368	542 (Backflow)

Table 4: Boundary conditions for Intake and Exhaust boundaries.

The remaining boundaries are all of the **WALL** type and follow the **Law of wall**, but the difference between them is the **velocity** boundary condition. On the one hand, there are the **Stationary and FIXED** boundaries that represent those parts of the system which remain static along the cycles. In all of the cases, the **temperature** boundary condition will be of the **Dirichlet** type basing on the scavenging, cylinder wall, piston wall and exhaust results obtained by CNR-STEMS. Similarly as in the previous paragraph, the corresponding temperature values can be observed in Table 5:

Boundary	**Temperature [K]**
Intake Walls	368
Intake Collector	368
Intake Ducts	368
Cylinder	400
Exhaust Ducts	542
Exhaust Collector	542
Exhaust Walls	542
Intake Piston Bottom	550
Exhaust Piston Top	550

Table 5: Temperature boundary conditions for the fixed boundaries.

As it can be seen in Table 5, one end of each of the pistons is set as a fixed wall boundary. Although this might seem illogical due to the fact of knowing that the whole piston should move, it has a mathematical justification: instead of representing the pistons as cylinders moving inside the liner, they are modelled as cylinders that stretch in order to reach the top dead centre and then, contract until the bottom dead centre (this is the reason why, in Figure 9, at the bottom dead centre, both pistons are just a disc and at the top dead centre, they are shown as a longer cylinder). Under these conditions, the intake piston bottom and the exhaust piston top must remain fixed and the other respective piston boundaries move with respect to them. Consequently, with this approach it is possible to represent the pistons' movement in an alternative way that **reduces the total simulation time** because the pistons are at full length only at the top dead centre; in any other position, they have a shorter length, reducing the total domain and so, the total cell number.

On the other hand, the **Translating MOVING** boundaries are those that change their position during the cycles, that is to say, in the actual case of study, those boundaries that refer to the pistons, with the exceptions of the ones mentioned in the previous

paragraph. For the purpose of realism, in the **velocity** boundary condition, the motion of the pistons is not the one automatically generated by the software (sinusoidal function calculated using the conventional theory known for internal combustion engines) because, as the engine is of the free piston type, there is no connecting rod-crank mechanism and so, their associated dimensions needed for the position calculations are not present. Therefore, the position profile is obtained thanks to the GT-Power simulation (discrete steps in which the piston position is represented as a function of the crank angle degrees)[2], which evidences that the behaviour is not perfectly sinusoidal, but a deformed sinusoidal function that can be seen in Figure 11. Similarly to the Stationary and FIXED case, the **temperature** in these boundaries is defined using **Dirichlet boundary conditions**, basing on the piston temperature provided by CNR-STEMS which has a value of **550 °C**.

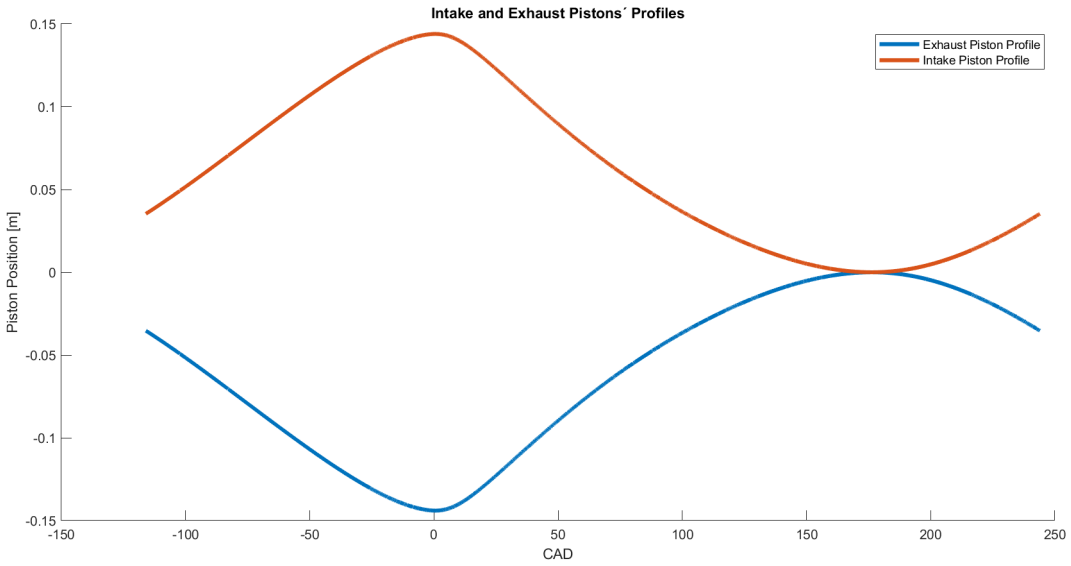

Figure 11: Intake and Exhaust Pistons´ Profiles. The 0 CAD position is when the intake piston top and exhaust piston bottom reach the top dead centre.

3.2.3 Regions, Initialization and Streams

Once all of the boundaries are completely defined, the following step is to setup the different regions in the domain. A region is a collection of boundaries where the initial conditions and events are set; and are useful also to report results in specific locations in the geometry, not just results for the whole of it.[12]

In the model, boundaries are grouped based on either which of them show to have the same initial conditions and/or which of them is of particular interest and hence, needs to be separated from the others. With these criteria, the regions in the model happen to be the following:

[2]Although it is known that talking about "crank angle degrees" might seem absurd for a free piston engine, it is just a reference variable calculated using the time step and the engine's angular speed.

Region	Boundaries
CYLINDER	Cylinder Intake Piston Top Intake Piston Bottom Exhaust Piston Bottom Exhaust Piston Top
INTAKE	Intake Intake Walls Intake Collector
EXHAUST	Exhaust Exhaust Walls Exhaust Collector
EXHAUST DUCTS	Exhaust Ducts Exhaust Piston Skirt
INTAKE DUCTS	Intake Ducts Intake Piston Skirt

Table 6: The regions defined and the boundaries that compose them.

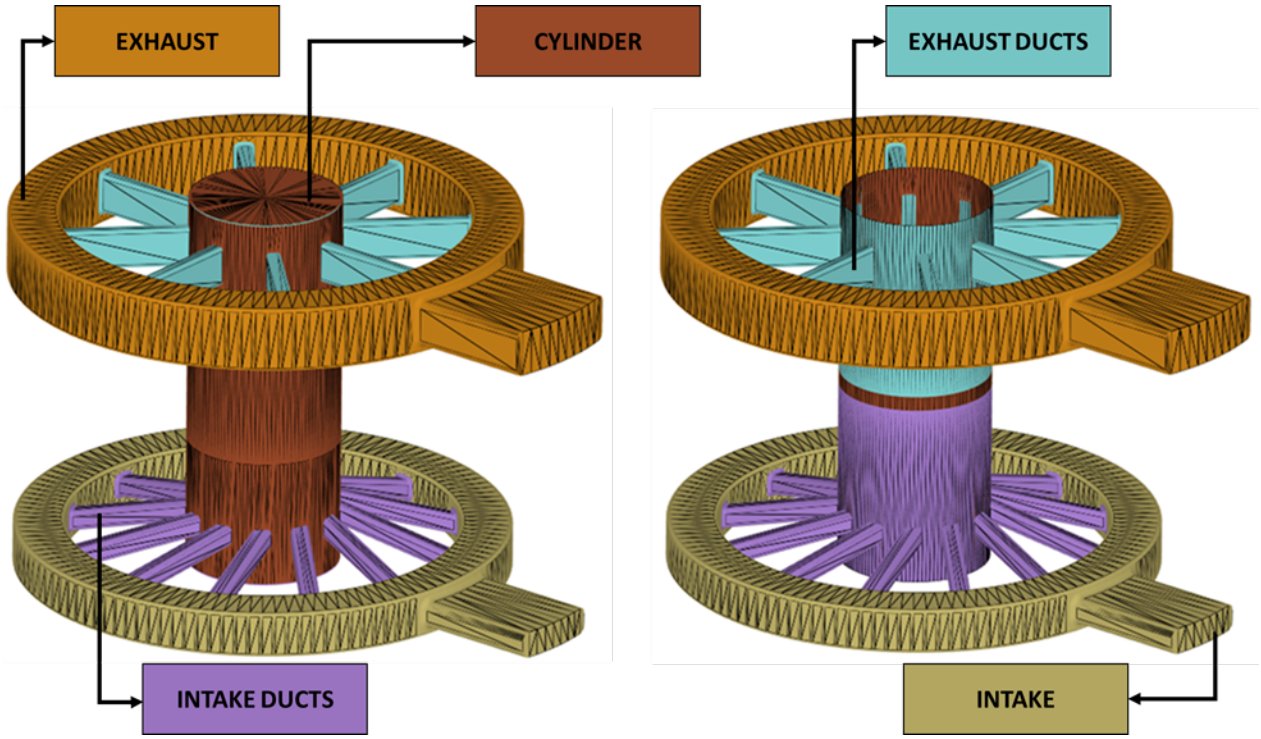

Figure 12: Isometric view of the regions present in the domain at the bottom dead centre (left) and top dead centre (right).

It must be mentioned that the Intake Piston Top and Exhaust Piston Bottom boundaries were chosen as part of the cylinder region because, although they do not physically belong to the cylinder, from the simulation point of view, they are the boundaries that enable the

closing of the cylinder at both ends. Additionally, the Exhaust and Intake Piston Skirts are assigned, respectively, to the EXHAUST DUCTS and INTAKE DUCTS regions because they are only involved in the fluid domain when they avoid the flow into the cylinder by blocking the ports, so, it appears reasonable to give the skirts the same properties as the regions to which they link when they interact with the fluid domain.

The following step consists in performing the initialization of each region, in other words, establishing the velocity, temperature, pressure and species at the very beginning of the simulation. The program will run **starting just before the exhaust valve opening at 80 CAD**[3] and will finish **at the top dead centre (360 CAD)**. This information is useful because it determines the initial conditions for the CYLINDER region: thanks to the GT-Power simulation, it is possible to obtain the profiles of different thermodynamic variables (see Figures 13 and 14) and with them, the values at a specific CAD, like for example, 80. For the remaining regions, the initial values selected are the same as those defined for the correspondent boundary conditions. All this information can be clearly visualized in Table 7[4].

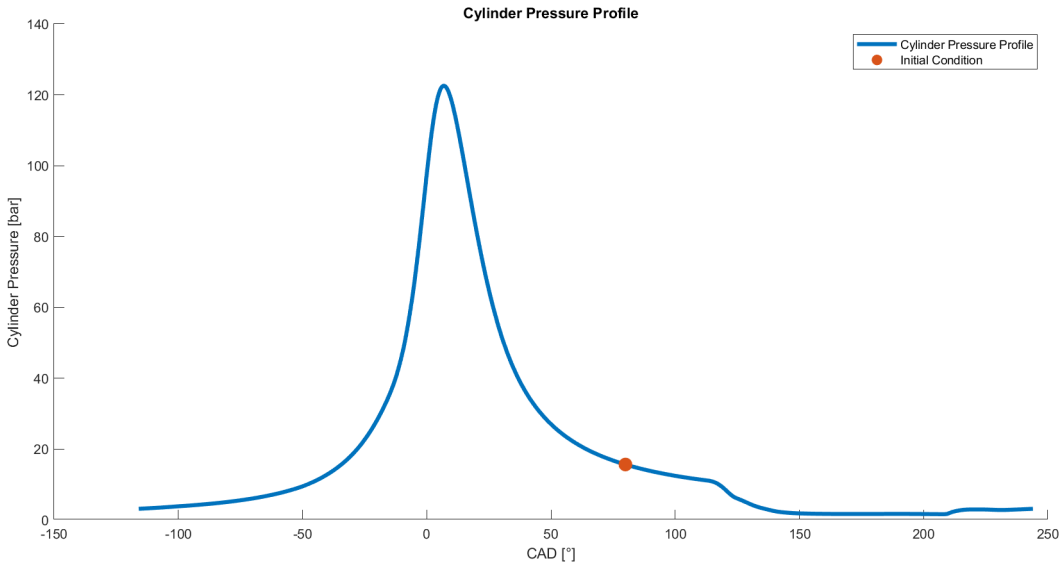

Figure 13: Cylinder pressure profile and initial pressure condition for the simulation.

[3]Crank angle degrees

[4]Species and passives are explained in section 3.2.4

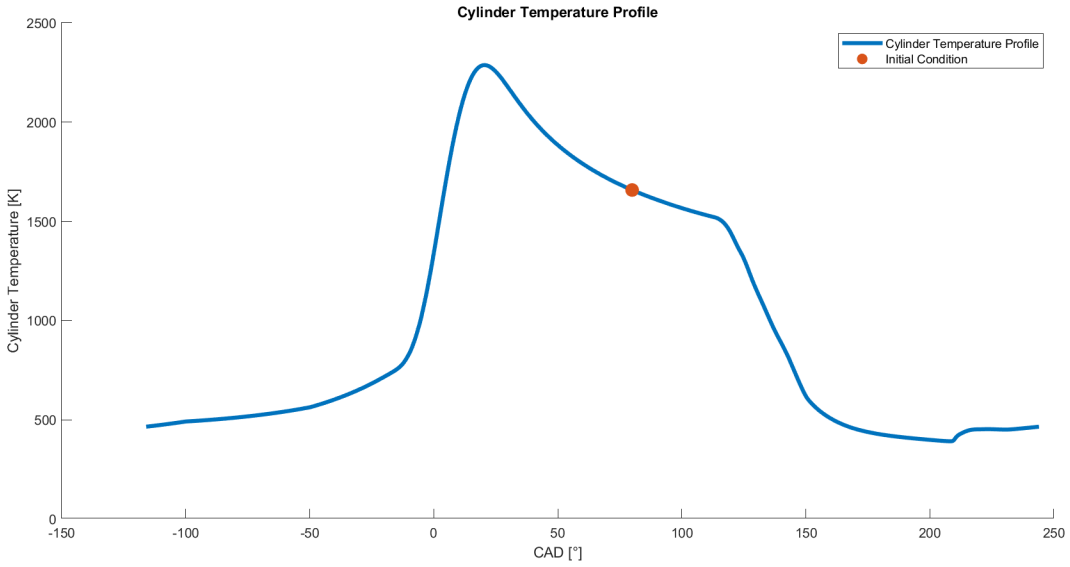

Figure 14: Cylinder temperature profile and initial temperature condition for the simulation.

Region	CYLINDER	INTAKE	EXHAUST	INTAKE DUCTS	EXHAUST DUCTS
Temperature [K]	1658,17	368	542	368	542
Pressure [bar]	15,67	2,53	1,92	2,53	1,92
Species	AIR (Mass fraction = 1)				
Passive (INTAKE)	0	1	0	1	0

Table 7: Parameter definition in each region.

Lastly, it is necessary to highlight the fact that **all of the regions previously mentioned share the same stream** because the same fluid flow crosses all of the regions during each cycle.

3.2.4 Events and Species

Having the boundaries and the regions fully determined, the following step is to define the events that occur during each engine cycle. In this particular case, the only event that needs to be established is the **permanent** connection between the corresponding regions in order to always enable the fluid flow between regions (so it is a so-called **open event**), only interrupted when the pistons' skirt is placed in a way that blocks the scavenging and exhaust ports. Therefore, the region connection in the model, following the denomination from Table 6, results being the one shown in Table 8 where the "Source Region" refers to the one that sends the flow to the "Sink Region" that receives it:

Source Region	Sink Region
INTAKE	INTAKE DUCTS
INTAKE DUCTS	CYLINDER
CYLINDER	EXHAUST DUCTS
EXHAUST DUCTS	EXHAUST

Table 8: Permanently open connections between regions

Additionally, as the main goal of this study is to provide a proper characterization of the gas filling of the engine, it must be mentioned the fact that this will be done by just considering **air** as the only fluid moving inside the control volume. To speed up the solver, instead of studying each of the air species separately, it is defined a **composite gas species** which is called **"AIR"** and is composed by **23,3% (mass fraction) of O_2 and 76,7% of N_2**; this composite species allows the study of the air fluid as a whole, accelerating the equation solving process, and then, if necessary, it is also possible to see the effects on each of the base species that define AIR.

Finally, in order to be able to study the scavenging efficiency, it is necessary to keep track of the fluid that enters at the Intake boundary. Therefore, it is required to define a **passive species** called **"INTAKE"** which does not influence the final results, but just permits to observe how the gases that enter at the intake distribute along the control volume throughout the cycles. Based on this information, it is reasonable to set the **value** of this passive species as **1** at the Intake boundary and **0** at the Exhaust boundary because all of it enters through the Intake port, none of it is received as backflow at the Exhaust port.

3.2.5 Time Step

As the simulation studies the transient behaviour of the engine, it is necessary to define the criterion to choose and control each time step at which results are computed. Considering that there are different mathematical and physical conditions that affect the selection of the time step, it does not seem reasonable to choose a fixed one, but a **variable** one: two consecutive steps could not be equal if they are not defined by the same cause. In this way, the **initial time step** of the simulation is the only one **user-imposed** and, after some of these steps, the software automatically develops certain calculations, based on physical and mathematical criteria, and defines the maximum time step that complies with all the restrictions imposed by them.[12]

Apart from the initial time step, the user must define the maximum and minimum possible time step that are used by the software to validate if the results obtained enter or not in a reasonable range. On the one hand, the minimum time step is relevant because if the time step applied was too small, the simulation would take an uselessly long time until it finds the required results. On the other hand, if the time step was too large, the accuracy and stability of results would be affected, so it is necessary to define a maximum time step. Accordingly, based on Converge Manual reccomendations, the following values are decided for the model [12]:

- Initial Time Step: 10^{-6} **s**
- Maximum Time Step: 10^{-5} **s**

- Minimum Time Step: 10^{-7} **s**

3.3 CFD Model Verification

All of the previously mentioned conditions conform the starting point for the actual CFD analysis of the opposed-pistons engine. The following steps consist in verifying that the mesh and the different settings are able to produce sufficiently trustworthy results. This is done by running a number of simulation changing different properties of the model and revising the effects on the overall results.

As it was mentioned before, **all of the simulations start just before opening of the exhaust valve at 80 CAD and finish at 360 CAD (top dead centre)** and the reason for this is the fact that **combustion is not modelled** throughout this study. Therefore, the simulation does not obtain combustion results, but uses the ones obtained via GT-Power to initialize the regions; and it finishes when the first cycle reaches the top dead centre because if it went further, the simulation would not be trustworthy because combustion should occur.

3.3.1 Grid Verification

The decision of the **base grid size** should consider the fact of not choosing an extremely coarse grid that causes results with insufficient precision nor an exaggeratedly fine mesh because, in this case, the time needed to solve the simulation would be uselessly long. Consequently, the value selected for the base grid size **in all the directions** is **4 mm** which is selected as a reasonable size considering that the base dimensions of the geometry exposed in Tables 1 to 3 are one or two orders of magnitude higher than this value.

Although the base grid size is a fundamental part of the mesh definition, another aspect of high relevance is the **fixed embedding** definition. The fixed embedding consists in applying a grid refinement on certain specific positions at certain specific interval of CAD in order to increase the precision of the results found only at those positions and only during the previously mentioned interval.[12] In the domain studied, different embeddings were defined in order to precisely analyse different processes and properties; all of them are explained next:

- **Cylinder**: This embedding is **permanently** active, considers the whole cylinder volume from end to end and is set in order to study and assess with adequate precision the different processes that occur inside of the cylinder.

- **Boundary**: In a similar way, this is also a **permanent** embedding defined along the cylinder, but, in this case, it is a superficial type of embedding that just refines a certain amount of layers nearby the lateral cylinder walls to properly represent the boundary layer generated there, its effects in the flow and, afterwards, in the combustion.

- **Region - Intake**: This **cyclic** embedding is activated at the INTAKE and INTAKE DUCTS regions when the simulation reaches the 85 CAD and until the 255 CAD, that is to say, from the scavenging ports opening until their closing, so as to properly study the scavenging process in the regions that influence the most this process.

- **Region - Exhaust**: As an analogous condition, there is a **cyclic** embedding set at the EXHAUST and EXHAUST DUCTS regions that refines the grid in a CAD interval between 80 and 265, in other words, since the exhaust ports open until they close, in order to properly analyze the gas outflow process in the corresponding regions where this happens.

In each of the cases, it is necessary to define the **scale** of the embedding because it is the property that enables the refinement of the grid: if the scale is "n", the embedding will divide the cell base grid size by 2^n. Apart from the scale, an important aspect, just for the boundary embedding, is the amount of **layers** at which this type of embedding will be applied in the cylinder wall.[12]

In this preliminary mesh analysis, different scales and number of layers will be tested until the adequate values are obtained. A **non hydrodynamic** type of simulation is launched in order to evaluate if the generated mesh is appropriate or not for the actual study. This kind of simulation runs the problem during the same CAD interval as in a conventional hydrodynamic simulation, but it deactivates any physical and thermodynamic process present because, in this way, it is possible to test if the actual grid is able to adapt itself and represent properly the situation of concern. An appropriate mesh will be the one that has a reasonable number of cells together with a relatively low wall time (time required to solve each CAD step).[12]

3.3.2 Sealing Failure Solution

With the mesh verification completed, the following step is to launch the hydrodynamic simulation. The first idea of this step was to test and optimize different parameters regarding the grid and the temporal analysis, but an unexpected problem appeared: a sealing failure occurred as the pistons approached the bottom dead centre.

As it was exposed in Section 3.2.1, sealing should be directly guaranteed by the fact that the pistons have a higher diameter than the cylinder and so, by enabling the triangle intersection, no fluid flow through any cavity blocked by the piston skirt is allowed. Therefore, detailed analysis of the pistons' grids and their intersections with the cylinder is developed in order to identify why there is a sealing problem generated if the volume design is correct.

Once the problem is identified, it will be fixed and a new simulation will be launched. **If the new simulation is able to reach the 360 CAD, then it is considered that the sealing problem has been solved**.

3.3.3 Simulation Running Time: AMR, CFL number and time step

After confirming the fact of having a completely functional simulation, the following step is to modify its settings to have it running during a reasonable period of time: neither too short because it would imply lack of precision in the final results; nor too long because because it would not be efficient for post-processing and for launching further simulations. Considering the fact that **just 280 CAD** (starting at 80 until 360) are simulated and that in **further simulations complexity will increase** because the **combustion model** will

be added, it is decided that a **reasonable running time** should be solving around **100 CAD per day**[5] for this kind of simulation.

To control the velocity of the simulation to solve the whole transient problem in the indicated CAD range, there are three parameters that will be edited: **the Adaptive Mesh Refinement (AMR), the Courant–Friedrichs–Lewy (CFL) number; and the maximum time step (see Section 3.2.5)**.

Adaptive Mesh Refinement (AMR)

The Adaptive Mesh Refinement (AMR) consists in refining the grid at certain locations when a certain variable surpasses certain value. In this way, it is possible to study complex phenomena by increasing the precision of the results only at certain specific positions based on a physical property of interest.[12]

Throughout the simulations, it is always set the **type** of AMR as **sub-grid scale (SGS) based**, that is to say, the embedding associated to the AMR is activated when the gradient of the specified field ("sub-grid field") is the highest. As in this study only gas filling is analysed, the most reasonable field to define as the one that controls the AMR is the **velocity** because it is the one that permits the proper study of scavenging and exhaust; and because other fields, like temperature and pressure, are more relevant and influential in what regards to combustion. Additionally, as the gas filling should be tracked along all the geometry, it is decided that **the AMR can be activated in all of the regions** (see Figure 12), and, as it is known that the most critical velocity values will occur when the scavenging and exhaust ports open and close, due to the eventual reduction of the flow area, the **grid is set to refine between 80 CAD and 265 CAD ("Cyclic AMR")**, that is to say, **from the exhaust ports opening until their closing** (that also includes the opening and closing of the scavenging ports).

The remaining Adaptive Mesh Refinement settings are the ones actually used to control the running time of the simulation. To begin with, one fundamental aspect is to determine the **maximum embedding level** which has exactly the same definition as the "scale" seen in Section 3.3.1, so its value affects the grid refinement, the precision of the results and the computational time. In second place, it should be established the **sub-grid criterion** for the velocity which is the absolute value of the velocity gradient above which embedding is activated in a cell and is defined as a percentage of the actual velocity in the cell. The higher the value of the sub-grid criterion, the lower the strictness of the AMR activation, that is to say, lower number of cells are being embedded, causing lower precision and computational time. To define the sub-grid criterion, CONVERGE recommends values between **0,1% and 10%** to obtain reasonable results.[12]

As a last remark, the **maximum cell number** is a way to limit the quantity of cells present in the grid so as to avoid generating an extremely refined mesh that increases

[5]In this writing, the amount of CAD per day are referred to a 12 cores case. It is known that, with a higher amount of cores, the CAD solved per day increases almost linearly (the behaviour is not perfectly linear because there is also the influence of the waiting time between cores).

absurdly the computational time. In case the maximum cell number is reached because there is a large number of cells that satisfy the sub-grid criteria, the software will automatically adapt all the criteria, making them less strict and reducing the number of cells affected by the AMR until the maximum limit is obtained; in other words, the number of cells that will suffer the embedding will be lower and will be only those with the highest velocity gradients.[12]

Courant–Friedrichs–Lewy (CFL) Number

The Courant–Friedrichs–Lewy (CFL) Number[6] is an adimensional coefficient that is useful to define the time steps (and so the CAD step) at which the CONVERGE solves the equations that govern the case of analysis. By definition, the CFL number is:

$$CFL = u \cdot \frac{\Delta t}{\Delta x} \tag{2}$$

where "u" is the speed at that cell; Δt the time step; and Δx the ratio between the cell volume and the cell's projected area in the most restrictive direction between CONVERGE's x,y and z axes.

Considering a case in which the CFL is the time step limiter (see Section 3.2.5), by looking at equation 2, it is evident that, as Δx is a parameter imposed by the mesh and u a result determined by the physical conditions of the problem, the value of Δt can be controlled in a proportional way by changing the value of CFL. In order to provide, stable and precise results with a reasonable time step, CONVERGE recommends to keep the CFL number in a **range between 0,5 and 3**.

3.4 CFD Model Simulation: Thermodynamic Study

In the actual condition, the model is completely defined and trustworthy results are guaranteed, so the remaining step is to launch simulations and analyse the results.

In first place, tridimensional graphs of the control volume at different CAD steps are obtained in order to evidence how the different fields evolve in time inside the engine. With this information, it is expected to derive certain conclusions about the effectiveness of the model to represent the gas filling (mainly scavenging and exhaust) inside the engine. The main fields that are evaluated are:

- Air mass
- Velocity Magnitude
- INTAKE passive species concentration

[6]Throughout this work, when the "CFL Number" is mentioned, it is always referred to what CONVERGE calls "Convection CFL".

The air mass is useful to characterize the gas filling inside the cylinder; the velocity magnitude helps to analyse if the gas movement throughout the volume is reasonable; and INTAKE enables the visualization of the trace of the gas as it enters the volume and how its quantity evolves during the cycle.

Moreover, there are some parameters related to the engine design and testing that are computed in order to verify if the engine's behaviour is logical from a thermodynamic point of view:

- **The Scavenge Ratio ("SR") and the Delivery Ratio ("DR")**: used to characterize the scavenging process because, as the only fluid in the inflowing charge is air, they represent up to what extent the atmospheric mass has been supplied to the engine during scavenging.
- **The Scavenging Efficiency ("SE")**: establishes how much of the total mass that remains after the exhaust closes corresponds to the air (INTAKE passive in the simulation) trapped in the cylinder after scavenging. In this case, an adapted definition is studied because, once again, the charge is composed just by air; the unburnt air mass refers to the mass that was inside of the cylinder before the INTAKE passive entered; and because no exhaust gas mass is considered due to the fact that no combustion is simulated.
- **The Trapping Efficiency ("TE")**: relates the trapped mass of air (INTAKE passive in the simulation) to the total amount that entered the cylinder during scavenging.
- **The Charging Efficiency ("CE")**: compares the actual engine gas filling with air with respect to the ideal one.

For all of them, there is a mathematical expression associated which can be seen below:

$$DR = \frac{m_{as}}{m_{dref}} = \frac{m_{as}}{\rho_{at} \cdot V_{sv}} = \frac{m_{as}}{\frac{p_{at}}{R_a \cdot T_{at}} \cdot V_{sv}} \tag{3}$$

$$SR = \frac{m_{as}}{m_{sref}} = \frac{m_{as}}{\rho_{at} \cdot (V_{sv} + V_{cv})} = \frac{m_{as}}{\frac{p_{at}}{R_a \cdot T_{at}} \cdot (V_{sv} + V_{cv})} \tag{4}$$

$$SE = \frac{m_{tas}}{m_{tr}} = \frac{m_{tas}}{m_{tas} + m_{ar}} \tag{5}$$

$$TE = \frac{m_{tas}}{m_{as}} \tag{6}$$

$$CE = \frac{m_{tas}}{m_{sref}} \tag{7}$$

where "m_{as}" is the mass of fresh charge supplied during scavenging; "p_{at}" the atmospheric pressure (equal to 101,325 kPa); "T_{at}" is the atmospheric pressure (equal to 293 K); "R_a" is the gas constant for air (equal to 287 $\frac{J}{kg \cdot K}$); "V_{sv}" is the swept volume; "V_{cv}" is the clearance volume; "m_{tas}" is the mass of fresh charge trapped; and "m_{ar}" is the mass of air that remains from a previous cycle.[7]

.

Finally, some plots of different parameters versus the CAD are also studied to determine if the situation represented by the CFD model is in correspondence with the GT-Power model developed by CNR-STEMS. This kind of plots also enable to visualize the evolution of different thermodynamic parameters during the cycle studied and conclude if that evolution follows an expected trend or not.

4 Results and Discussion

With the methodology already defined, the following step is to properly apply it to obtain the corresponding results and evaluate the model. In the following sections, different simulations will be studied and their results will be analysed in order to derive varied conclusions with the final objective of reaching a trustworthy model able to represent the gas filling in an opposed-pistons engine.

4.1 Grid Verification

To begin with the mesh verification, the starting point for the fixed embedding is defined as follows:

- Scale for all of the embeddings except the boundary: 2
- Scale for the boundary embedding: 3
- Number of layers of boundary embedding: 4

With these parameters already set, the non-hydrodynamic simulation is executed and the following grid (which shows one colour for each region) is obtained during the different CAD intervals:

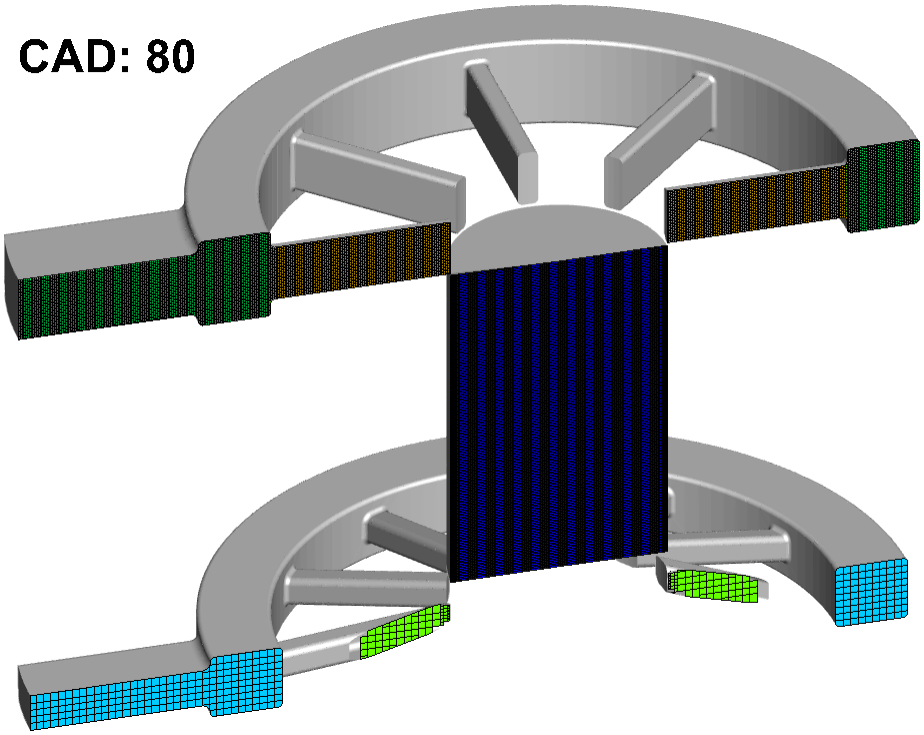

Figure 15: Slice showing the grid at 80 CAD (Region - Intake embedding still not activated).

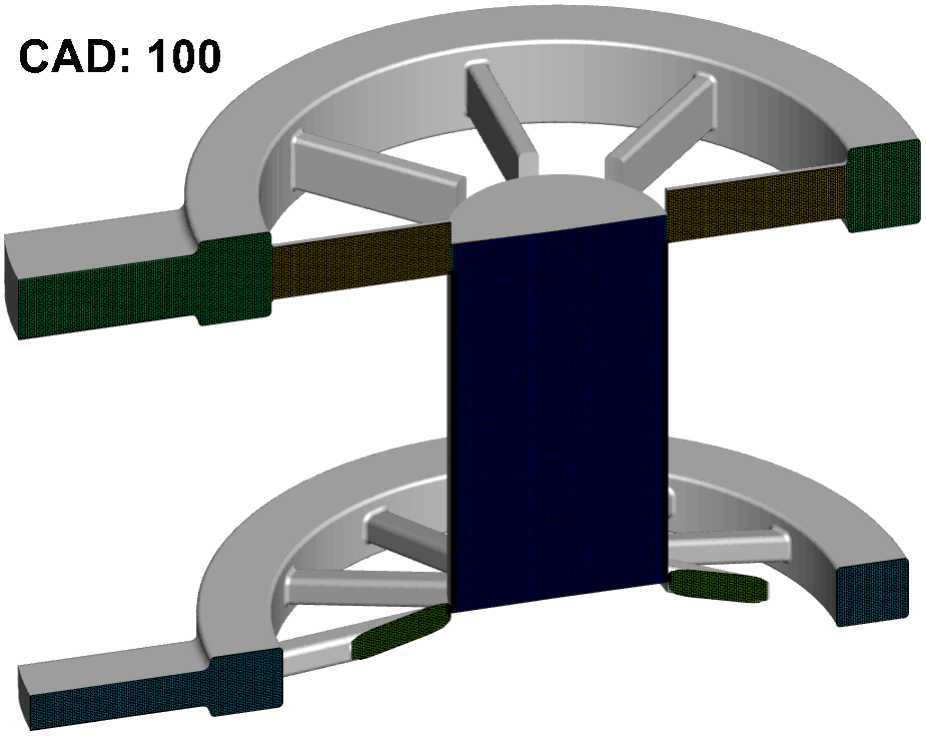

Figure 16: Slice showing the grid at 100 CAD (All of the embeddings activated).

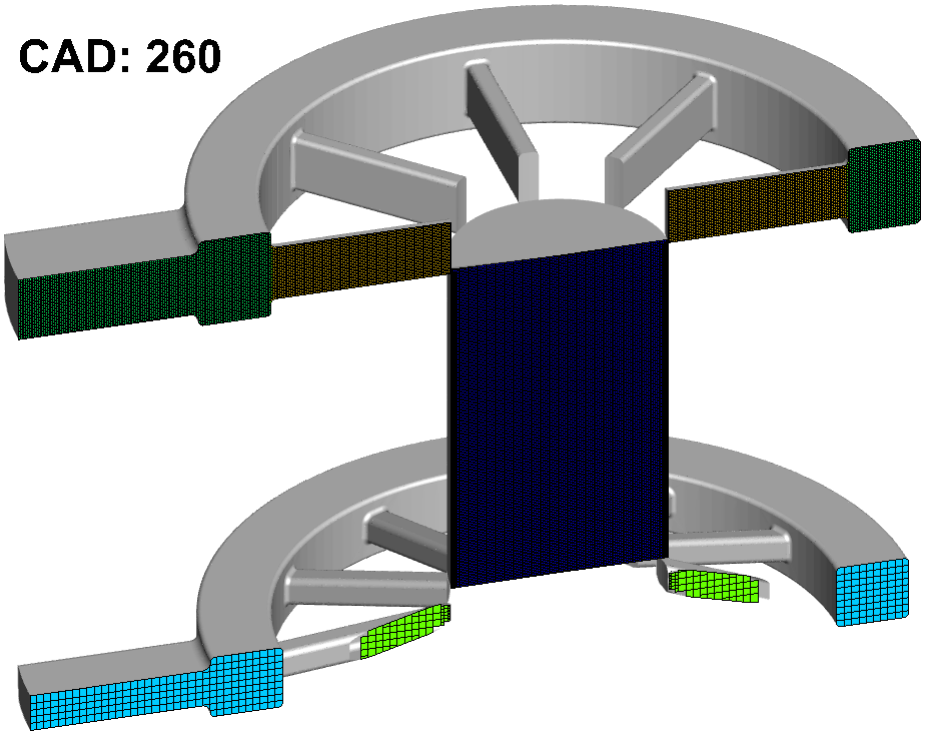

Figure 17: Slice showing the grid at 260 CAD (Region - Intake embedding deactivated).

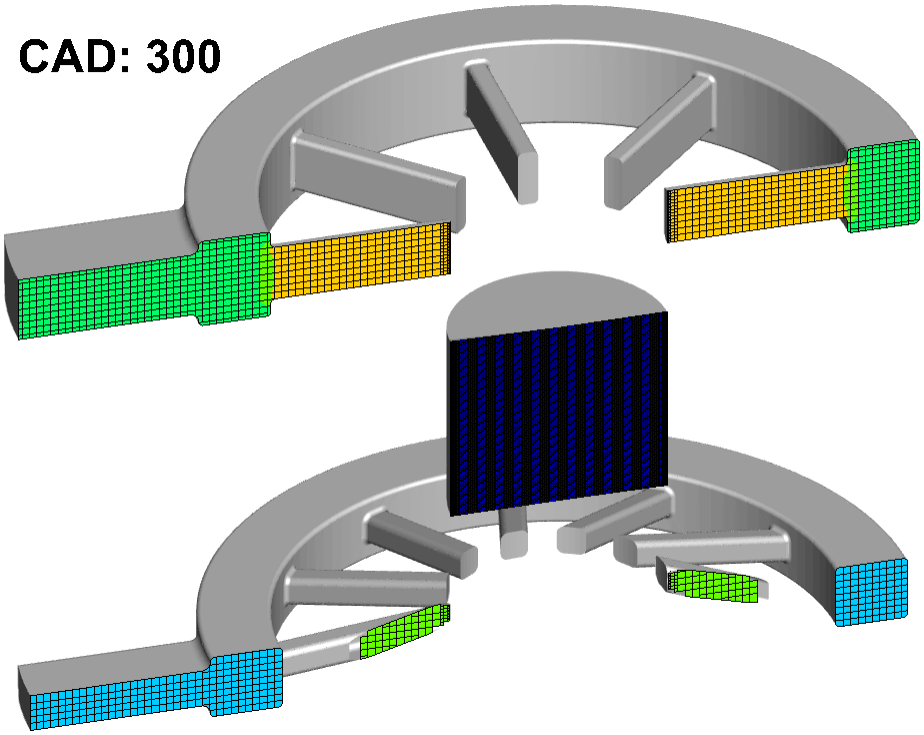

Figure 18: Slice showing the grid at 300 CAD (Region - Intake and Region - Exhaust embedding deactivated).

As a first consideration, as it can be seen in Figure 19, it is plotted the total number of cells in the domain as the crank angle varies. The domain shows to have a reasonable tendency to increase the number of cells until the BDC[7] and reduce the cell number as the TDC[8] is reached. Furthermore, three discontinuities are present in the number of cells at the positions illustrated in Figure 20 which are:

- **85 CAD**: after the exhaust already opened, but not yet the intake.
- **255,9 CAD**: after the intake closed, but not yet the exhaust.
- **266,7 CAD**: after the exhaust closed.

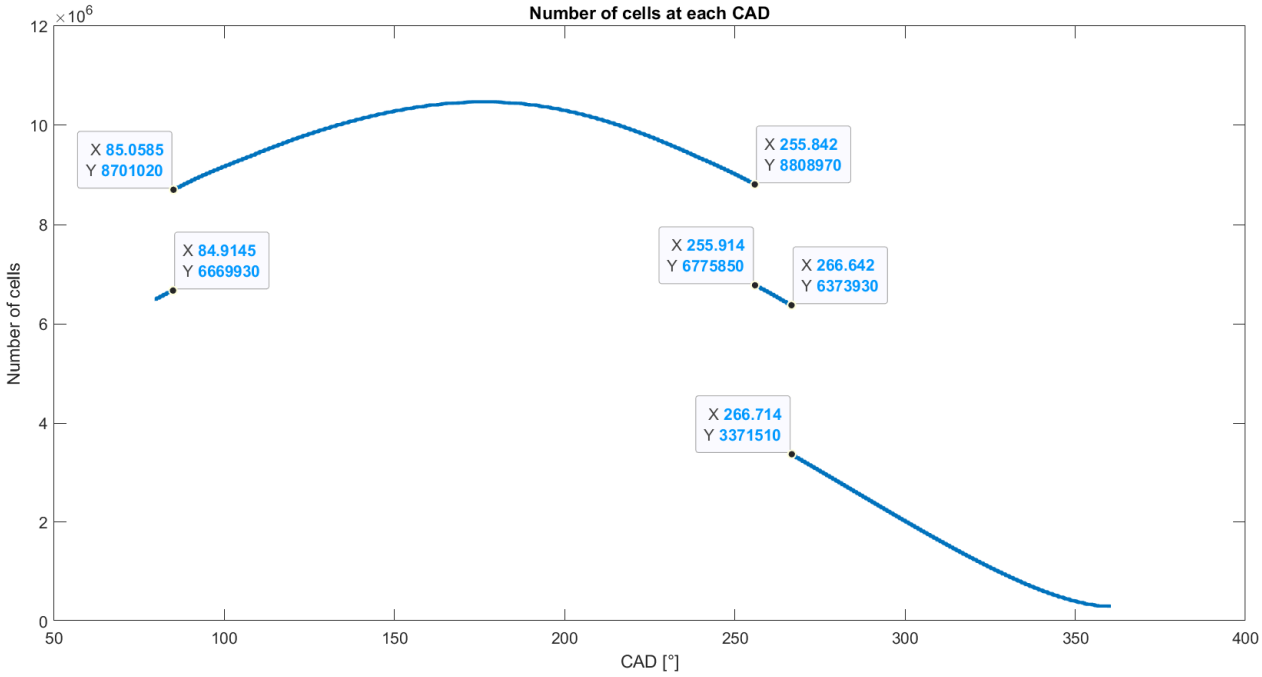

Figure 19: Total number of cells at each CAD.

[7]Bottom dead centre at 180 CAD.
[8]Top dead centre at 360 CAD.

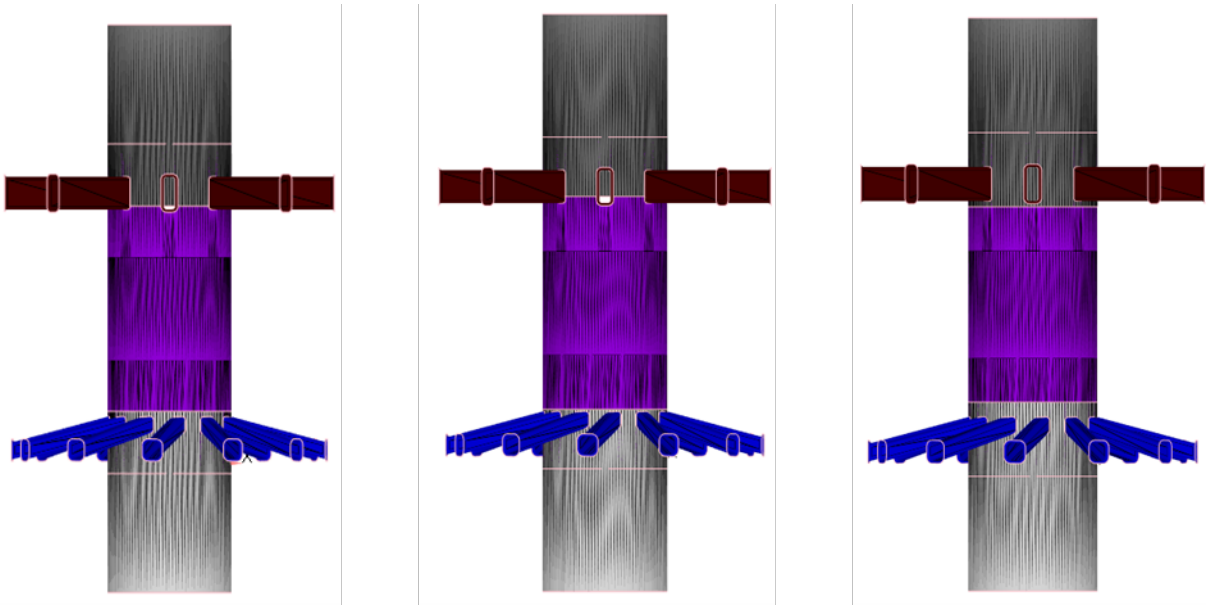

Figure 20: Pistons' position at (from left to right) 85°, 255.9° and 266.7°.

By analysing the cell number per region as the CAD increases (see Figure 21), it is shown that the shape of the curve from Figure 19 is mainly given by the CYLINDER region curve. In addition, the remaining regions have an almost piecewise constant cell number which has the consequence of generating the discontinuities in the figure previously mentioned:

- The discontinuity at 85 CAD is given by the INTAKE and the INTAKE DUCTS regions.
- Similarly, the same happens with the discontinuity at 255,9 CAD.
- With respect to the discontinuity at 266,7 CAD, it is a consequence of the discontinuity at the EXHAUST and EXHAUST DUCTS regions.

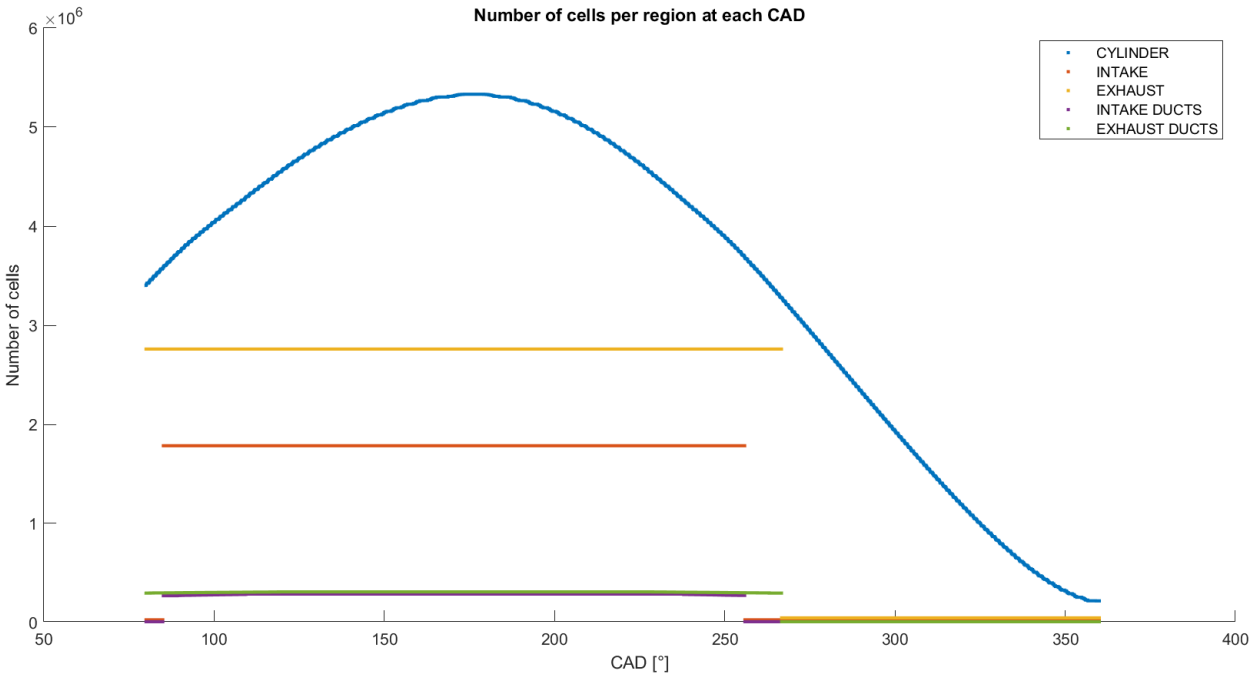

Figure 21: Number of cells per region at each CAD.

Lastly, it is plotted in Figure 22 the time required to compute the results at each angle step. It is shown that (neglecting dispersions) the values remain around 20 and 40 seconds and, as the piston approaches the BDC, the time gets reduced to between 15 and 20 seconds. These values remain (showing the previously mentioned discontinuities) until both ports close and once this happens, the solving time starts to reduce from 15 seconds until 2 seconds.

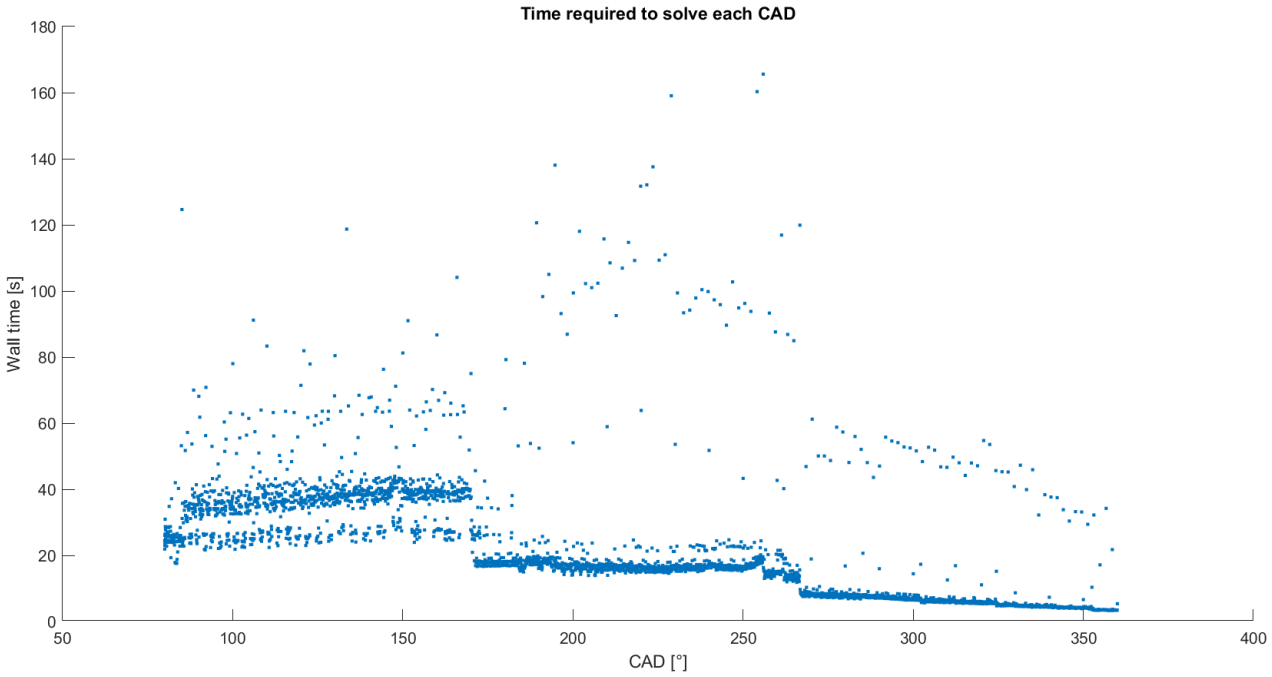

Figure 22: Time required to solve each CAD.

By analysing Figures 19 to 22, it is reasonable to conclude that the grid requires certain modifications. The actual cell number (around 10^7) and time for solving each CAD (around 30 seconds) are relatively high considering that this analysis just evaluates the mesh and not any other thermodynamic property that might require some complex equation solving. Therefore, it is appropriate to conclude that it is necessary to resize the different parameters of the fixed embedding previously defined and the chosen values are the following ones:

- Scale for all of the embeddings except the boundary: 1
- Scale for the boundary embedding: 2
- Number of layers of boundary embedding: 3

Having established the previous values, the grid gets modified in this way:

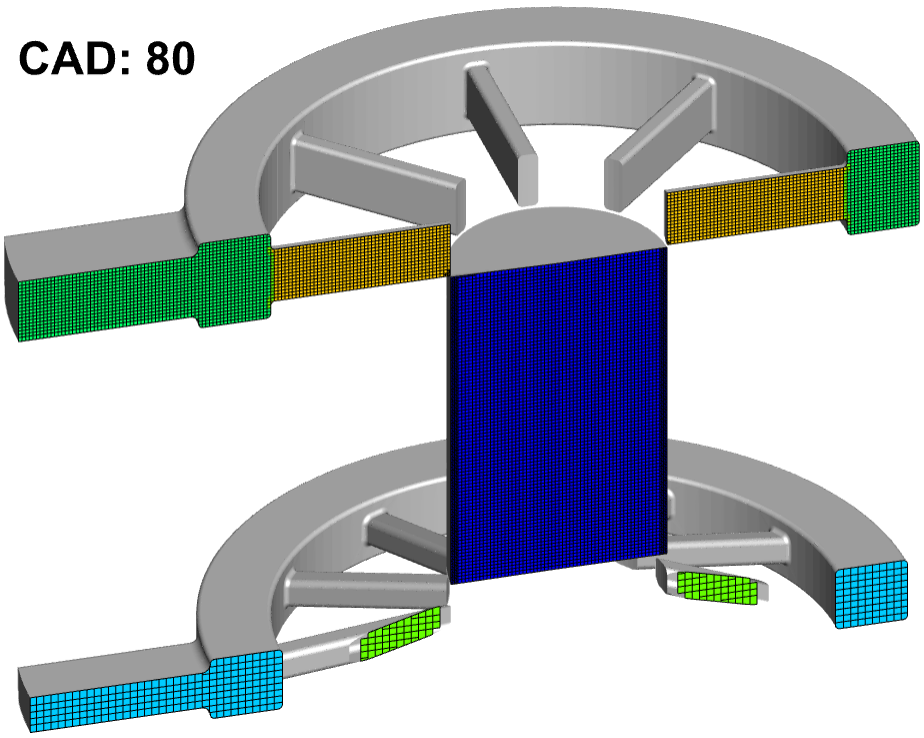

Figure 23: Slice showing the new grid at 80 CAD (Region - Intake embedding still not activated).

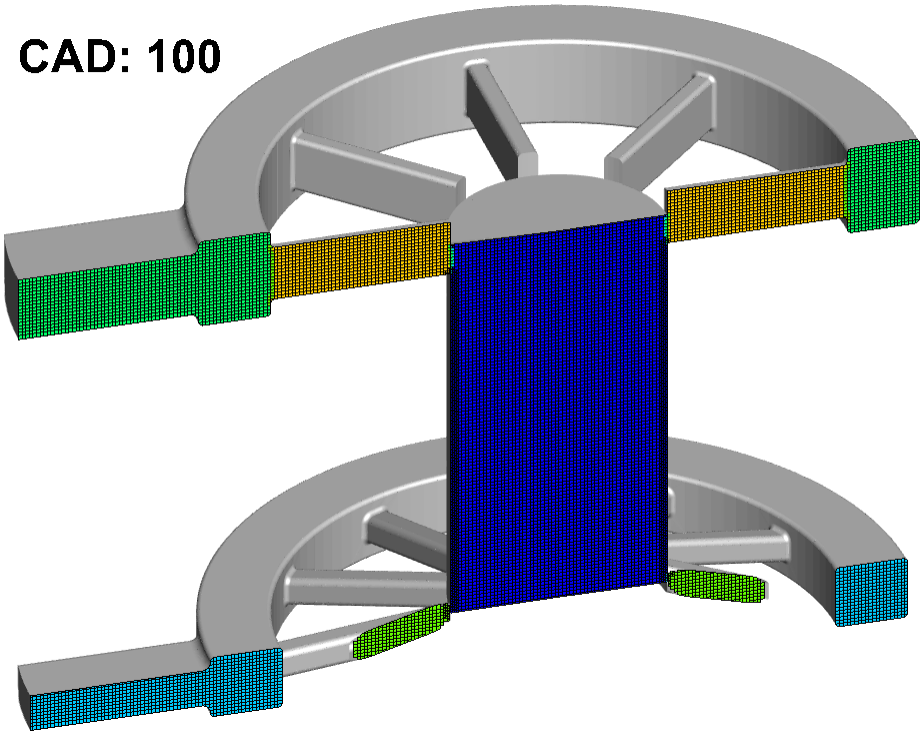

Figure 24: Slice showing the new grid at 100 CAD (All of the embeddings activated).

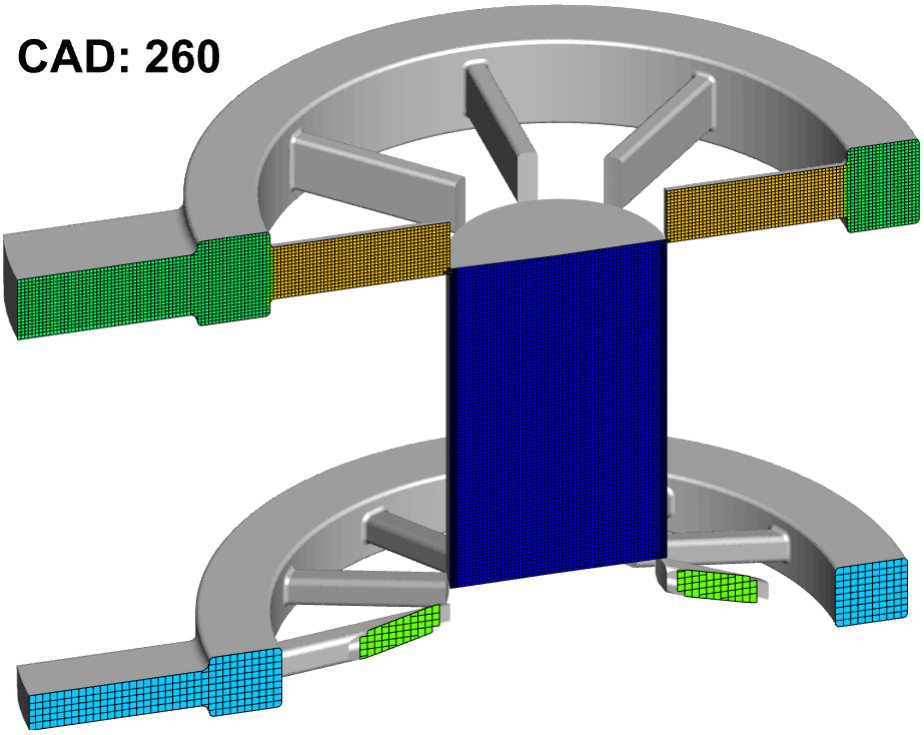

Figure 25: Slice showing the new grid at 260 CAD (Region - Intake embedding deactivated).

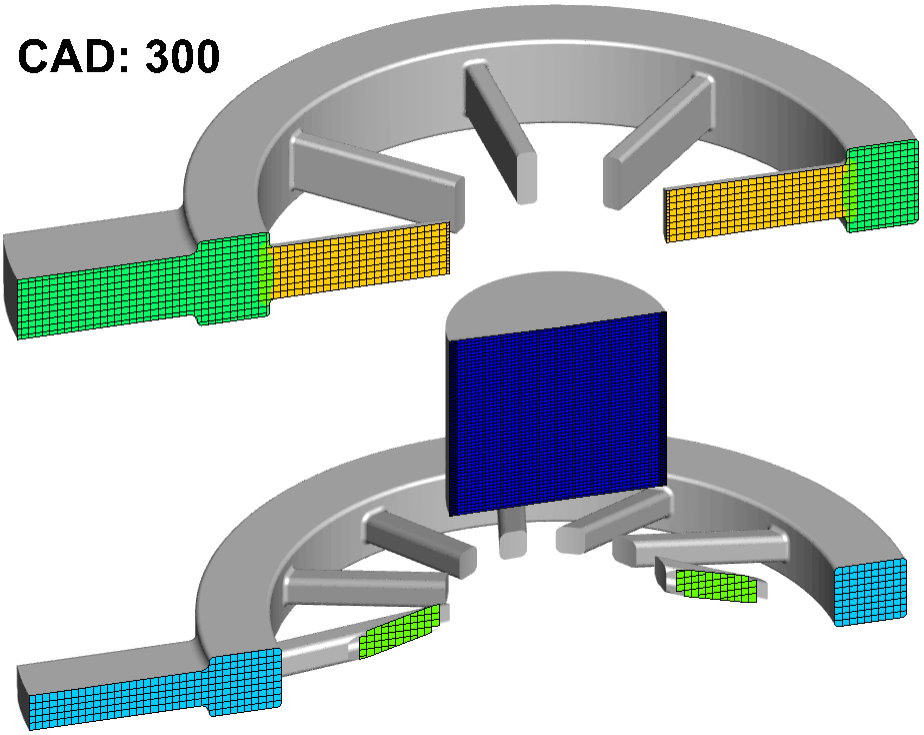

Figure 26: Slice showing the new grid at 300 CAD (Region - Intake and Region - Exhaust embedding deactivated).

Once again, in order to verify if the amount of cells has reached a reasonable value, the total amount of cells and the numbers of cells per region are plotted. It is clearly seen that

the discontinuities remain present in the same CAD values; this means that the simulations shown before and the ones shown below represent the same conditions. However, it is also evident in the following pictures that the number of cells has decreased appreciably.

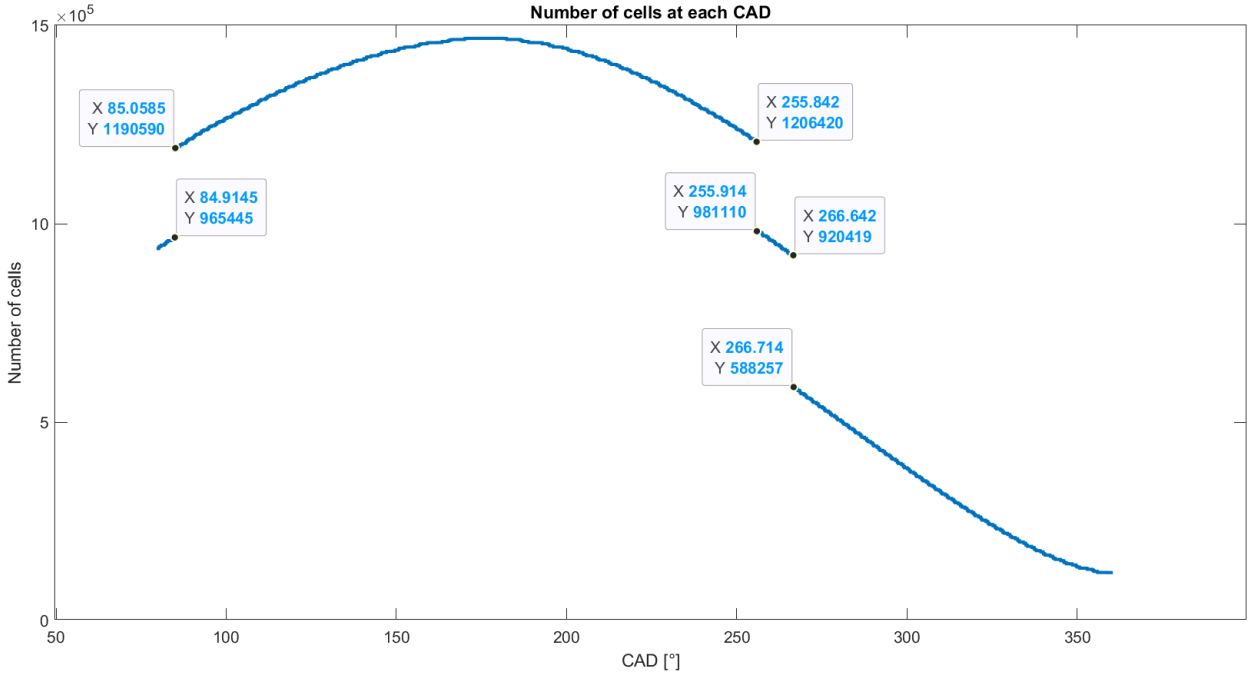

Figure 27: Total number of cells at each CAD.

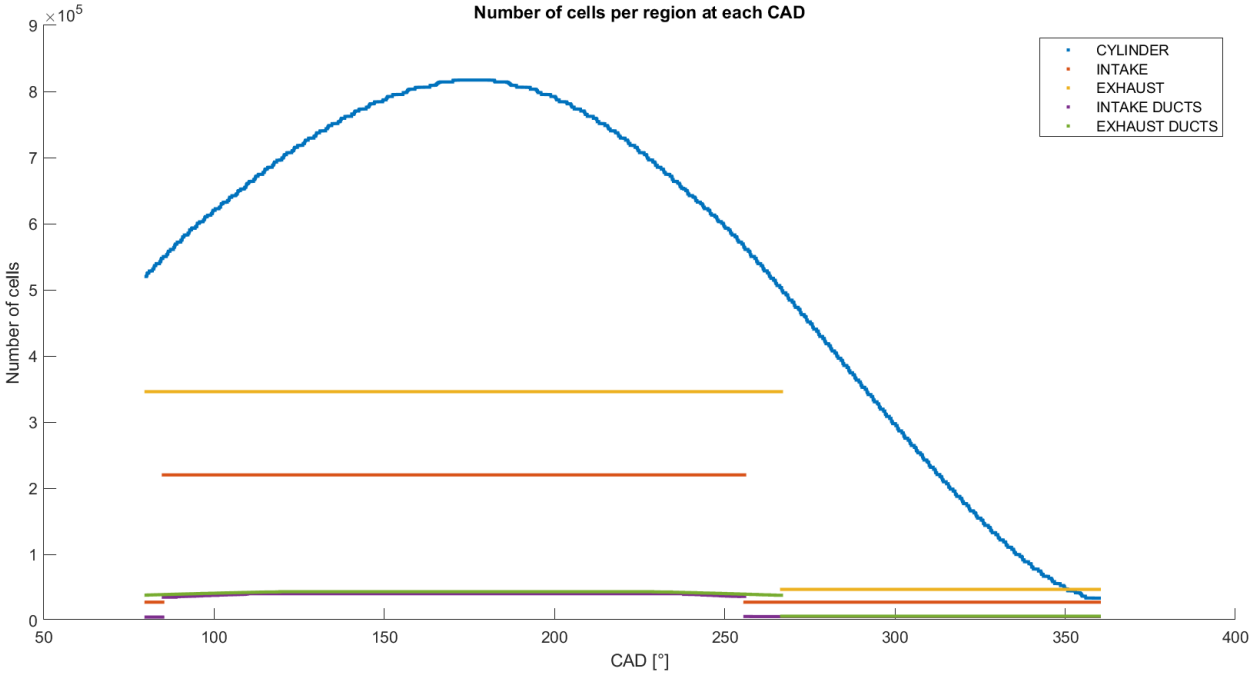

Figure 28: Number of cells per region at each CAD.

In a similar way as before, with the cell number already shown, it is now plotted the

wall time at each CAD and it has clearly presented a difference with respect to the previous conditions. It is shown that (neglecting dispersions) the values remain around 5 seconds with a decreasing trend as the piston moves to the BDC and then, when it returns to the TDC, the minimum value of around 2,5 seconds is reached.

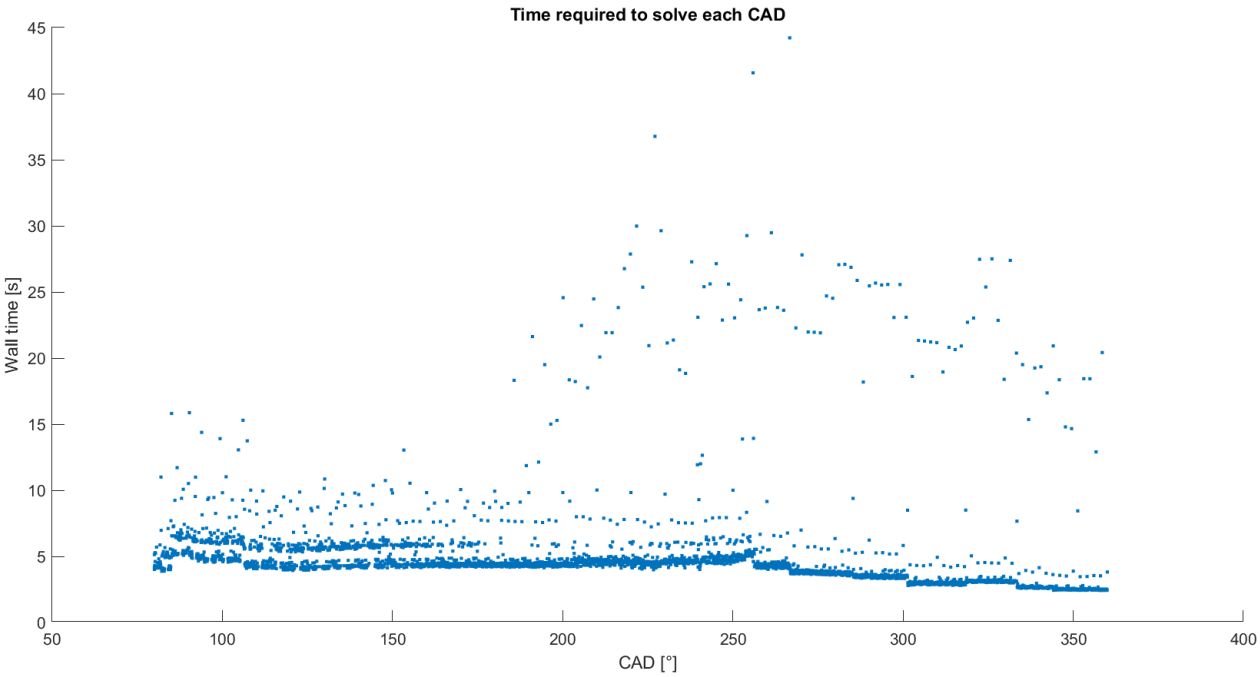

Figure 29: Time required to solve each CAD.

As a last remark of this last simulation, it must be mentioned that:

- **No recoveries**[9] were found, so no fatal errors or problems with the convergence of the iterations are detected
- **All of the time steps** are **one order of magnitude higher** than the minimum (see Section 3.2.5), obtaining results with adequate precision with low computational price.

In this new condition, the total cell number has shown to have decreased one full order of magnitude (from 10^7 to 10^6) and the time it takes to solve each crank angle degree is around 6 times less than in the previous simulation. Therefore, as the new condition shows to have generated satisfactory results for a non-hydrodynamic simulation, it is decided that **the conditions set for the fixed embedding in this last simulation will be the ones defined for testing the hydrodynamic simulation** in the following step of the project.

4.2 Sealing Failure Solution

After analyzing the whole grid, it is discovered the real cause of the sealing failure: **wrong piston triangulation.**

[9]If the iteration does not converge or a fatal error is detected, the software will try to solve the iteration once again but with half the value of the previous time step; this last situation is a "recovery". [12]

As it can be see in Figure 30, the piston triangulation is so regular that causes some edges of the triangles to be almost perfectly coincident with the cylinder's edges. In consequence, in this conditions, triangle intersection is not happening because there is an unwanted alignment between edges that avoids contiguous triangles to intersect and so, no intersection means inadequate sealing conditions.

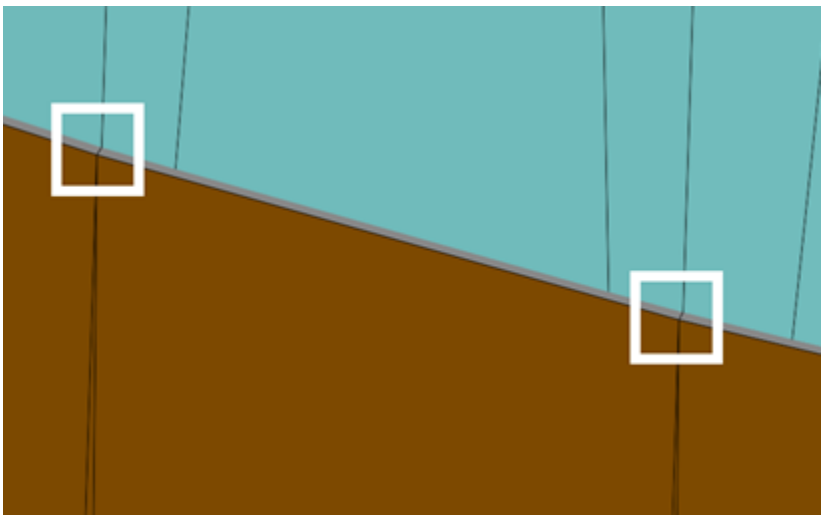

Figure 30: Initial triangulation. In grey, the Intake Piston Top; in brown, the Intake Piston Skirt; and in turquoise, the Cylinder

As a solution, it is evident that triangle intersection must be guaranteed, so what it is done is to generate a **random discretization** at the Intake Piston Top (and Exhaust Piston Bottom too) in order to reduce the probabilities of generating a grid that has edges aligned with the cylinder's. If the probabilities of coincidence between edges is reduced, then triangle intersection will tend to occur (see Figure 32) and so, **sealing problems should disappear**. The random discretization is only kept at the border of the Intake Piston Top and Exhaust Piston Bottom because it is where the intersections happen; and the remaining part of them are re-triangulated to keep the original piston shape (see Figure 31).

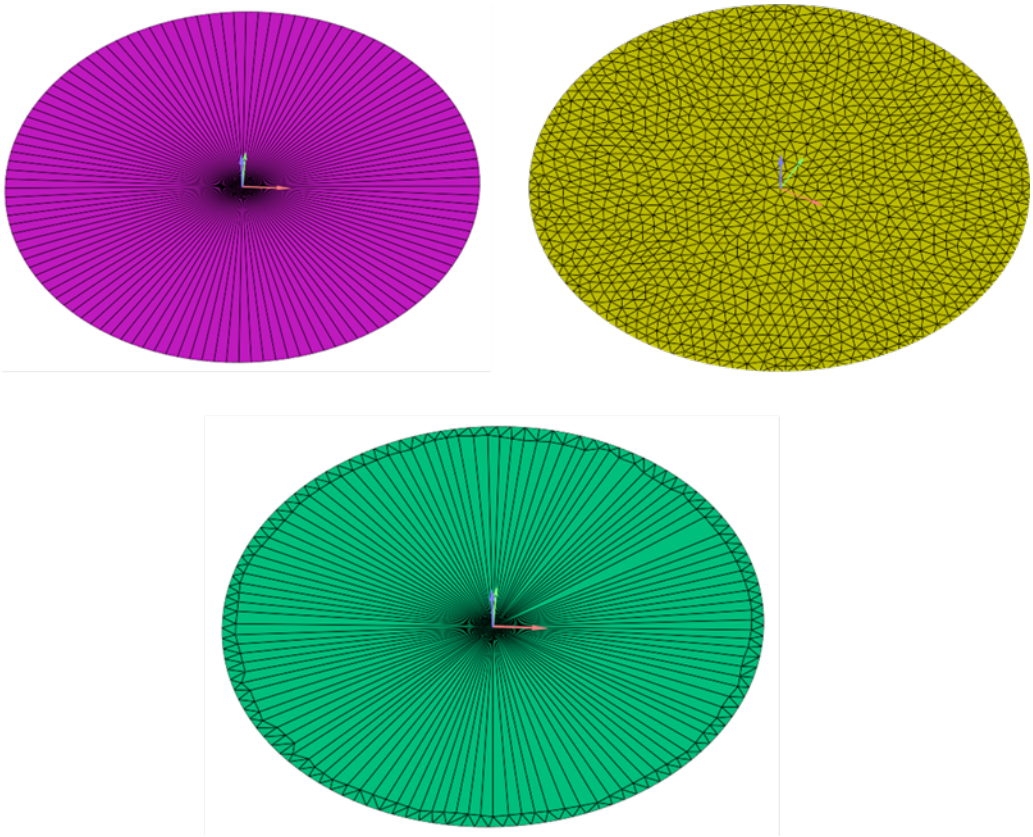

Figure 31: In pink, original piston triangulation; in yellow, piston with random triangulation; in green, final piston boundary with both random and regular triangulations.

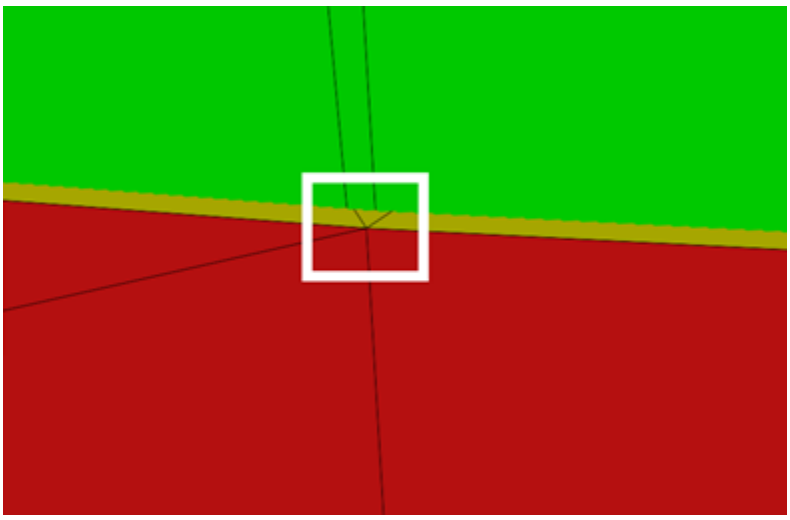

Figure 32: New triangulation. In light brown, the Intake Piston Top; in red, the Intake Piston Skirt; and in green, the Cylinder

However, even though this situation had the potential of solving the sealing issue, the situation changed without improving: now the sealing problem appeared at around 94 CAD. Therefore, after considering all the possible reasons for this to happen, it is concluded that the best alternative is to **change the base grid size** because:

- by slightly changing the previously set value (see Section 3.3.1), the whole grid is constructed and so, vertexes occupy a different position that avoid the allignment between cylinder and piston edges without affecting appreciably the initial mesh layout.

- the CAD step at which cylinder and piston edges are aligned can be avoided due to the fact that, if the CFL number is the time step limiter (see Section 3.3.3) and the grid size is modified, the CAD step value should unavoidably change.

Considering all this, it was decided to select a **new base grid size of 4,1 mm**.

With this new settings, a new simulation is run and it reaches 360 CAD, hence it is concluded that **the sealing problem has been solved.**

4.3 Simulation Running Time

As a starting point, there are some parameters that are set with values based on previous experience (see Table 9), but they just work just as a trial and will for sure be modified once the first simulation is run and its duration is determined.

Parameter	**Value**
CFL Number	1
AMR	
Maximum Embedding Level	3
Sub-grid criterion [%]	1
Maximum Cell Number	$4 \cdot 10^6$

Table 9: Trial values for the initial simulation.

With the previous information, the first hydrodynamic simulation (that will be referred to as "SIM 3" from now onwards) is launched to initially test if its duration reaches acceptable values. Unfortunately, this is not the case: **the simulation only solves 3 CAD a day**. Therefore, the simulation is stopped because, for sure, some modifications need to be applied. To have a clearer idea of the reason why this situation is occurring, some tridimensional graphs of the velocity magnitude[10] in the domain are provided:

[10]It is known that the velocity values are appreciably high, but this finds its meaning in another problem that is discussed in Section 4.4.4. Anyway, the graphs are still useful as a reference for the field and mesh.

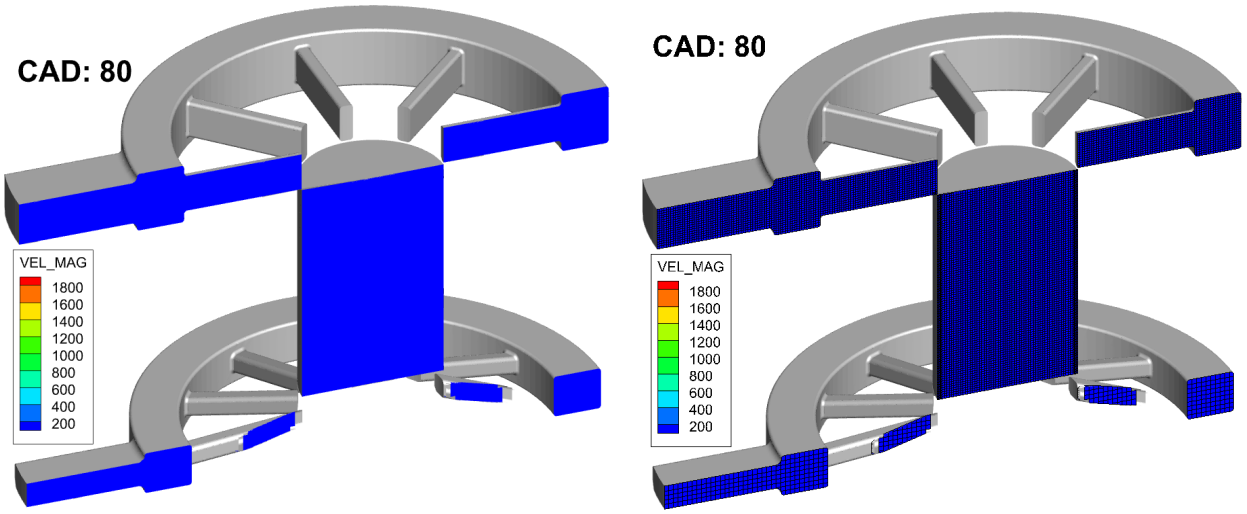

Figure 33: Velocity magnitude field (in $\frac{m}{s}$) in the control volume at 80 CAD with (right) and without (left) the mesh. In this case, it is shown a slice that permits better exhaust visualization.

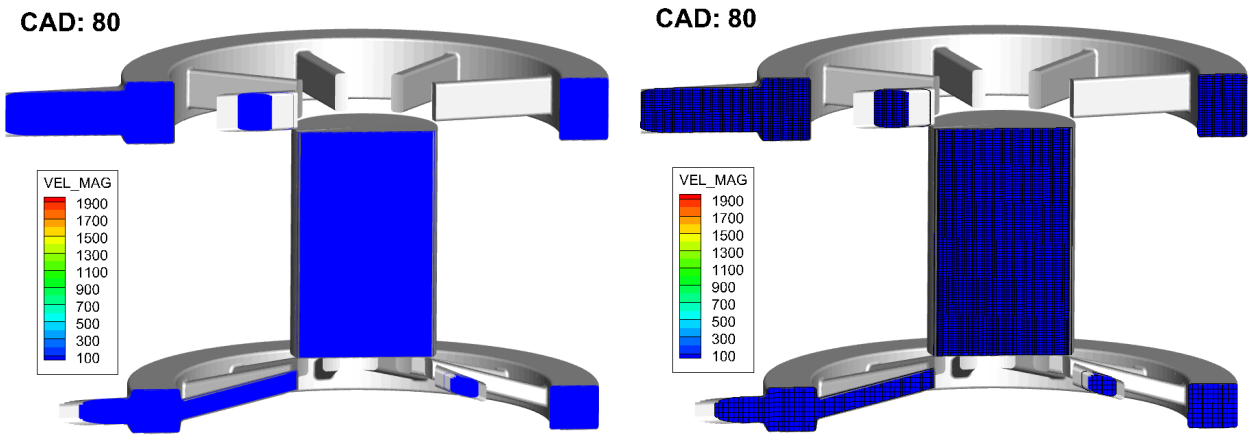

Figure 34: Velocity magnitude field (in $\frac{m}{s}$) in the control volume at 80 CAD with (right) and without (left) the mesh. In this case, it is shown a slice that permits better scavenging visualization.

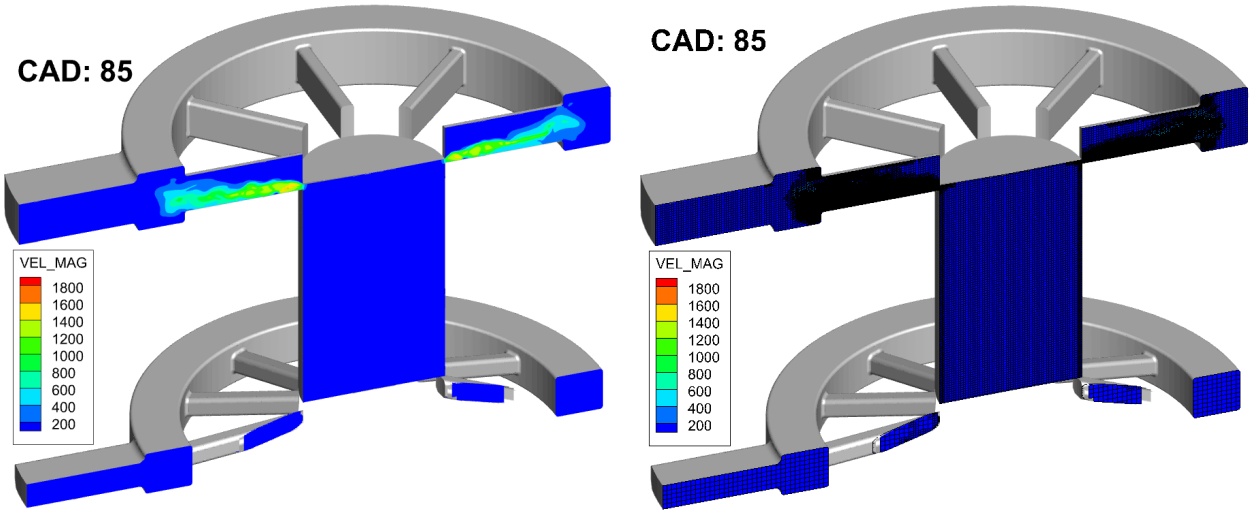

Figure 35: Velocity magnitude field (in $\frac{m}{s}$) in the control volume at 85 CAD with (right) and without (left) the mesh. In this case, it is shown a slice that permits better exhaust visualization.

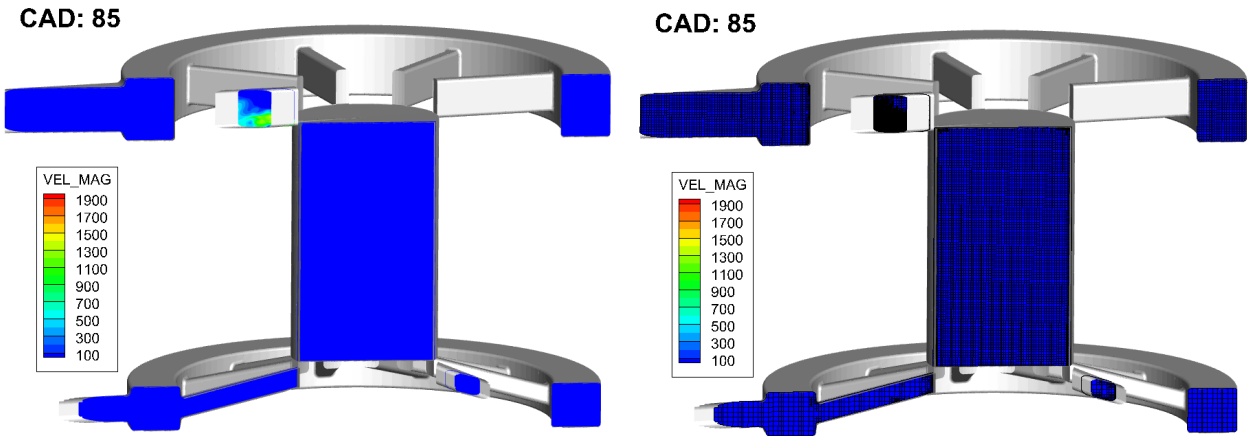

Figure 36: Velocity magnitude field (in $\frac{m}{s}$) in the control volume at 85 CAD with (right) and without (left) the mesh. In this case, it is shown a slice that permits better scavenging visualization.

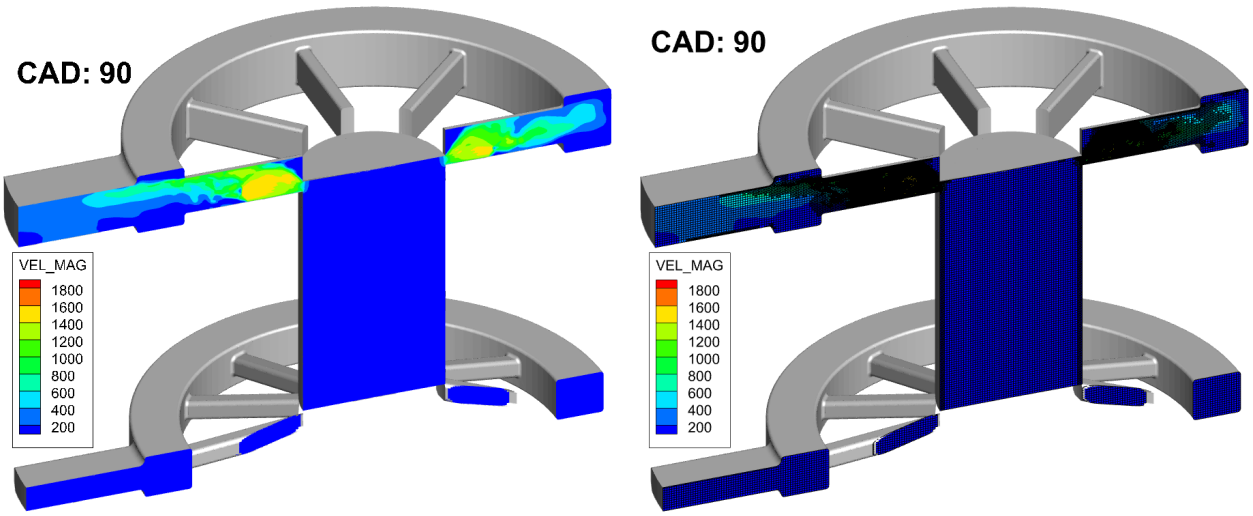

Figure 37: Velocity magnitude field (in $\frac{m}{s}$) in the control volume at 90 CAD with (right) and without (left) the mesh. In this case, it is shown a slice that permits better exhaust visualization.

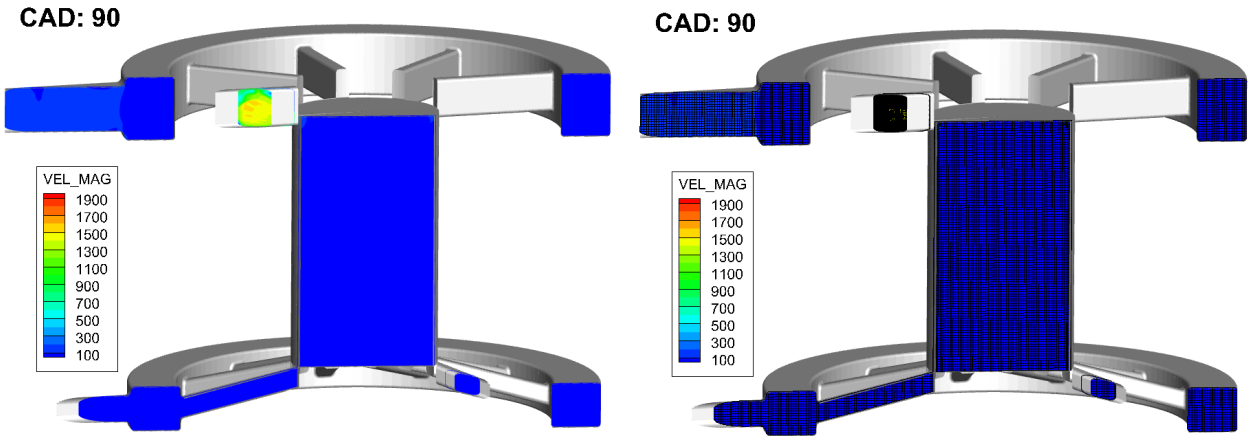

Figure 38: Velocity magnitude field (in $\frac{m}{s}$) in the control volume at 90 CAD with (right) and without (left) the mesh. In this case, it is shown a slice that permits better scavenging visualization.

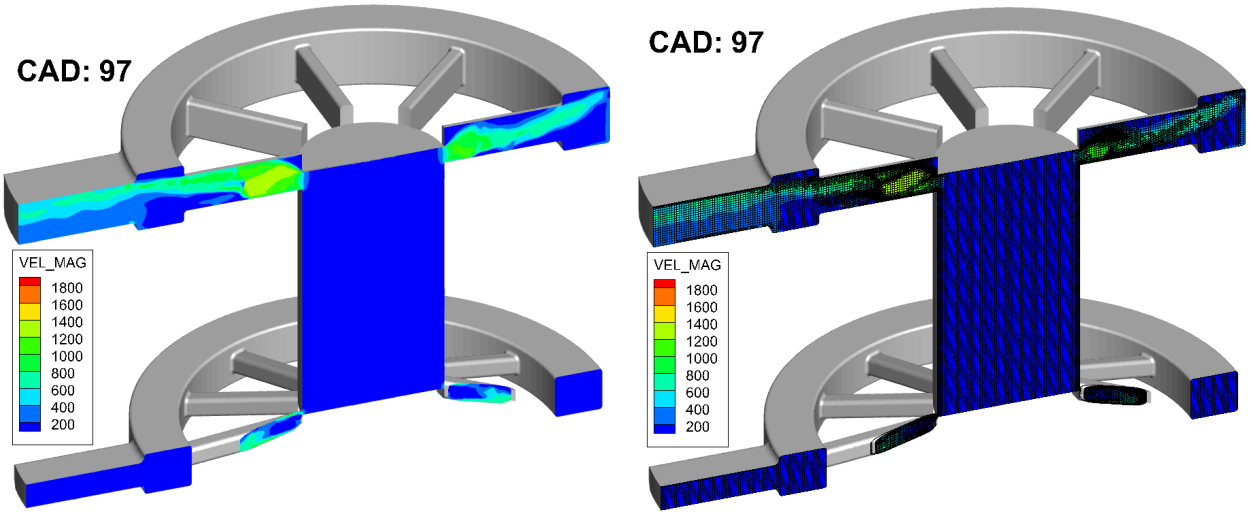

Figure 39: Velocity magnitude field (in $\frac{m}{s}$) in the control volume at 97 CAD with (right) and without (left) the mesh. In this case, it is shown a slice that permits better exhaust visualization.

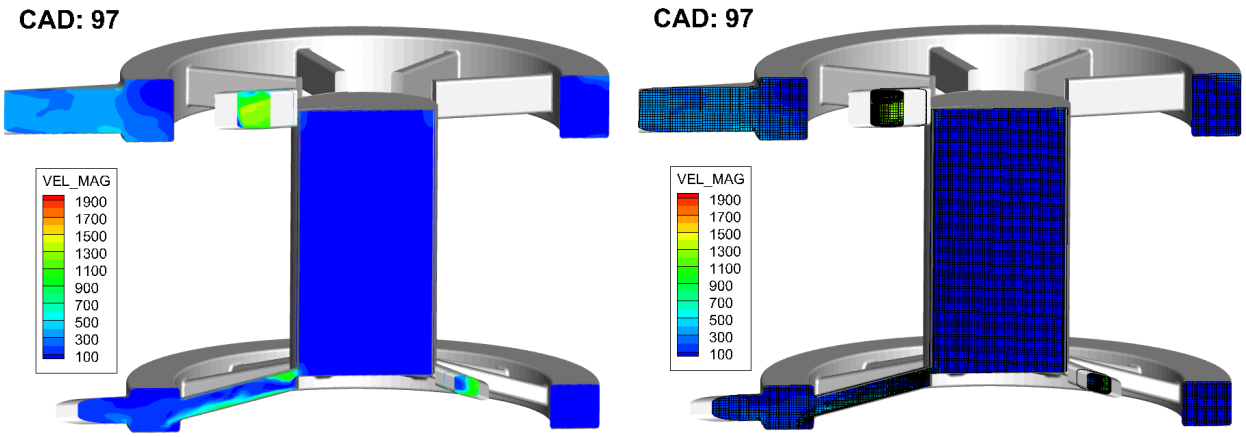

Figure 40: Velocity magnitude field (in $\frac{m}{s}$) in the control volume at 97 CAD with (right) and without (left) the mesh. In this case, it is shown a slice that permits better scavenging visualization.

By observing Figures 33 to 40, it is confirmed that the AMR is working correctly: the left figures show the different velocity fields and the right figures evidence the fact that embedding is activated in cells where velocity experiences a sudden change due to, for example, port opening.

In consequence, as **the AMR working conditions appear not to be the problem**, the following step is to analyze the temporal parameters of the simulation. Below this paragraph, the wall time and the time step profiles are plotted to properly determine if any of them is more determinant as a cause of this problem:

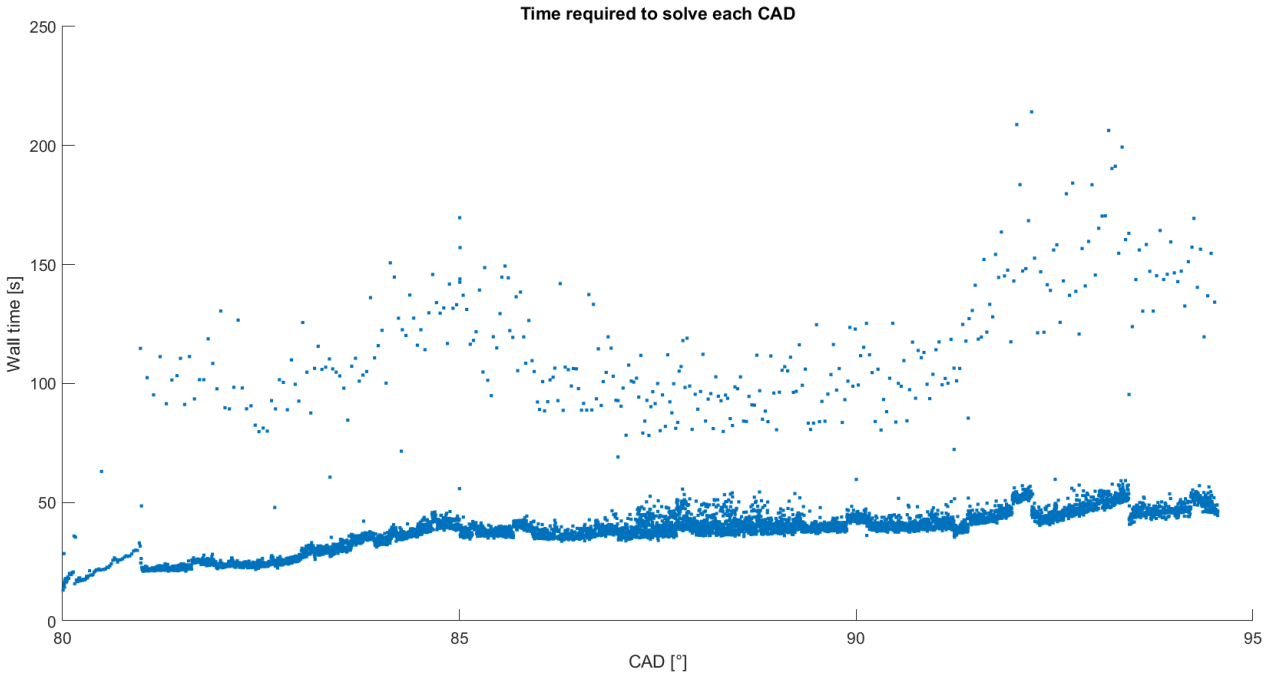

Figure 41: Time required to solve each CAD in SIM 3.

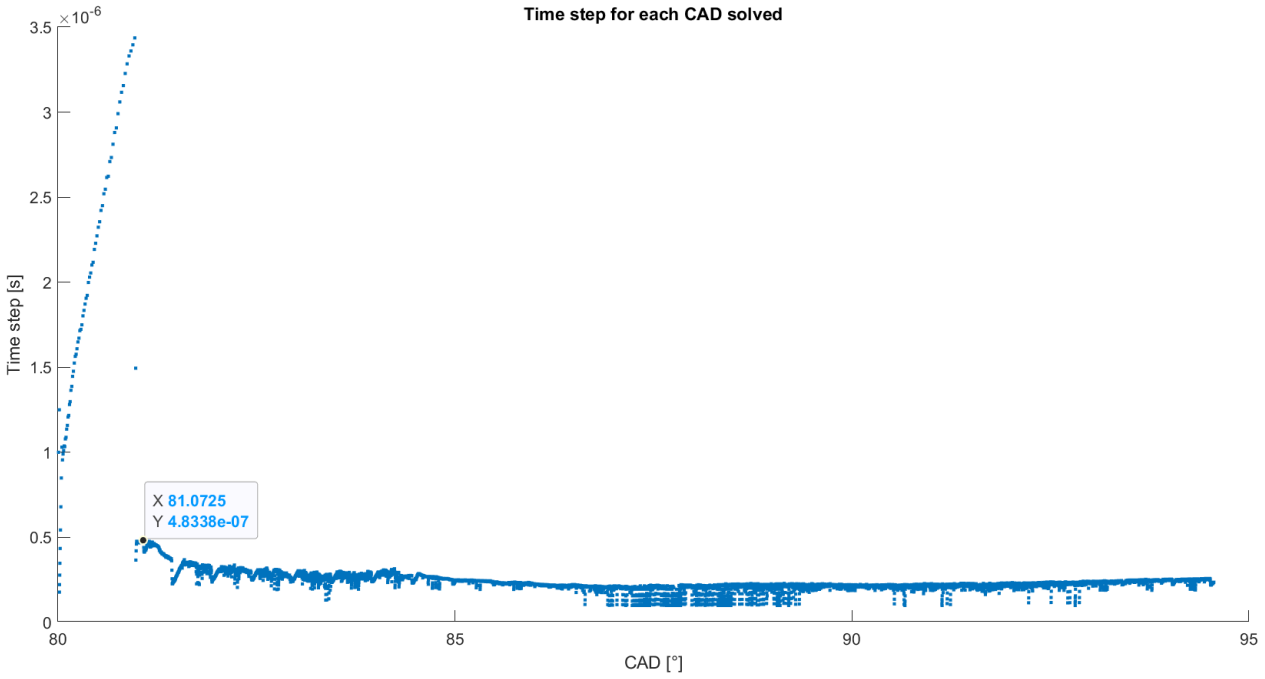

Figure 42: Time step for each CAD solved in SIM 3.

From Figure 41, it is reasonable to say that the **time taken for solving each time step** is not the main problem because it ranges around **40 seconds** (neglecting dispersions) which is not an extremely large value. However, the time step does seem to be the cause of the extended duration of the simulation because, after the exhaust opening (at around 81 CAD), it **rapidly descends to values at around** 10^{-7} **which are too close to the**

minimum value (see Section 3.2.5) and this is not a positive sign because it indicates that, in order to obtain an adequate precision in solving the problem, the software needs to discretize the time domain to extremely low values.

In an attempt to solve the issue, following Equation 2, **it is increased the value of the CFL number to 2**, so as to also increase the time step in the cases where the CFL is the time step limiter (which are 90% of the steps if it is taken SIM 3 as a reference). Under these conditions, a new simulation called "SIM 4" is run and it is expected to obtain better results.

Although this solution seems promising and it actually provides some improvements, these ones are not so influential and are even accompanied by other new problems that before were not present. To begin with, the overall duration did improved, but it just duplicated: **the solver provides results for 6 CAD per day**. This condition is still considered not appropriate for the current simulated case, so the simulation is run for 30 CAD to obtain enough information and then stopped once again. Additionally, considering that CONVERGE has solved the problem in 10846 CAD steps, 1456 recoveries are identified including, among others:

- temperature extrapolation error
- negative densities or pressure
- maximum turbulence iteration

Hence, it is not right that **in 10 % of the steps for which a solution is found, at least one recovery occurs**. Furthermore, the effects on the wall time and time step are also negative:

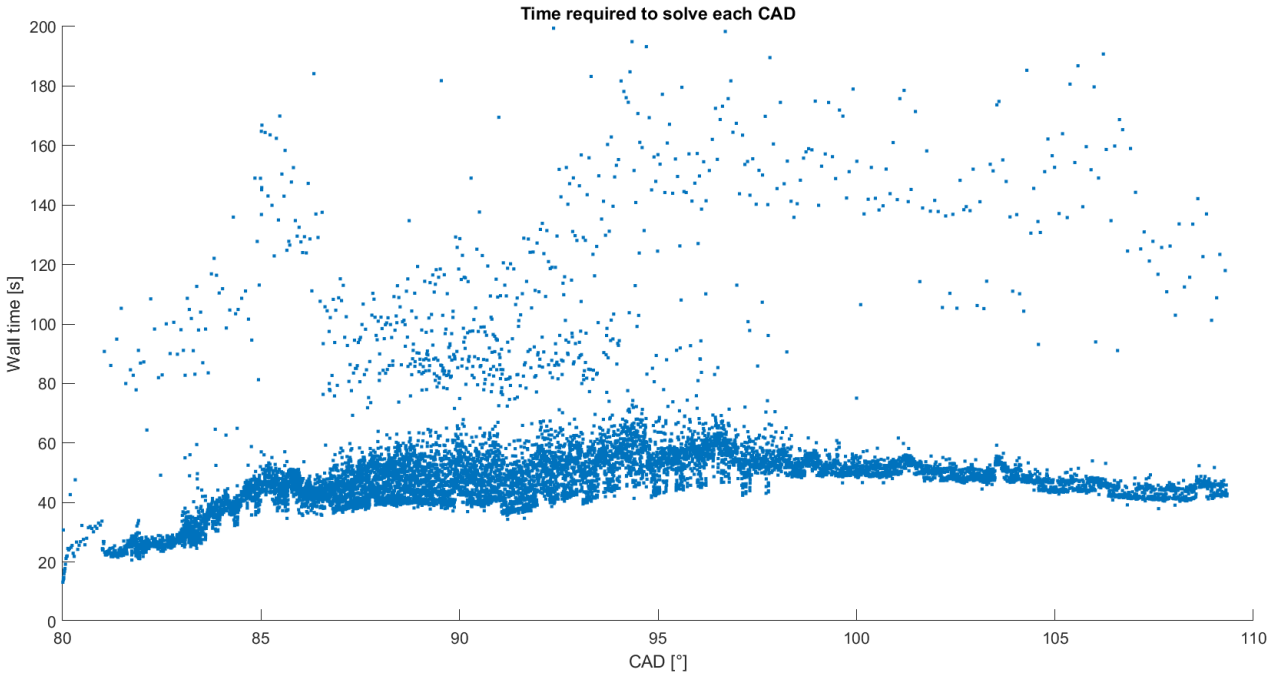

Figure 43: Time required to solve each CAD in SIM 4.

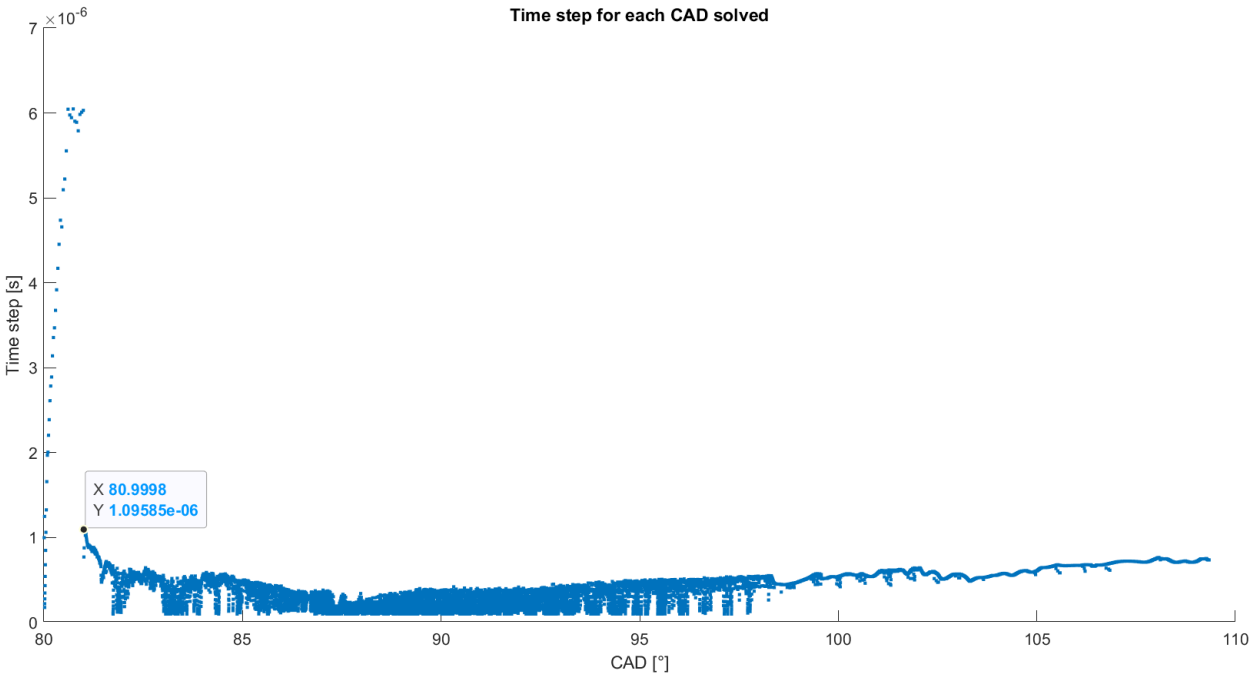

Figure 44: Time step for each CAD solved in SIM 4.

In Figure 43, it is evident that the **wall time has slightly increased** which, in principle, is not so severe; but the real problem is the fact that **the amount of dispersion has increased abruptly and to huge values**, having even the case of taking 3 minutes to solve just one step. With regards to Figure 44, the situation is not better: the tendency is to have time step values higher than in SIM 3, but, anyway, **similar to the minimum allowed case** and, what is worse, at some specific CAD values, the time step is **at its minimum** (this means that the actual settings do not enable CONVERGE to study the temporal domain at that CAD step with the required precision because the time step value needed is lower than the minimum possible).

Therefore, following the definition of the CFL number in Equation 2, it is found a way of modifying the time step in an attempt to keep it away from the minimum value: maintaining the same CFL number and considering that it is not possible to modify the speed, if the "Δx is increased, then the time step should also increase. By knowing this, it is chosen to **modify the AMR settings** in order to generate less strict conditions for its associated embedding and the decisions taken are:

- **Reduce the maximum cell number**: before it was $4 \cdot 10^6$ and now $2 \cdot 10^6$
- **Increase the sub-grid criterion**: from 1% to 3%

Under this new conditions, a new simulation, called "SIM 5", is run in order to verify that the modifications permitted the solution of the previously mentioned problems.

As a starting point, the actual grid is compared to the ones from SIM 3, to properly visualize the effects of the changes in the AMR settings:

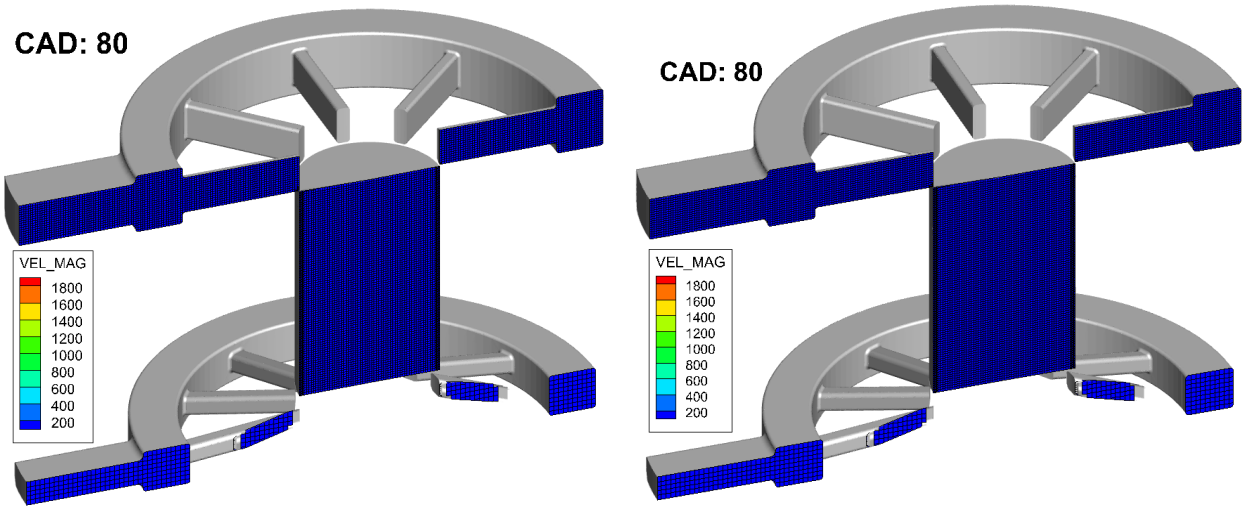

Figure 45: Velocity magnitude field (in $\frac{m}{s}$) in the control volume at 80 CAD in SIM 3 (left) and SIM 5 (right). In this case, it is shown a slice that permits better exhaust visualization.

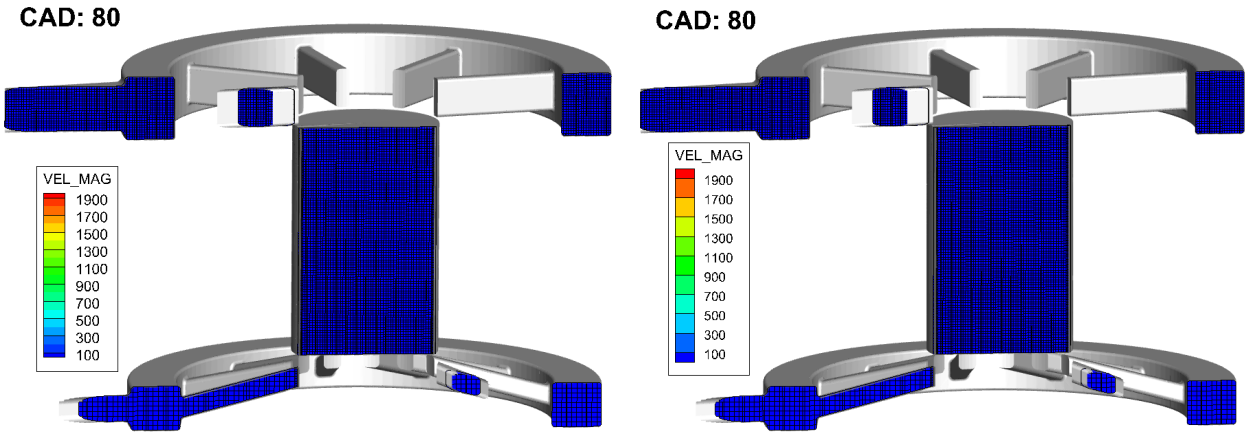

Figure 46: Velocity magnitude field (in $\frac{m}{s}$) in the control volume at 80 CAD in SIM 3 (left) and SIM 5 (right). In this case, it is shown a slice that permits better scavenging visualization.

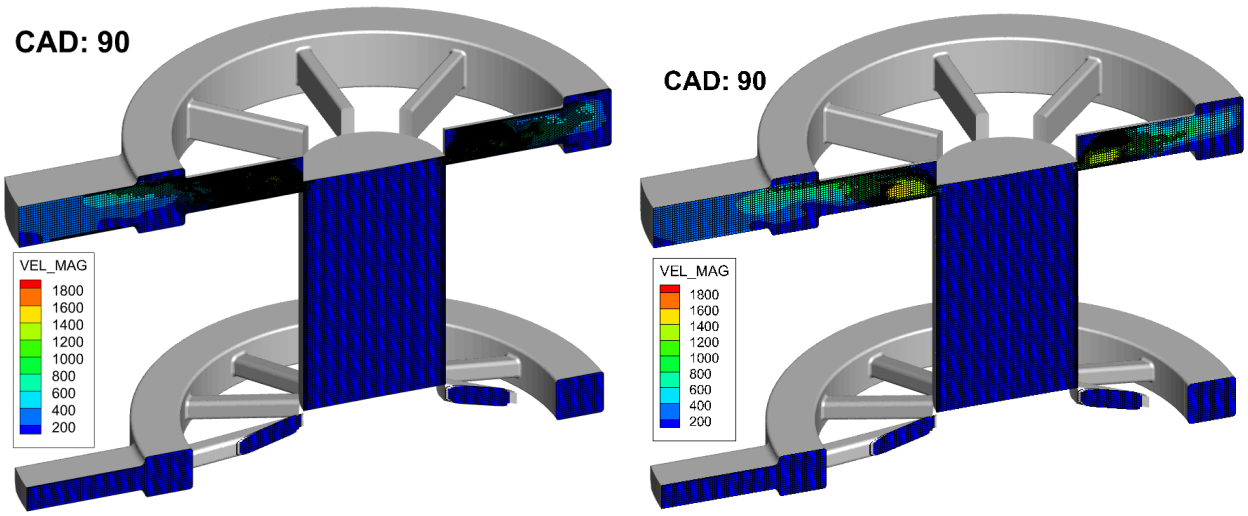

Figure 47: Velocity magnitude field (in $\frac{m}{s}$) in the control volume at 90 CAD in SIM 3 (left) and SIM 5 (right). In this case, it is shown a slice that permits better exhaust visualization.

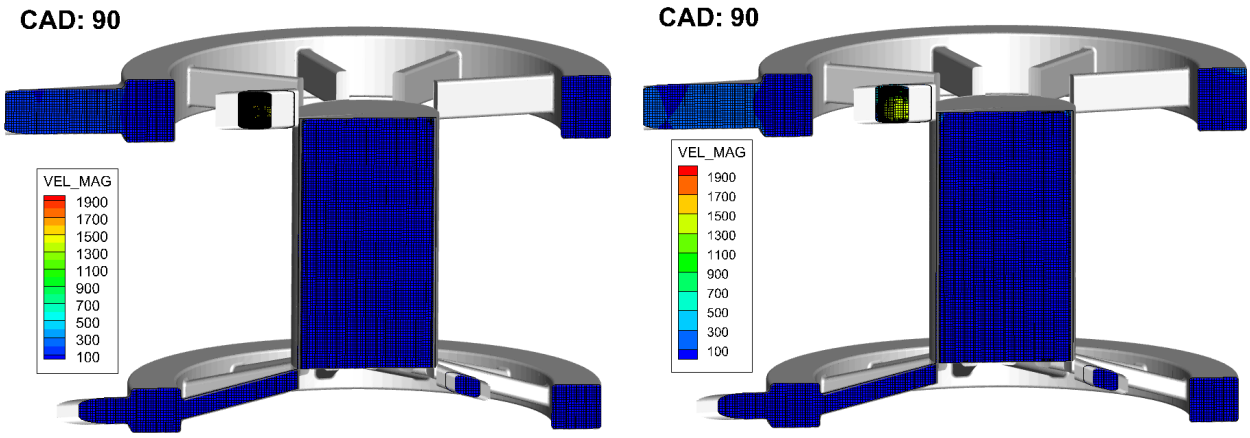

Figure 48: Velocity magnitude field (in $\frac{m}{s}$) in the control volume at 90 CAD in SIM 3 (left) and SIM 5 (right). In this case, it is shown a slice that permits better scavenging visualization.

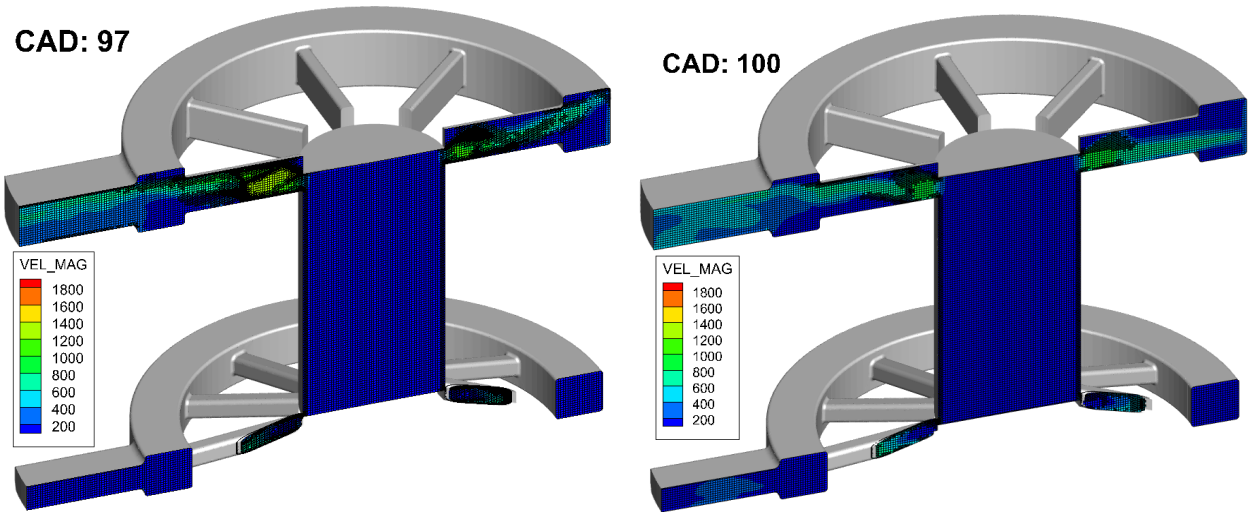

Figure 49: Velocity magnitude field (in $\frac{m}{s}$) in the control volume at 97 CAD in SIM 3 (left) and 100 CAD in SIM 5 (right). In this case, it is shown a slice that permits better exhaust visualization.

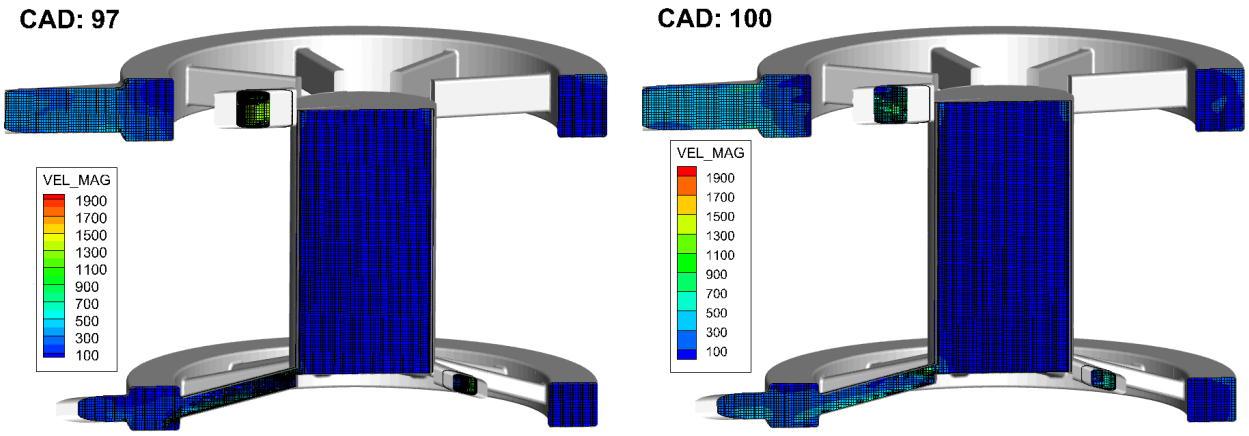

Figure 50: Velocity magnitude field (in $\frac{m}{s}$) in the control volume at 97 CAD in SIM 3 (left) and 100 CAD in SIM 5 (right). In this case, it is shown a slice that permits better scavenging visualization.

The previously seen images show that, before the AMR activation (see Figure 45 and 46), both grids remain the same, but when the exhaust opens, the Adaptive Mesh Refinement begins to act and differences start to appear (see Figures 47 to 50). As in SIM 5 the sub-grid criterion is increased, the threshold above which AMR starts working increases, so less number of cells are embedded in SIM 5 than in SIM 3. Apart from that, and anticipating a problem that will be dealt later in this section, the maximum number of cells is reduced, hence in SIM 5 the AMR might not able to embed all the amount of cells that it should, but a lower amount that could be even lower than in SIM 3.

Moreover, it must be mentioned that with this new conditions the duration of the whole simulation decreased considerably: **65 CAD per day are solved**. Nevertheless, it will be seen that the graphs will only reach around 183 CAD because at this point appeared the sealing problems discussed in Section 3.3.2. Similarly to SIM 4, 1203 recoveries of the same types as before are present in 17947 CAD steps, so the negative condition of having **recoveries in approximately 10% of the CAD steps** has not been solved yet.

As it can be seen in Figure 51, the wall time is positively affected by the new AMR conditions because the average value has been reduced one order of magnitude and also the number and value of the dispersion have been decreased. Regarding the time steps, as evidenced in Figure 52, the overall situation has improved because, for most of the simulation, the time step has a value around 10^{-6} s which is contained between the maximum and minimum ranges (see Section 3.2.5). However, it must be mentioned the fact that, after the exhaust ports opening and some CAD after the scavenging ports opening, the time step presents some values which are noticeably close or even equal to the minimum one and, as it has been exposed before, this should be avoided.

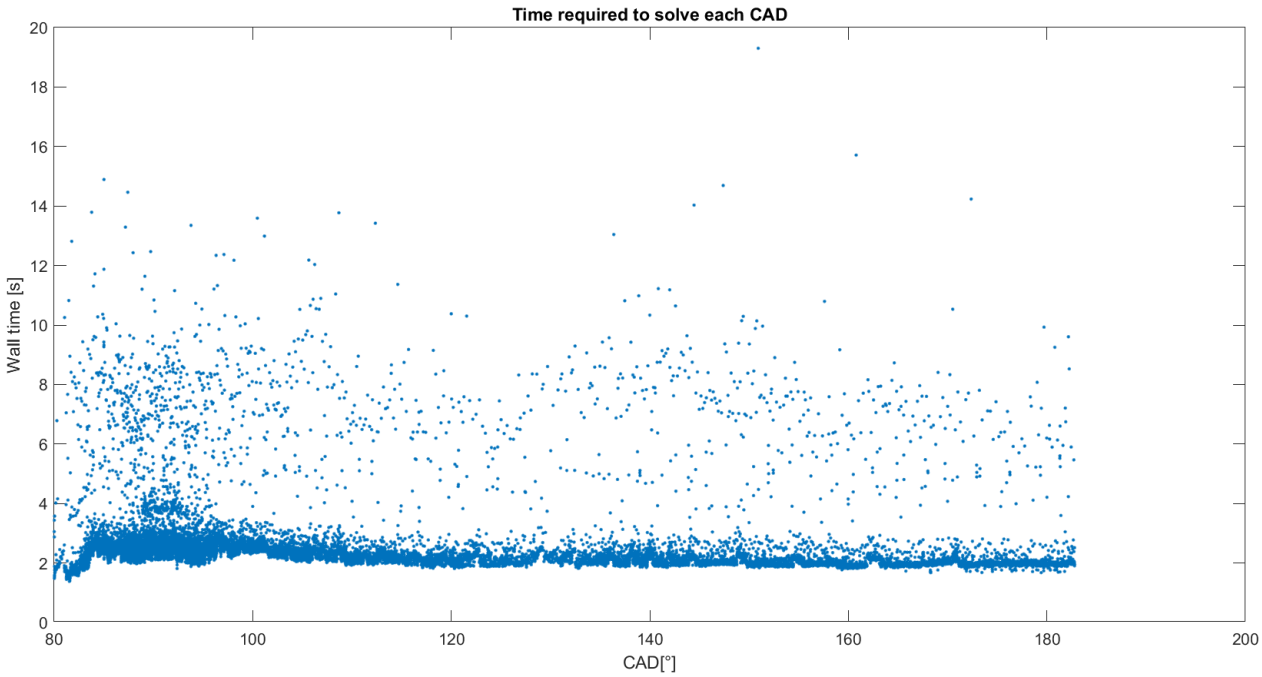

Figure 51: Time required to solve each CAD in SIM 5.

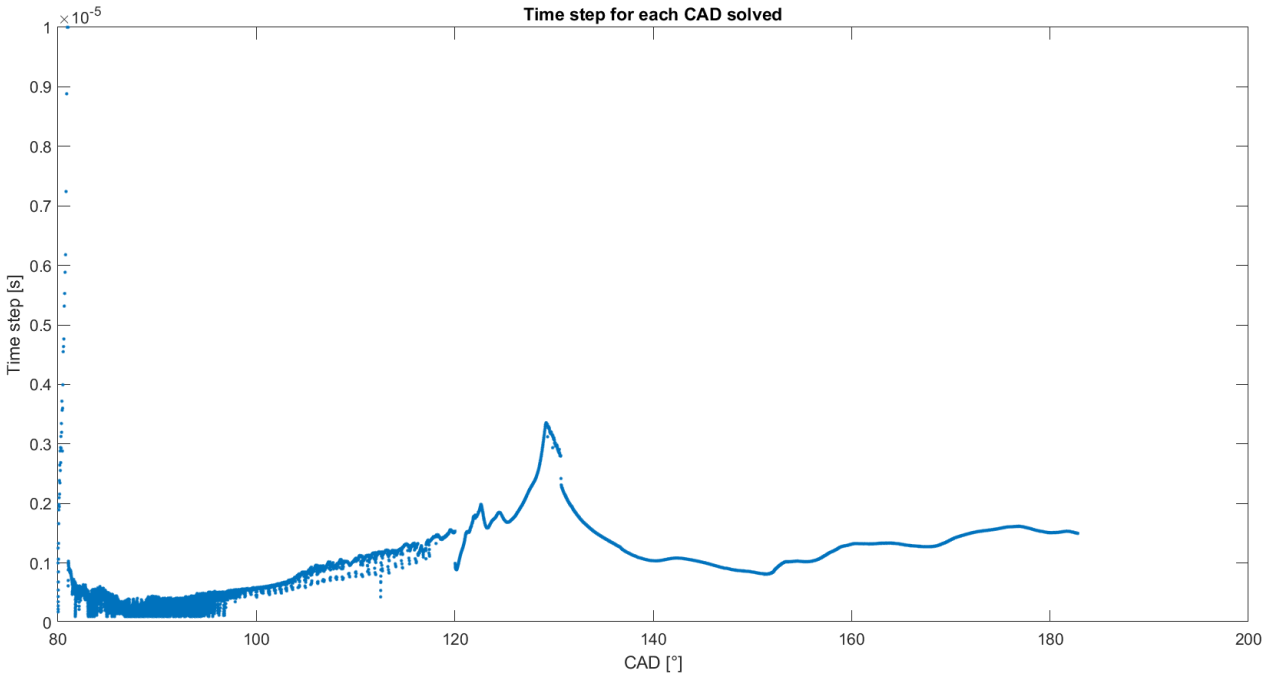

Figure 52: Time step for each CAD solved in SIM 5.

As a last negative remark of SIM 5, in order to verify if the changes applied to the AMR did not compromise the precision of the results, it is plotted the total cell number as a function of the crank angle degrees and the conclusion is that **the generated grid is not precise enough**. As it can be seen in Figure 53, some CAD after the exhaust port opening , the grid arrives to the maximum allowed number of cells ("cell saturation"); this means that some other cells should be embedded but are not, so the results provided are not as precise as they should be. As a first hypothesis, this was attributed to the fact of reducing the maximum cell number in SIM 5, but as it can also be observed in Figure 53, SIM 4 also suffered cell saturation. Therefore, a new solution should be provided to solve this saturation condition and allow the grid to have the precision that the problem requires.

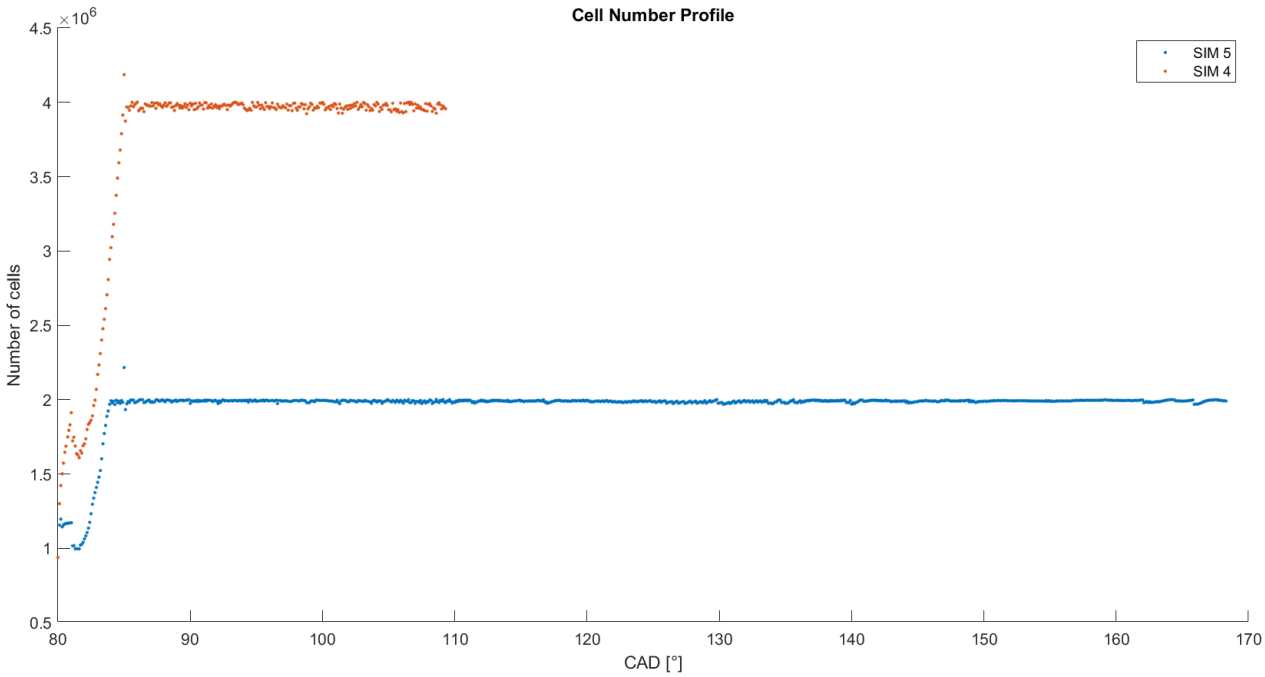

Figure 53: Total number of cells at each CAD for SIM 4 and SIM 5.

Considering all the modifications and results obtained from SIM 3 to SIM 5, a new simulation is run with several changes in its setup which are discussed below. This new simulation will be referred to as "SIM 6" and is expected to give encouraging results because it combines the values of all of the parameters previously modified, based on the results that they provided.

To begin with, based on SIM 4, it can be concluded that increasing the CFL number is not so influential in terms of the simulation speed and it is accompanied by some negative consequences, like recoveries and reduced time step values. As a result, it is decided to maintain it at low values specially during the important stages of the simulation and, instead of setting a constant value, a **cyclic temporal profile for the CFL number** is defined in order for its value to adapt to the corresponding stage of the simulation:

- At the beginning of the simulation (**80 CAD**), as it is just before the exhaust opening, the value is set to **1** as a starting point for the analysis.
- Some CAD after the exhaust opening (specifically at **86,5 CAD**), due to the high pressures and velocities, it is required a lower CFL number to properly develop the study with an increased time precision, so a value of **0,6** is chosen. This value remains until some CAD just before the scavenging port opening.
- The **scavenging phase** is less critical in terms of pressure and velocity values, so it is set a **CFL equal to 1** since it begins (at around **91,5 CAD**) until the exhaust closes port at **265 CAD**.
- As the remaining steps of the simulation are not so important for the gas filling analysis, the CFL number is imposed to have a value of **2**. Anyway, as neither the AMR nor

most of the fixed embeddings are activated during these stages, it is expected that the time step limiter will not be the CFL number, but the maximum time step value (explained in Section 3.2.5).

To sum up, the temporal profile of the CFL number can be evidenced in Table 10:

CAD [°]	0	80	86,5	91,5	265	360
CFL number	2	1	0,6	1	2	2

Table 10: CFL temporal profile.

Similarly, based on the temporal precision that the different processes that occur inside the volume require, it is decided to also define a **cyclic temporal profile for the maximum time step value**. The value defined in Section 3.2.5 remains throughout most of the simulation, with the exception of some instants before the exhaust and scavenging ports opening (**at 81,5 and 90 CAD respectively**) when its value is reduced to 10^{-6} during some CAD (**until 83 and 91,5 CAD respectively**) to increase the precision of the analysis in case the time limiter for any step in that range ends up being the maximum one. To summarize, it is exposed the temporal profile for the maximum time step of the simulation in Table 11.

CAD [°]	0	81,5	83	90	91,5	360
Maximum Time Step [s]	10^{-5}	10^{-6}	10^{-5}	10^{-6}	10^{-5}	10^{-5}

Table 11: Maximum time step temporal profile.

Lastly, it has been seen in SIM 5 that the parameter that provides the most positive consequences by making it less restrictive is the AMR. Therefore, there are various modifications applied to the different parameters that compose the Adaptive Mesh Refinement configuration in order to permit an adequate problem solving:

- The **maximum cell number** is set to 10^7, instead of $2 \cdot 10^6$ in order to be sure of avoiding cell saturation and to refine as many cells as the software considers necessary.
- The **sub-grid criterion** is increased from 3 to **5** which is not such an abrupt change, so precision is not extremely affected, but still allows a lower number of cells to be embedded and reduces the computational time.
- The **embedding level** is reduced from 3 to **2** which reduces the computational time to a great extent and, for the actual project phase, it is considered to still provide reasonable precision to the results.

Having these new settings defined, SIM 6 is launched and, fortunately, positive results in terms of the temporal parameters are obtained. To begin with, the simulation is able to **reach the 360 CAD** without crashing, with frequency of **95 CAD solved per day** and showing **no recoveries at all**. In the following figures, it can be clearly seen the differences between the grid generated with SIM 5 and with SIM 6. In a similar way to the comparison between SIM 5 and SIM 3, it is shown that before the AMR activation both grids

are approximately equal because they have the same base grid size and fixed embeddings' configuration, but, as soon as the exhaust ports open and the AMR starts to refine the mesh, the differences are evidenced. As in SIM 6 the maximum cell limit has been increased together with an embedding level reduction, the grid shows higher number of cells from the base grid being embedded (even higher than in SIM 3 at times if compared with Figures 33 to 40), but with a coarser refinement. This previous condition also enables to conclude that the increase in the sub-grid criterion did not affect considerably the precision of the results because the number of cells affected by the AMR has increased. not reduced.

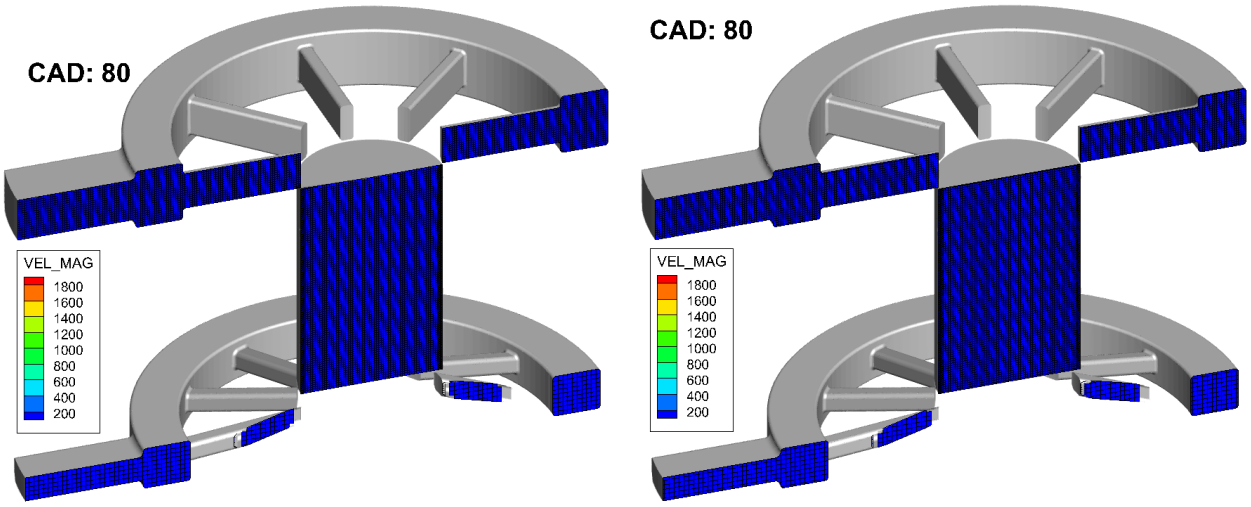

Figure 54: Velocity magnitude field (in $\frac{m}{s}$) in the control volume at 80 CAD in SIM 5 (left) and SIM 6 (right). In this case, it is shown a slice that permits better exhaust visualization.

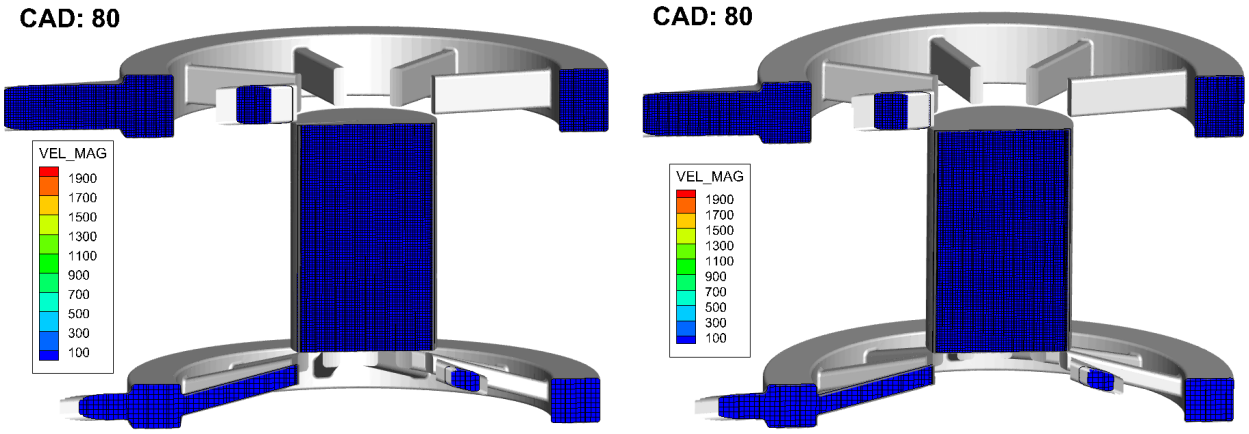

Figure 55: Velocity magnitude field (in $\frac{m}{s}$) in the control volume at 80 CAD in SIM 5 (left) and SIM 6 (right). In this case, it is shown a slice that permits better scavenging visualization.

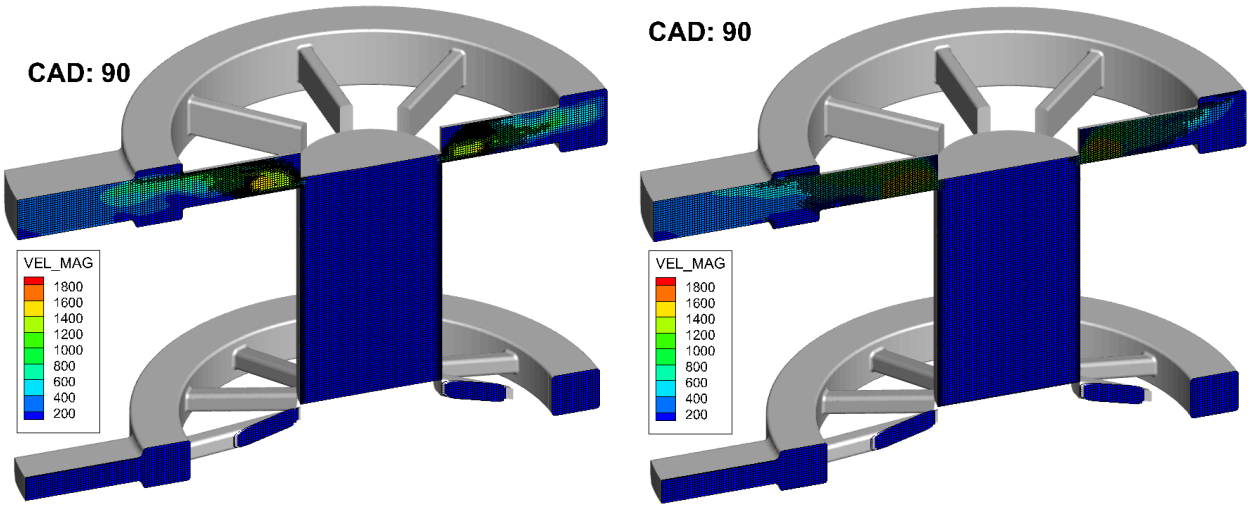

Figure 56: Velocity magnitude field (in $\frac{m}{s}$) in the control volume at 90 CAD in SIM 5 (left) and SIM 6 (right). In this case, it is shown a slice that permits better exhaust visualization.

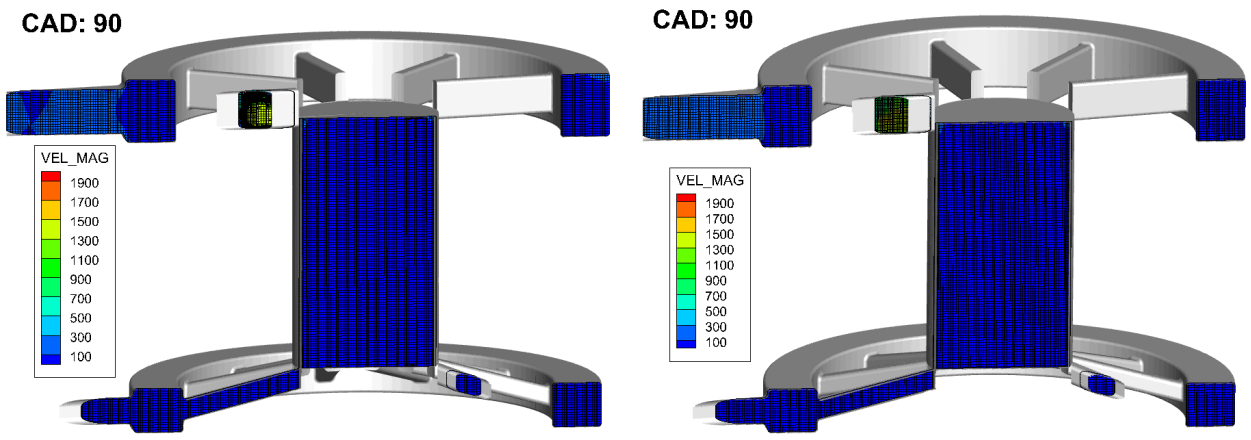

Figure 57: Velocity magnitude field (in $\frac{m}{s}$) in the control volume at 90 CAD in SIM 5 (left) and SIM 6 (right). In this case, it is shown a slice that permits better scavenging visualization.

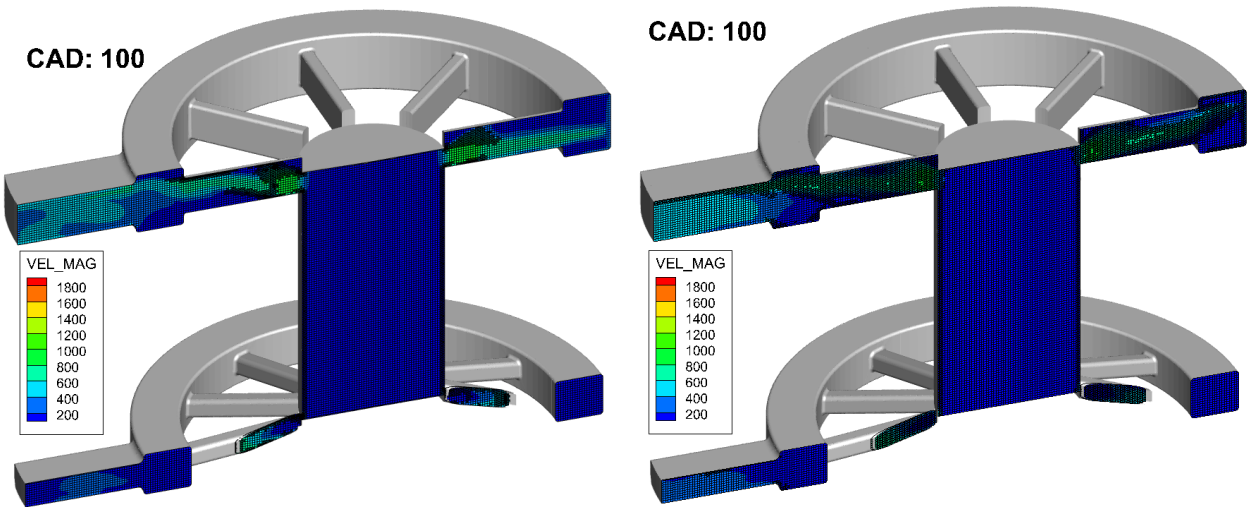

Figure 58: Velocity magnitude field (in $\frac{m}{s}$) in the control volume at 100 CAD in SIM 5 (left) and SIM 6 (right). In this case, it is shown a slice that permits better exhaust visualization.

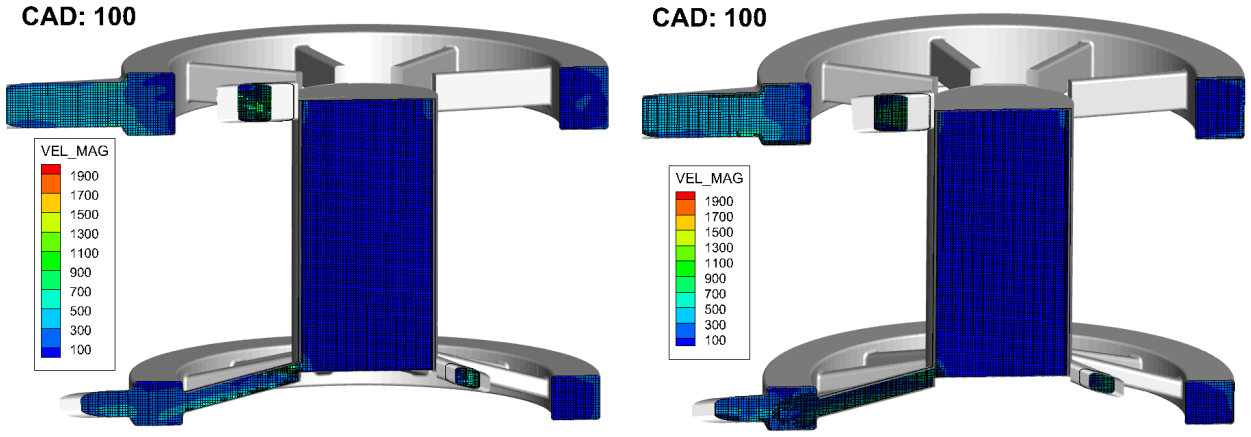

Figure 59: Velocity magnitude field (in $\frac{m}{s}$) in the control volume at 100 CAD in SIM 5 (left) and SIM 6 (right). In this case, it is shown a slice that permits better scavenging visualization.

In second place, as visualized in Figure 60, the wall time presents values which are similar to those seen in Figure 51 with even lower number of dispersions, so this means not only that **the time needed to solve each CAD step is acceptable**, but also that it has a value that is **kept stable during most of the CAD steps** regardless of what does each time step is representing from a physical point of view.

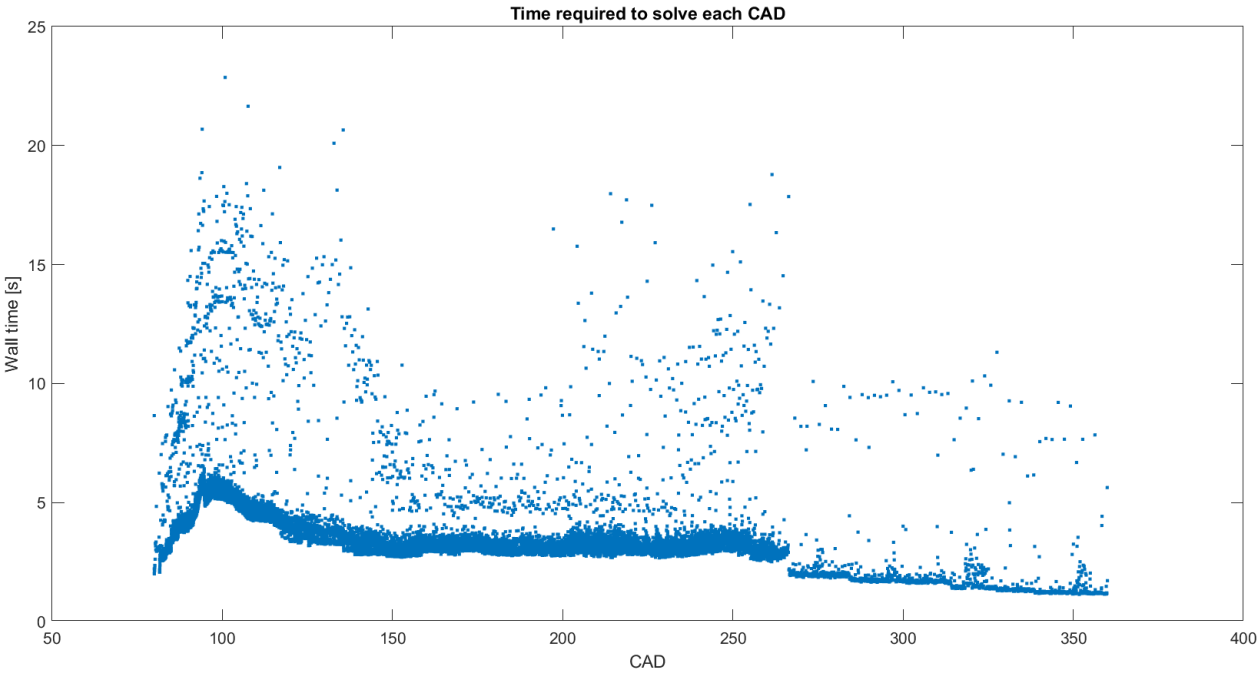

Figure 60: Time required to solve each CAD in SIM 6.

Thirdly, similarly to Figure 52, Figure 61 shows that, for the different CAD steps, the **time step presents a value of the order of** 10^{-6} **s** which, once again, is a positive result because it is contained in the previously defined range. Nevertheless, it should be mentioned that, **after both of the ports close at around 265 CAD, the time step occurs to be the maximum one** (see Section 3.2.5) which is **not a negative situation** because CONVERGE imposes this to avoid instabilities that might be generated if the mathematical conditions of the problem were the ones that set the time step. The time steps that result from the model's mathematics have relatively high values after the ports' closing due to:

- the **fluid motion being simple to solve** because the velocity is quite low compared to when cylinder and ducts are connected.
- the **AMR and cyclic embeddings not being activated any more**, so the grid stops being refined and, for a constant value of the CFL number, this means that the time step shound unavoidably increase (see Equation 2).
- the **CFL number having the maximum value in this CAD range** because this might mean that at a certain point it would no longer be the time step limiter because the constraint that it imposes would be satisfied anyway.

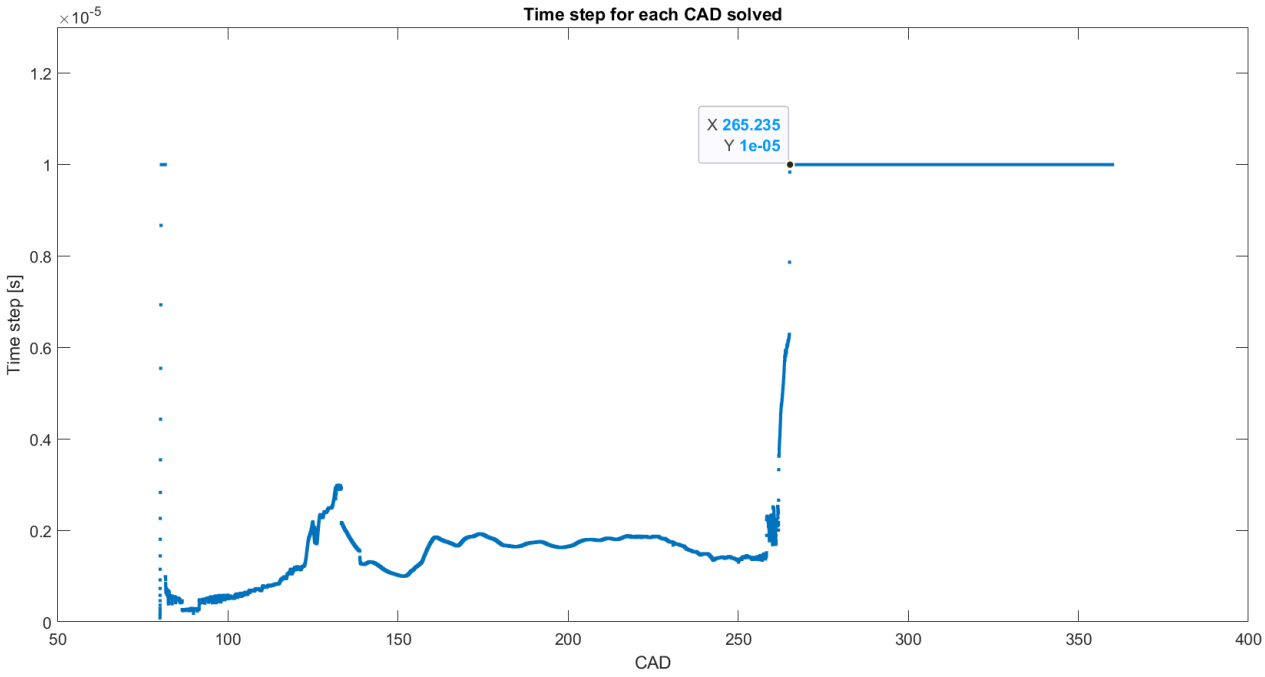

Figure 61: Time step for each CAD solved in SIM 6.

As a final observation, it is plotted in Figure 62 the total amount of cells in SIM 6 and it is seen that, unlike Figure 53, the model does not arrive to the cell saturation condition (it never reaches the maximum value of 10^7 cells). Hence, in this way, it is possible to conclude that **the results obtained have the maximum precision that the actual settings allow** because solver is able to embed all the cells that required it. Additionally, considering also the results obtained in Section 4.1, it is reasonable to state that **the total number of cells obtained is adequate** because it is not an extremely high value for this initial stage of the model where only only gas filling is analysed, but it is sufficient to provide the results with the necessary precision.

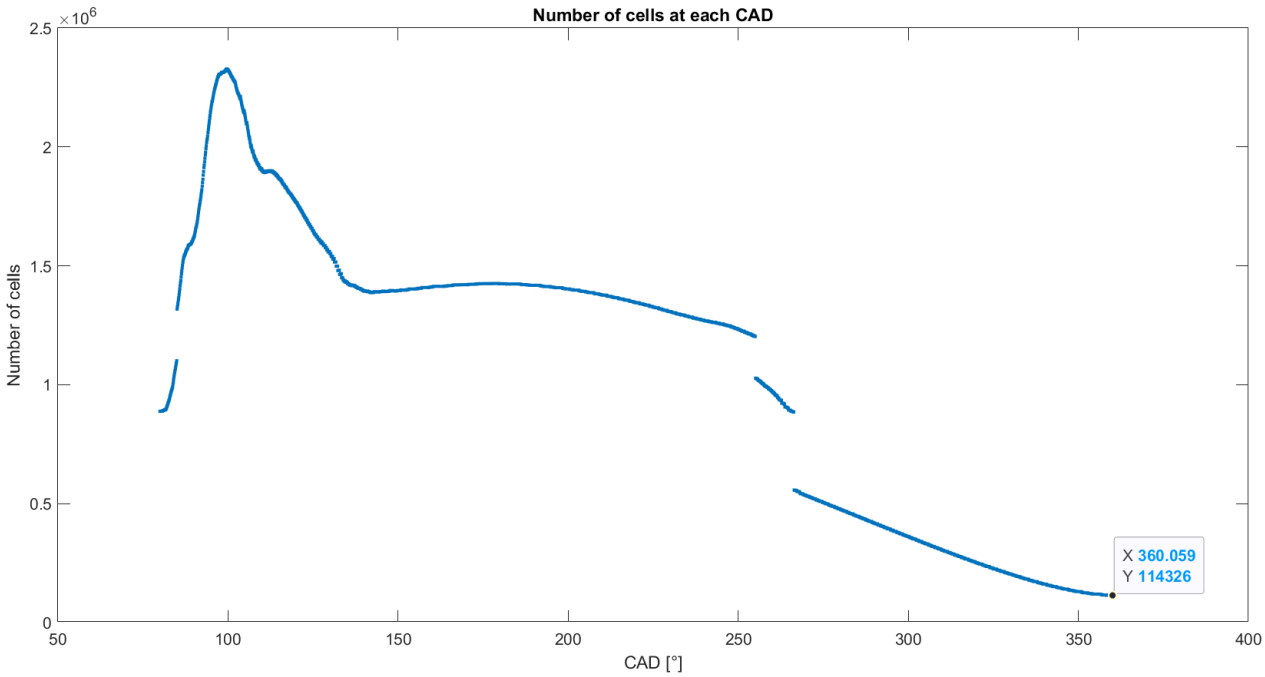

Figure 62: Total number of cells at each CAD for SIM 6.

In conclusion, as SIM 6 has shown promising outcomes in regards to its duration, the temporal characteristics and the AMR execution, it is decided that **its results are trustworthy enough to execute a first analysis on them** and that **its settings will be the starting point for further simulations**, like for example, adding the combustion modelling.

4.4 Thermodynamic Study

After verifying the grid, solving the sealing problem and providing a reasonable duration to the simulation, the model´s results are finally ready to be analysed from a thermodynamic point of view in order to characterize the engine's design.

4.4.1 Velocity, Air Mass and INTAKE concentration fields

To start with, in the following pages a variety of tridimensional figures are exposed which show the evolution of the air mass, velocity and INTAKE passive species concentration fields. Two different slices (both of them without the grid for better visualization) of the domain are shown because one of them permits better visualization of the behaviour at the exhaust ducts and the other at the intake ducts.

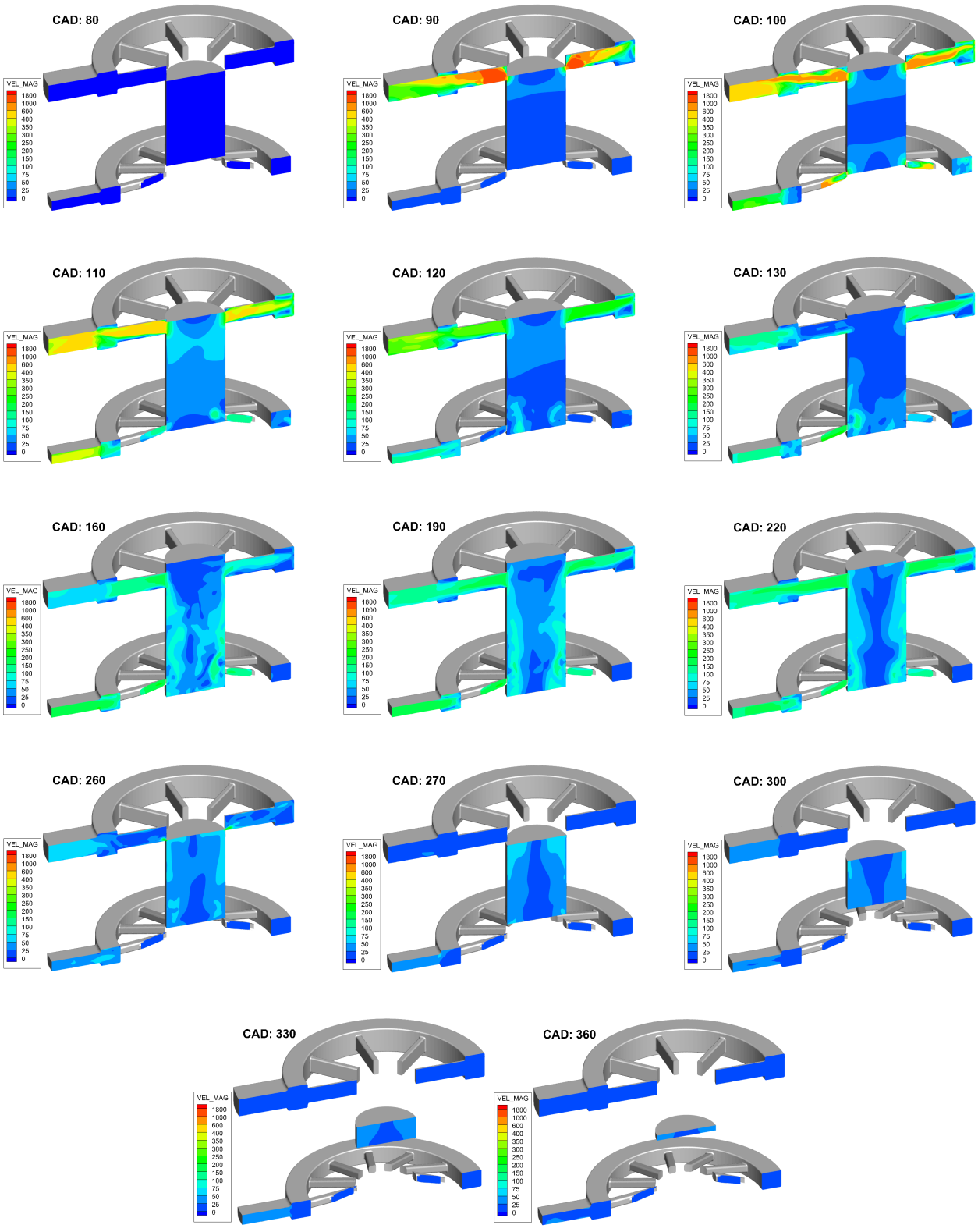

Figure 63: Velocity magnitude field (in $\frac{m}{s}$) for various CAD values with a slice that permits better visualization of the exhaust ducts.

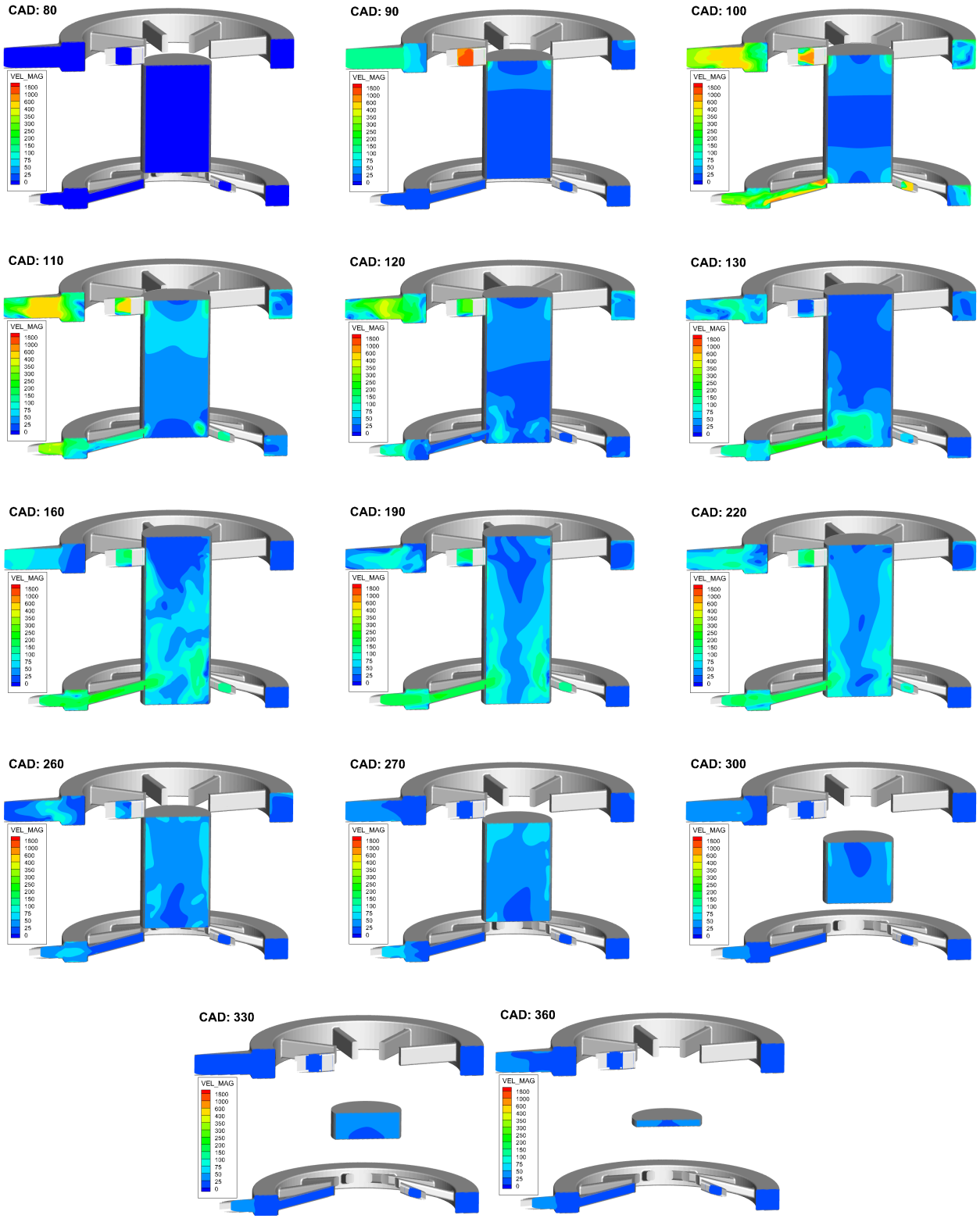

Figure 64: Velocity magnitude field (in $\frac{m}{s}$) for various CAD values with a slice that permits better visualization of the intake ducts.

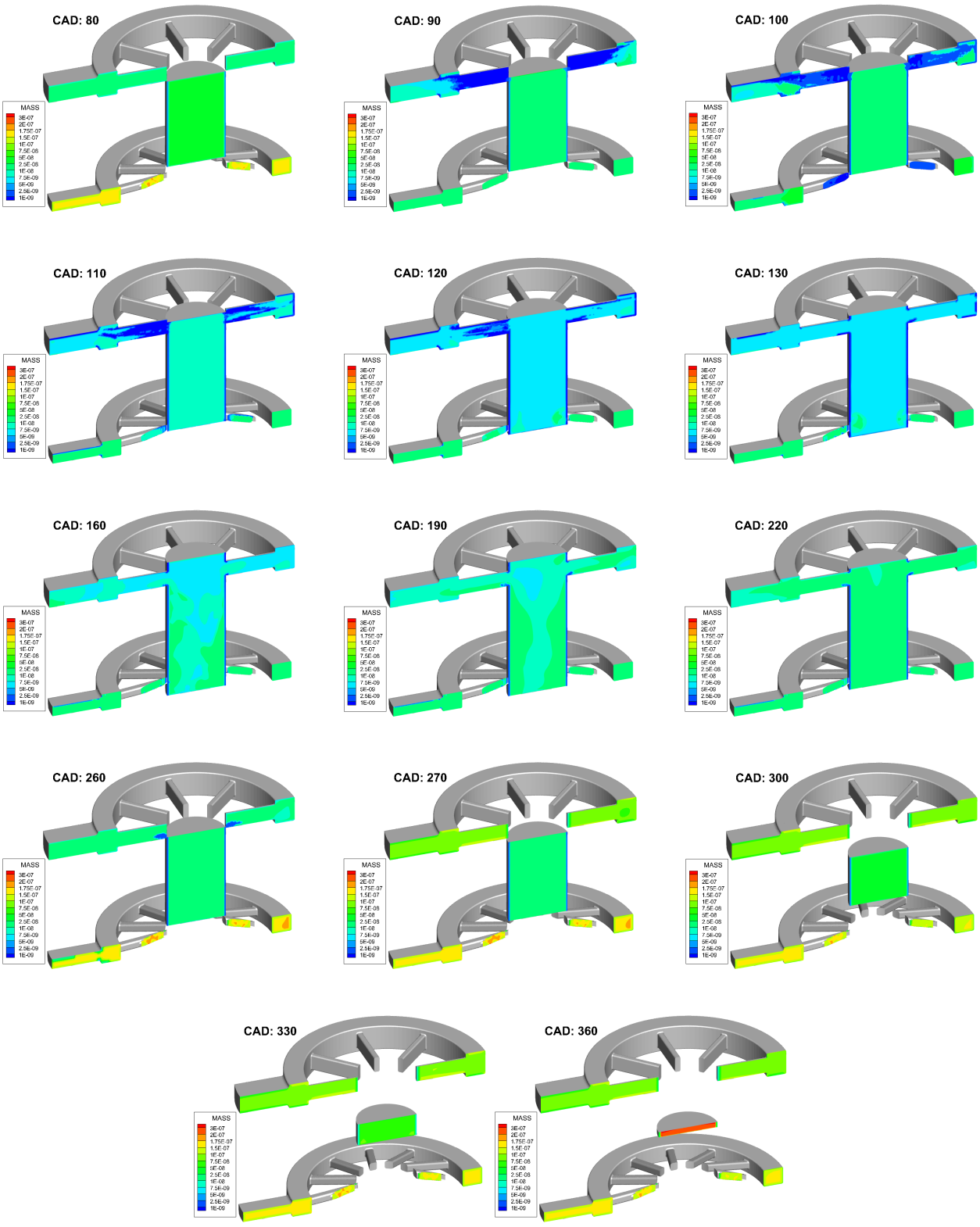

Figure 65: Air mass field (in kg) for various CAD values with a slice that permits better visualization of the exhaust ducts.

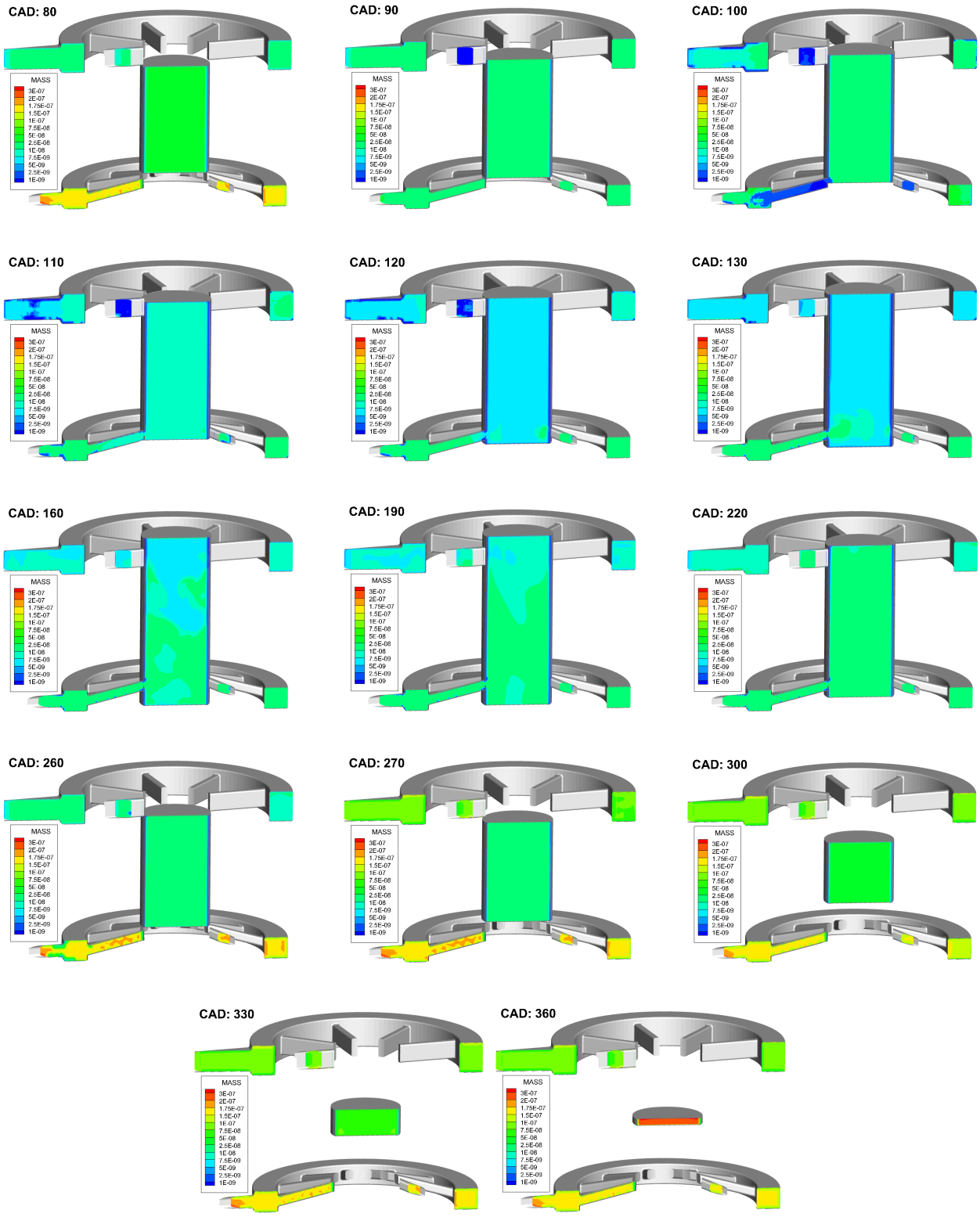

Figure 66: Air mass field (in kg) for various CAD values with a slice that permits better visualization of the intake ducts.

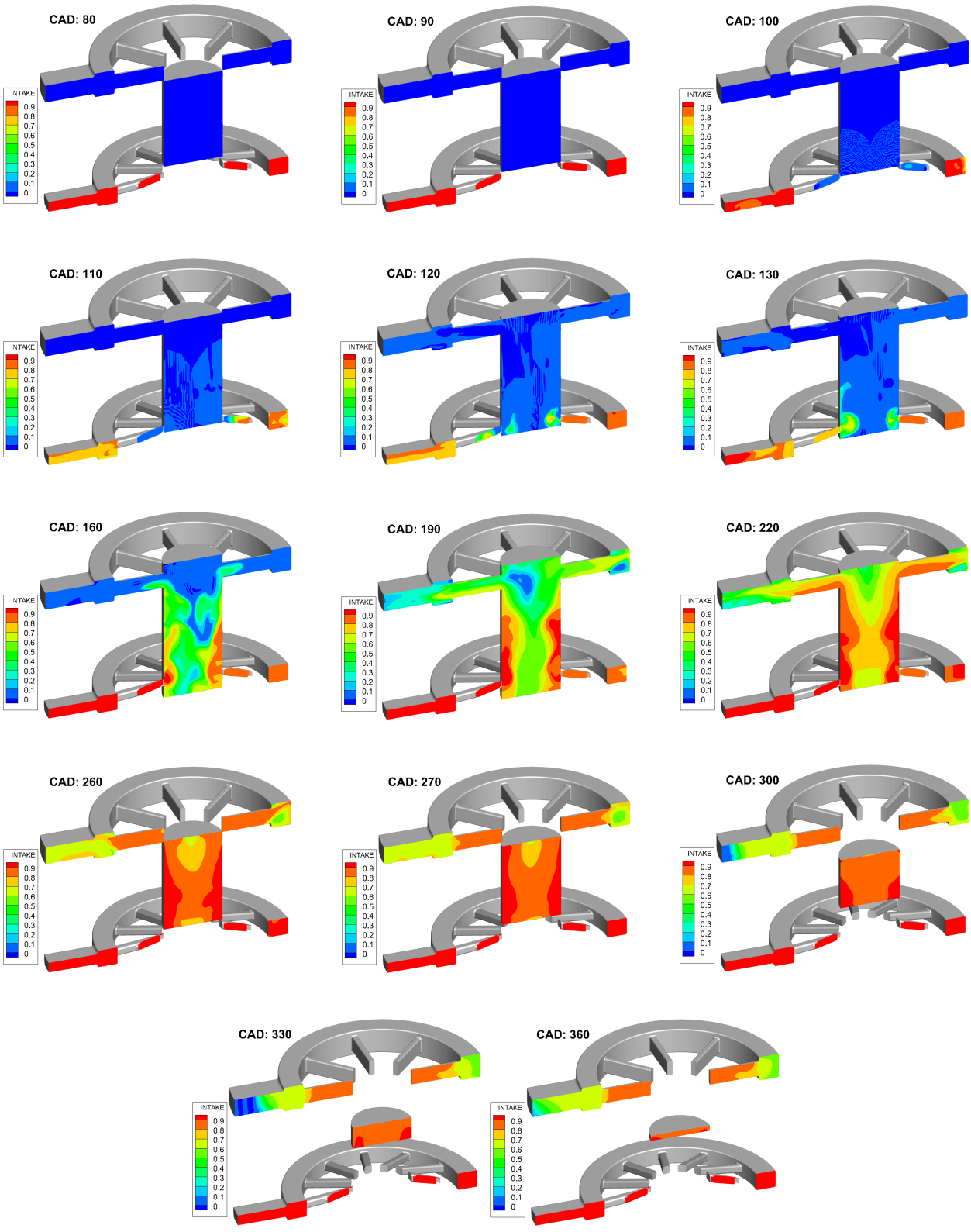

Figure 67: INTAKE species concentration for various CAD values with a slice that permits better visualization of the exhaust ducts.

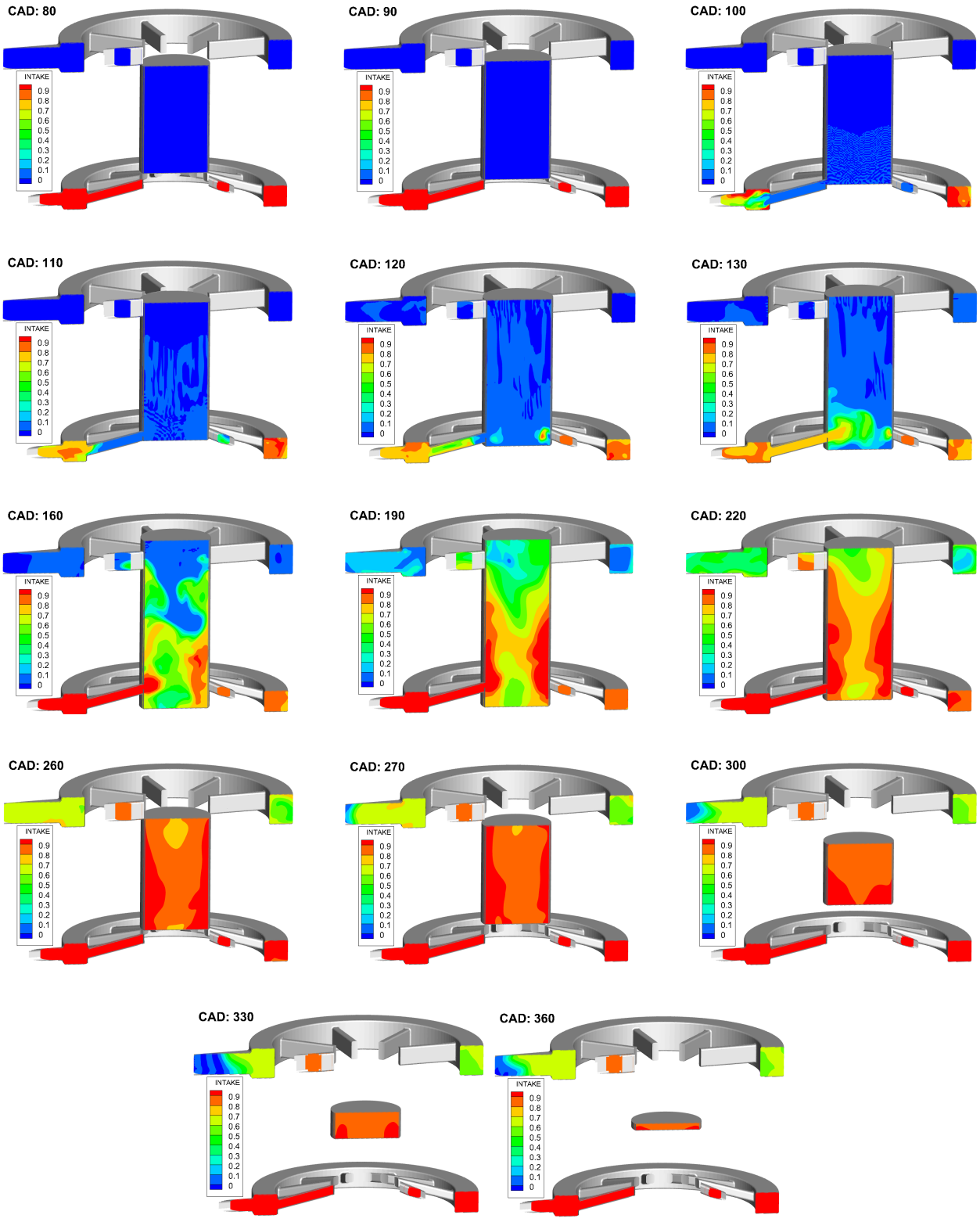

Figure 68: INTAKE species concentration for various CAD values with a slice that permits better visualization of the intake ducts.

The velocity field exposed in Figures 63 and 64 clearly shows how the (initially stationary at 80 CAD) fluid inside the cylinder is rapidly expelled to the exhaust ducts (seen in the image corresponding to the 90 CAD when the exhaust ports are already opened, but not the scavenging ones). Then, from the graph at 100 CAD onwards, it is represented how the opening of the scavenging ports generates the inflow of fresh air with a **swirling motion** that forces out the fluid that was previously present in the cylinder volume. When the 255 CAD are reached, the scavenging ports are closed, so the velocity profile at 260 CAD only evidences how the flow organizes itself to reach the exhaust that will close at 265 CAD; this is why there is no more flow inside any of the ducts starting from the 270 CAD. During the remaining CAD steps, the fluid is just compressed inside the cylinder, so its velocity field is gradually reducing in magnitude because the only elements that are generating the fluid movement are both pistons ends.

With regards to Figures 65 and 66, they evidence how, after the exhaust ports open (represented by the picture at 90 CAD), the air inside the cylinder moves out, pushing the fluid inside the exhaust duct, so the amount of air present in that region abruptly decreases. From this point on, the mass of air inside the cylinder gradually drops as it escapes through the exhaust ducts, but eventually starts to increase again due to the fact that the scavenging ports have also opened: this reduction and then growth condition of the amount of air inside the cylinder can be appreciated in the graphs from 90 CAD until 260 CAD when the scavenging ports are already closed. From that moment onward, the quantity of air inside the volume is almost constant (there is a fraction of air that is still forced out until the exhaust ports closed at 265 CAD) and the change of colour in the in the geometry is just because the system has reached the top dead centre, so the same mass of air is occupying a smaller volume: the clearance volume.

In last place, Figures 67 and 68 certainly represent the movement of the air from the intake inside the cylinder. To begin with, logically air is not entering the cylinder until the scavenging ports are opened, this is why, in the first pictures, the cylinder remains blue. As the CAD value increases, it is shown how the INTAKE gas moves inside the cylinder with a **swirling motion** and gradually fills the volume (gradually changing the cylinder colour from blue to green to orange). As a matter of fact, it is also possible to visualize (for example at 220 CAD) that there are some orange streamlines that enter the cylinder, stay next to its walls and escape through the exhaust ducts, in other words, **short-circuiting** is also represented. After the exhaust closes, see the image corresponding to 270 CAD, the cylinder remains mainly coloured by red, orange and yellow colours, that is to say, there is a high INTAKE species concentration inside; this means that the **scavenging is effective** because the inflowing gas is able to displace most of the gas that was inside the cylinder and fill its volume with fresh charge.

However, it must also be mentioned that there are some **irregularities present in the results**:

- The velocity values at the intake and exhaust opening are extremely high.
- When the scavenging ports open, instead of increasing the air mass inside the cylinder, the air quantity inside the intake ducts is shown to decrease.

- The air mass takes long time to fill again the cylinder volume (at 190 CAD is shown an almost complete filling).
- When the scavenging ports open, instead of the INTAKE species entering the cylinder, the cylinder's air mass fills the intake ducts (this is why at 100 and 110 CAD THE intake ducts are blue and not red anymore). The INTAKE species is shown to start entering the cylinder only at 120 CAD.
- The three fields represent a fluid jet entering the volume at 120 CAD, not before, even though the scavenging ports opened at around 91,5 CAD.

After a dedicated research, the reason for all this situations was discovered and it is discussed extensively in Section 4.4.4.

4.4.2 Ratios and Efficiencies

Having explained the behaviour of the different variables, the next step is to compute the value of the different ratios and efficiencies that reign the problem; this is possible thanks to the INTAKE passive which allows to specifically control the flow of the air mass that enters from the Intake Ducts to the Cylinder.

Delivery Ratio	Scavenge Ratio	Scavenging Efficiency	Trapping Efficiency	Charging Efficiency
1,885	1,815	0,891	0,523	0,95

Table 12: Efficiencies and ratios obtained with the simulation.

Based on the theory provided by Blair ([7]), it can be affirmed that **for the value of scavenge ratio obtained, the scavenging and trapping efficiency results are logical** because uniflow engines show to have typically high scavenging efficiencies, but relatively low trapping efficiencies for high loads (or, in other words, high delivery and scavenge ratios) typical of heavy duty engines. The high values for the charging and scavenging efficiencies mean, respectively, that the **gas** that flows inside the engine **fills the cylinder in a completely effective way**; and that most of the **fresh charge** that enters the cylinder is able to **displace to the exhaust the gases that were previously present inside the cylinder**. However, the reduced value of the trapping efficiency indicates that a large amount of the air that goes into the engine's cylinder does not get trapped there, so this implies, as it was mentioned before, that there is a considerable amount of **short-circuiting** which can also be clearly seen in Figures 67 and 68.

4.4.3 Plots for Model Validation

To continue, the CFD model is put under verification by comparing the pressure profile inside of the cylinder with the one obtained with the GT-Power model developed by CNR-STEMS. If both profiles were relatively similar, this would mean that SIM 6 is representing exactly the same condition as CNR-STEMS is modelling and no modification should be applied.

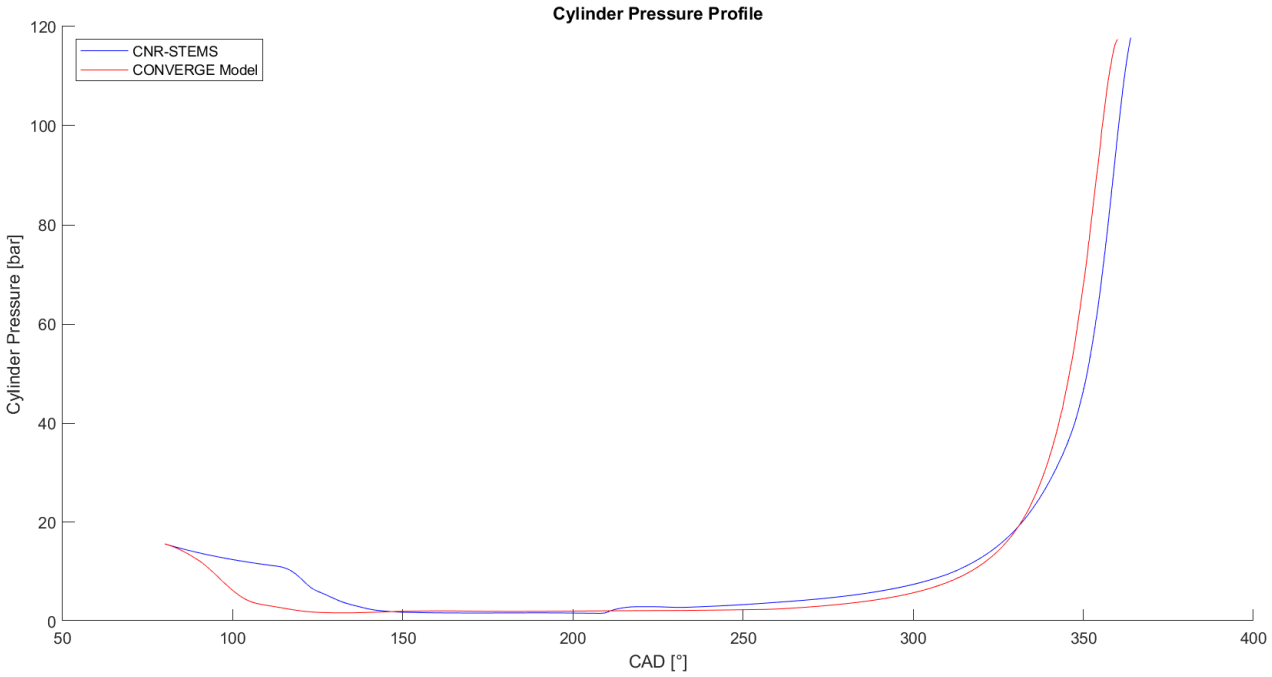

Figure 69: Cylinder pressure profiles obtained with CONVERGE and GT-Power.

Unfortunately, both profiles do not coincide. In first place, it can be seen that **from the beginning until around 150 CAD**, both profiles show a considerable difference, experiencing the **CONVERGE model a more abrupt decrease in the cylinder pressure**. Additionally, as the CAD value increases, it is eviidenced that **the minimum pressure value in SIM 6 is lower**, but it **starts growing before the GT-Power model**. All these differences imply that it is necessary to apply certain change/s to the model and all this situation is discussed in Section 4.4.4.

Similarly, in order to further study the problem identified with the pressure profile, the profile for the INTAKE passive species content inside the cylinder is placed below together with the efficiencies and ratios profiles which are all a consequence of the former.

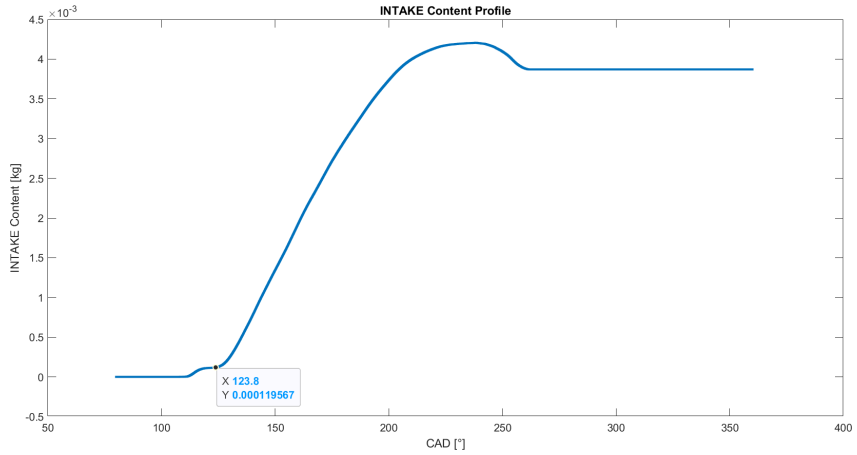

Figure 70: Profile for the INTAKE passive species content inside the cylinder.

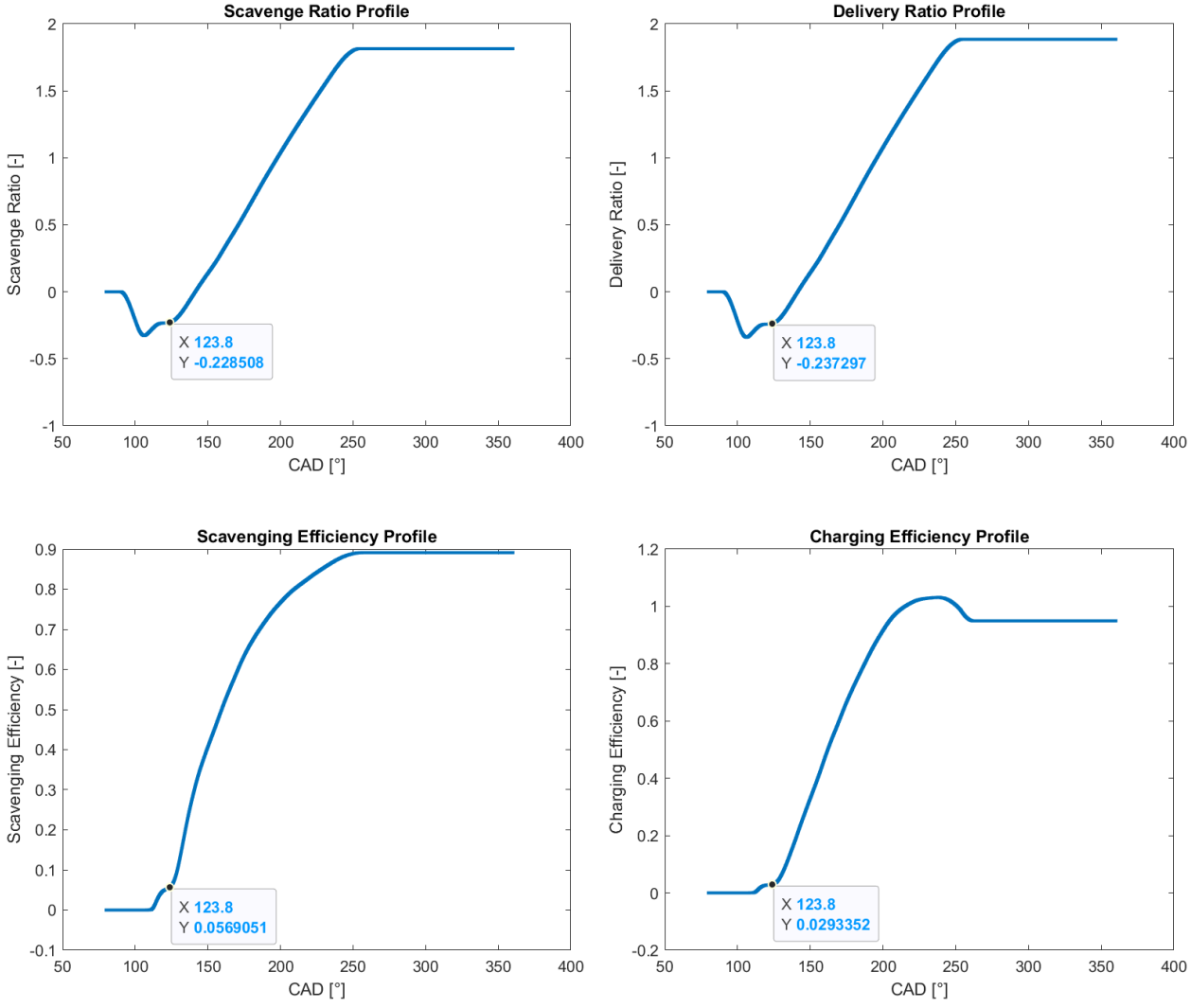

Figure 71: Profiles for the scavenge ratio, delivery ratio, scavenging efficiency and charging efficiency.

By observing Figures 70 and 71, it is possible to identify a common issue in all of the graphs displayed: **the behaviour does not start when it should but some CAD afterwards**. In all of the cases, the growing trend should start at around 91,5 CAD when the scavenging ports open causing the INTAKE species to enter the cylinder, but this behaviour begins at around 123,8 CAD. In addition, a more critical aspect is the fact that the scavenge and delivery ratios profiles present **negative values** at the beginning of the simulation which is not logical at all because it would mean that air mass is exiting the cylinder. Therefore, it can be concluded that **the initial differences in the pressure profiles** from Figure 69 are related to the fact that **the flow from the intake ducts to the cylinder is not occurring as it should** and this problem is discussed in Section 4.4.4.

4.4.4 Backflow and Ports' Position

After discovering all the previously mentioned problems, an exhaustive revision to the model was performed until the reason for them was identified: **backflow**. Figure 72 is a zoom at the intake ducts showing the INTAKE species concentration profile and, as it can be appreciated by the arrows, backflow exists during a relatively high CAD interval. When the scavenging ports open at about 90 CAD, the fluid is forced from the cylinder to the intake ducts during 20 CAD. After this interval, the fluid begins to flow back to the cylinder, but the inertia of the previous backflow causes that no fresh charge is able to enter the cylinder until 120 CAD. At this point the fresh air is just beginning to enter the cylinder and to conform the completely stabilized air jet shown at 130 CAD. As it can be concluded, this situation is not correct due to the fact that it **delays the whole scavenging process**: **all the sequence until the air jet is conformed lasts 40 CAD**, when it should actually occur shortly after the scavenging port opening.

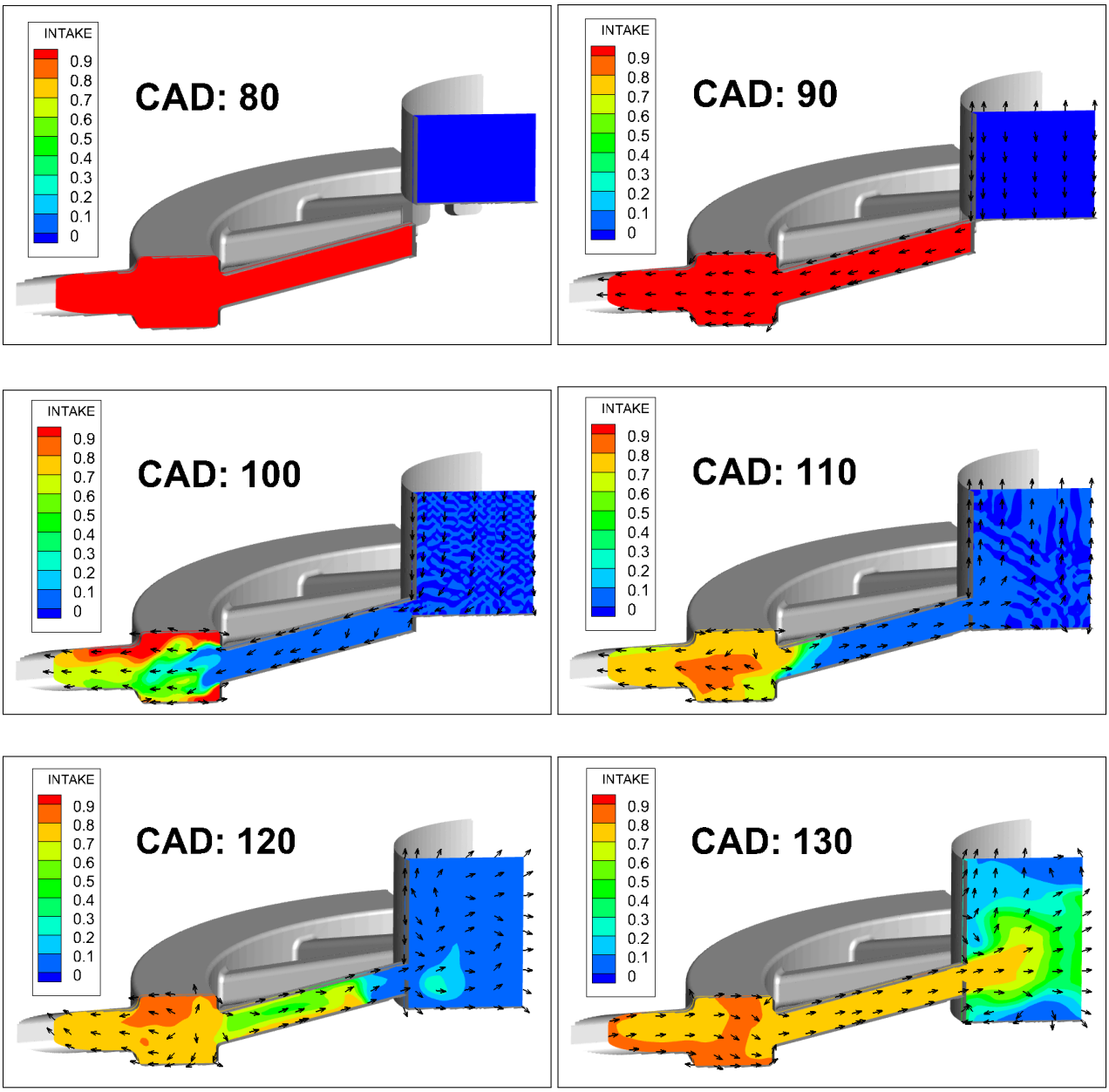

Figure 72: Initial backflow inside the engine.

Although it is known that some backflow can occur depending on when do the scavenging ports open, in this case backflow is a severe problem because it occurs **since the opening of the scavenging ports at about 91,5 CAD until a value near the 123,8 CAD**. In consequence, graphs from Figures 70 and 71 show inconsistencies like the delay in the starting point of the behaviour and the negative ratios' values because the intake ducts are not filling the cylinder with air, but receiving air coming from the cylinder. Additionally, it is now clear the delay in the appearance of the air jet entering the cylinder volume in Figures 63 to 68, because previously the inflowing air needed to act against the inertia of the backflow. As a last remark, backflow now appears as the main cause for the delay in the gas filling of the engine and for the behaviour inside the intake ducts represented in the

previously mentioned figures.

However, there is no apparent reason for backflow to occur: all of the design decisions and inputs to the CONVERGE model were either supported by theory or recommended by CNR-STEMS. After re-examining the whole model once again, a peculiar issue was discovered: in Section 3.1, it is mentioned the fact that the scavenging ports were designed to open at 131 CAD and the exhaust ports at 120 CAD, but in the CFD model, as it has been stated numerous times throughout this writing, they, respectively open at 91,5 CAD and 81,5 CAD. Thus, **there is a failure in the way the model represents the port opening** because in both cases it happens around **40 CAD before the design values**.

In Figure 73, it is evident the reason of this issue: **the linear interpolation to determine the ports' position**. As it can be seen in the previously mentioned figure, the linear and the sinusoidal curves separate from each other during a certain range of CAD values, hence the **linear interpolation was an imprecise design decision for locating the ports**. In consequence, the position in millimeters that corresponds to the ports' opening approximated with the linear interpolation ("Linear Approximation Intake/Exhaust Opening" in the graph) is actually associated to a lower CAD value in the sinusoidal trend ("Actual Intake/Exhaust Opening" in the graph), in other words, the ports' positions are associated to lower CAD values because the sinusoidal profile that defines the piston movement is at the left of both of the linear interpolation functions in Figure 73.

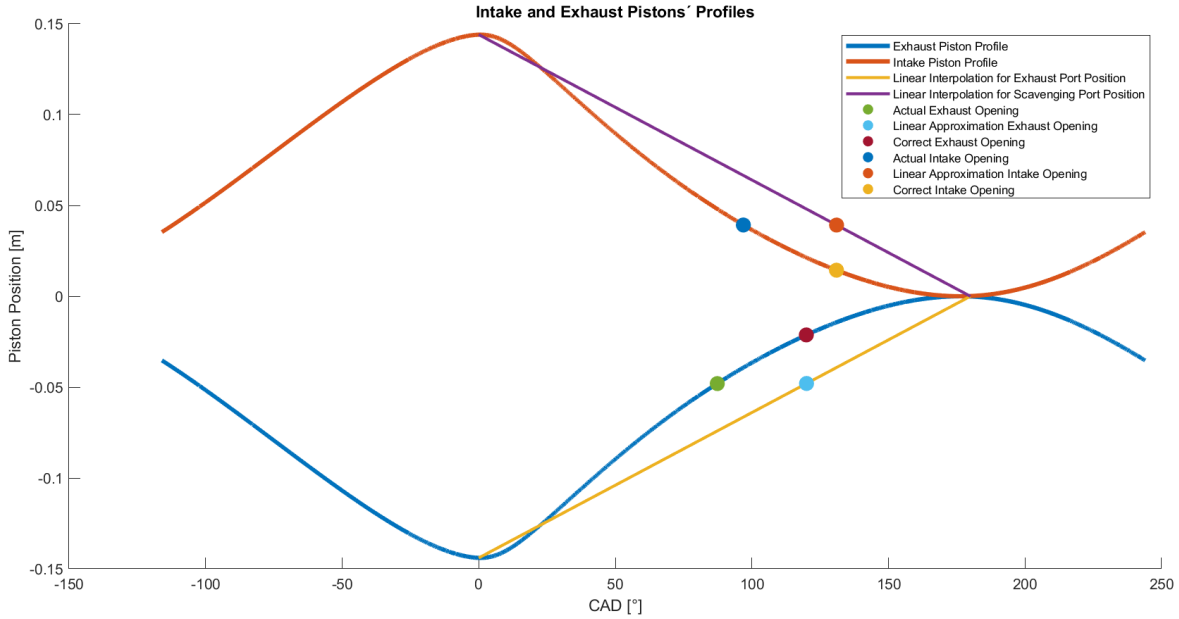

Figure 73: Intake and Exhaust Pistons´ Profiles withe both linear interpolations and different opening points.

Consequently, as the pressure profile used for the initialization (see Figure 13) is in correspondence with the sinusoidal piston position profile, the pressure value that the cylinder experiences when each set of ports open is not the required one, but also an anticipated one. Therefore, following the trend from Figure 13, **at port opening condition, pressure is higher than what it should be**, so, as it is also appreciably higher than the pressure at the intake, the air inside the cylinder is forced inside the ducts with a **significantly high velocity** (see Figures 63 and 64).

5 Conclusion

Throughout this writing, it was discussed the design and implementation of a CFD model to study the behaviour of an opposed piston two-stroke engine with the detail of having a free piston layout.

In an initial simulation stage, the non-hydrodynamic simulations allows to test the initial behaviour of the model designed and to properly evaluate the fixed embeddings' configuration. The objective achieved in this step is the fact of finding the appropriate settings of the fixed embeddings that result in an effective model with adequate values of total cell number, wall time and time step, together with no recoveries.

As a following step, when running the hydrodynamic simulation, the model was experiencing a sealing problem that generated a failure in the simulation before it finished solving the case. Fortunately, by changing the base grid size and discretization layout, the model is able to guarantee proper sealing during all the CAD steps of the simulation without failing.

In third place, it is required to guarantee the adequate simulation duration and this is done by properly setting the CFL number, the maximum time step and, most important of all, the Adaptive Mesh Refinement parameters. In the end, it is possible to obtain a simulation that, using 12 cores, takes 1 day to solve 95 CAD without showing recoveries. Additionally, the simulation also shows an acceptable time to solve all of the CAD steps, each of them related to a specific time step value which, in all of the cases, is inside the required interval. As a last remark, no cell saturation occurs, so the model is able to represent the studied situation with the highest precision that its settings allow.

In regards to the thermodynamic analysis, it can be stated that the model is able to effectively study the evolution of the different variables of importance and to represent the relevant processes of interest like the gas filling, the scavenging, the swirling motion and the short-circuiting. Moreover, the results obtained for the efficiencies and ratios typical of two-stroke engines show to have reasonable values for a heavy duty uniflow engine.

All in all, as far as the CFD model is concerned, the results obtained and the verification done permit to state that the different parameters defined in the settings enable an accurate study of the gas filling inside the engine during the first cycle and so, the combustion appears to be the following stage to add in the engine modelling.

However before dealing with combustion, there is a problem that is not directly related to the CFD model itself, but to the initial geometry design: the linear interpolation used for the ports' positioning was not precise enough, so their location generates their anticipated opening. As a consequence, as the pressure inside the cylinder is higher than expected, it occurs the backflow to the intake ducts which affects the scavenging process and so, the CFD model is not able to represent the same working conditions as the GT-Power model previously used as an input.

In order to solve this issue, there are two alternatives that can be implemented in further improvements of the model:

- Re-designing the CAD geometry and adapting the CFD model in a way that the scavenging and exhaust ports are placed in the positions named "Correct Intake/Exhaust Opening" in Figure 73.

- Adapt the GT-Power model for a scavenging and exhaust ports' opening at, respectively, 91,5 CAD and 81,5 CAD and insert this new piston profiles as boundary conditions in the corresponding boundaries as explained in Section 3.2.2.

As a last comment, throughout this writing the design and modelling was completely centred in studying the uniflow scavenging configuration, but, once the existing problems regarding the ports' location are solved and the a new simulation is launched and verified, it could be interesting for a further analysis to compare its results with the ones obtained in equivalent simulations with other layouts, like for example the loop scavenging analysis developed in [13].

References

[1] SoCalGas. *Benefits of Natural Gas.* URL: https://www.socalgas.com/for-your-business/natural-gas-vehicles/benefits. (accessed: August, 2023).

[2] Terrapass. *What Does It Mean to Be Carbon Negative?* URL: https://terrapass.com/blog/what-does-it-mean-to-be-carbon-negative/. (accessed: August, 2023).

[3] Kostusa. *Cool News You Can Use: Light Duty Vs. Heavy Duty Antifreeze.* URL: https://kostusa.com/cool-news-you-can-use-light-duty-vs-heavy-duty-antifreeze/#:~:text=Light%20duty%20engines%20are%20those,%2C%20buses%2Cor%20construction%20equipment. (accessed: August, 2023).

[4] Heavy Equipment Maintenance Solutions LTD. *Heavy Duty Engine Stand: A Comprehensive Guide.* URL: https://www.hemsltd.com/blog-heavy-duty-engine-stand/#:~:text=A%20heavy%20duty%20engine%20is,heavy%20loads%20and%20extreme%20temperatures. (accessed: August, 2023).

[5] J. Ma; H. Zhao; P. Freeland; M. Hawley; et al. "Numerical Analysis of a Downsized 2-Stroke Uniflow Engine". In: *SAE International Journal of Engines* (2014).

[6] J. Turner; R. Head; J. Chang; N. Engineer; et al. "2-Stroke Engine Options for Automotive Use: A Fundamental Comparison of Different Potential Scavenging Arrangements for Medium-Duty Truck Applications". In: *SAE Technical Paper* (2019).

[7] Gordon P. Blair. *Design And Simulation Of Two-Stroke Engines.* Society of Automotive Engineers, Inc., 1996.

[8] John B. Heywood. *Internal Combustion Engine Fundamentals, Second Edition.* McGraw-Hill Education, 2018.

[9] Jaclyn E. Johnson; Jeffrey D. Naber. *Alternative Fuels and Advanced Vehicle Technologies for Improved Environmental Performance (Second Edition).* Elsevier, 2022.

[10] Paul Breeze. *Stirling Engines and Free Piston Engines.* Academic Press, 2018.

[11] E. Mattarelli; C. Rinaldini; T. Savioli; G. Cantore; et al. "Scavenge Ports Ooptimization of a 2-Stroke Opposed Piston Diesel Engine". In: *SAE Technical Paper* (2017).

[12] Convergent Science. *Converge 3.1 Manual.* 2023.

[13] A. Nicastro; M. Baratta; D. Misul; C. Beatrice; et D. Di Maio. “Modellazione e analisi CFD preliminary per un caso innovativo di motore a 2 tempi”. In: (2023).